Alma Mater Studiorum – Università di Bologna

DOTTORATO DI RICERCA IN

Meccanica e scienze avanzate dell'ingegneria

Ciclo XXVII

Settore Concorsuale di afferenza: 09/A2

Settore Scientifico disciplinare: ING-IND/13

Design of a new harrow type wool transport mechanism to reduce fibre entanglement

Presentata da: JURAMIRZA ABDIRAMATOVICH KAYUMOV

Relatore e Coordinatore Dottorato

Prof. Vincenzo Parenti-Castelli

Esame finale anno 2015

Contents

List of figures

List of tables

Abstract

The wool is entangled at several stages of its processing. In the conventional scouring machines, the prongs or the rakes agitate the wool and lead the fiber entanglement. Several scouring systems have been commercialized in order to reduce the fiber entanglement. In spite of the existing technologies, the conventional scouring machines are widely used in wool processing.

In this thesis, a new approach for the harrow type wool transport mechanism has been introduced. The proposed mechanism has been designed based on the motion of the conventional harrow type wool transport mechanism by exploiting new synthesis concepts. The developed structure has been synthesized based on the Hrones and Nelson's "Atlas of four bar linkages". The four bar linkage has been applied for the desired trajectory of the developed wool transport mechanism. The prongs of the developed mechanism immerse the wool into the scouring liquor and gently propel forward toward the end of the machine with approximately straight line motion in a certain length instead of circular or elliptical motion typical of the conventional machines.

Introduction

The wool processing requires the scouring at its initial stage, to remove the contaminants of the raw wool. Dust and vegetable matters can be removed in burring machines. Grease and suints are removed in bowls of the scouring machine which are filled by hot water containing soda-soap or some alkali [1, 2, 3, 4]. During the scouring process, the wool can be entangled by the motion of transport mechanism of the conventional scouring machine. The entanglement cause many problems at the next stages of the wool processing.

Conventional wool scouring machines consist of 4-5 bowls [4]. Three of them are filled with hot water and the remaining two with pure cold or sometimes hot water for rinsing purposes. Each bowl has a wool transport mechanism and in between the bowls there are squeeze rollers. Prongs or rakes of the mechanism immerse the wool into the scouring liquor which is filled in bowl and propel it to the end of the bowl.

Basic mechanical motions of aqueous scour bowl design have not changed greatly, and the most of the wool still scoured in aqueous system using rake and harrow machines [4].

In the most conventional Harrow type wool scouring machines, the motion of the harrow is achieved by crank and cam mechanisms. The desired motion can be obtained by changing the cam profile. Weight of the harrow mechanism is counterbalanced by masses properly located. The harrow rotates in a circular (Figure 2) or elliptical motion (Figure 3). As a result of these rotation, the circulation of the scouring liquor is obtained. Wool fibres follow the harrow motions. In this case fibres can be mixed with each other respectively, and fibre entanglement can be increased. J.R.Cristoe reported that [5], the concept of working points is introduced to describe how wool can become entangled during the scouring. According to this report, the severity of entanglement induced is a function of the severity of each working point coupled with the number of working points (Figure 1a). The following four different ways [5] can be used to reduce fibre entanglement:

- Modification of existing machines;
- Radically changing the design of the scouring machine;
- Changing the scouring medium;
- Changing the scouring configuration.

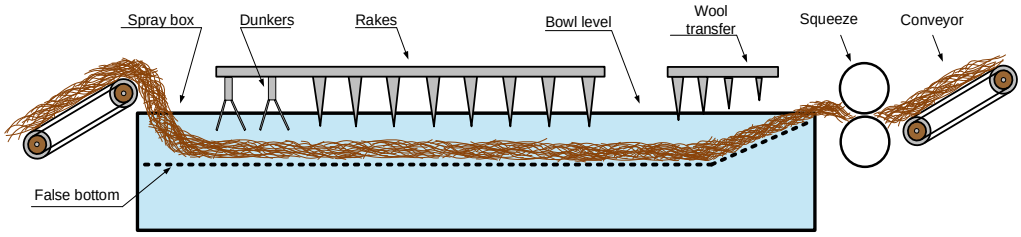

Figure 1a. Working points of the scouring bowl (Adapted from [5])

As cited in [5], in order to reduce fiber entanglement, the number of different scouring systems were developed, but, only the following three reached commercial use; Commonwealth Scientific Research Organization's (CSIRO) Jet scour [6], the University of New South Wales Aqueous Compression Jet scour [7] and the Fleissner Suction drum [8].

The goal of this work is reduce fibres entanglement by improving the motion of the conventional harrow type wool transport mechanism.

In the developed mechanism, the harrow can rotate with an approximate linear motion in a certain distance. At this distance, wool is propelled and cleaned between the harrow and scouring liquor. Wool can be floated gently in a straight line toward the end of the machine (Figure 3).

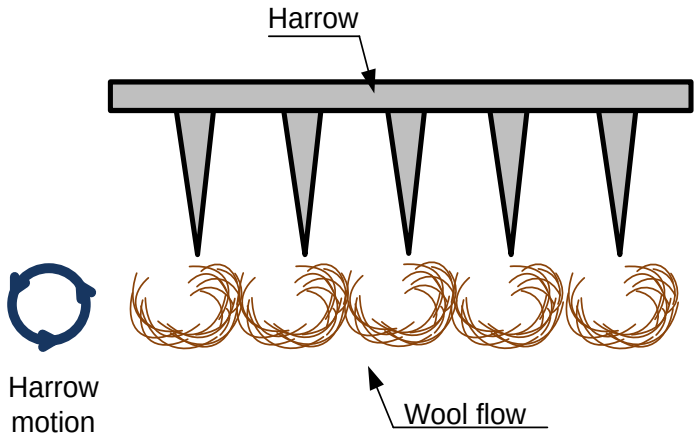

Figure 1. Circular motion of the harrow

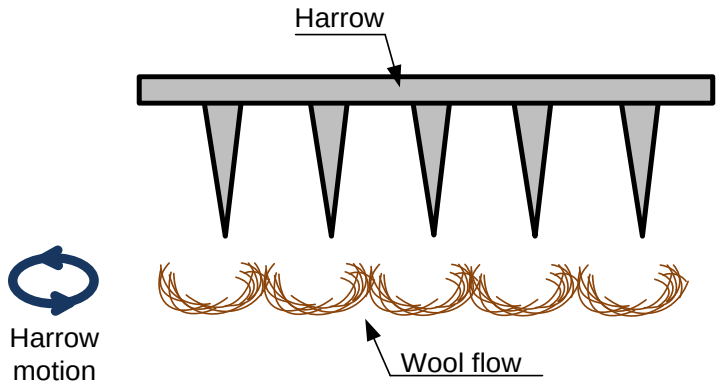

Figure 2. Elliptical motion of the harrow

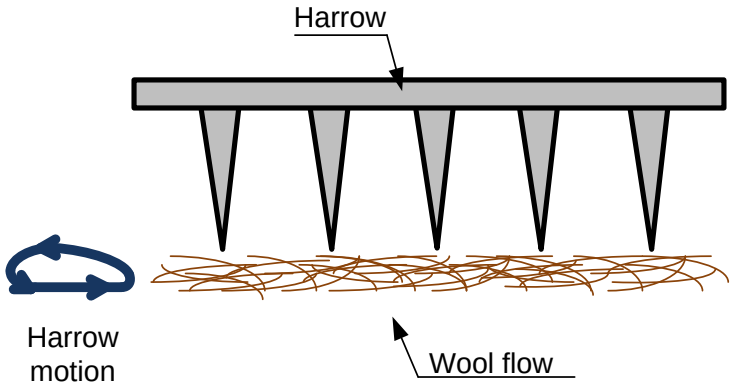

Figure 3. Approximately straight line motion of the proposed mechanism

The first chapter of this thesis is dedicated to the analysis of the state of the art, i.e. to the previously carried out researches in the field and the description of the conventional wool scouring machines. The second chapter illustrates the kinematics and the kinetostatics of the proposed mechanism. The third chapter describes the design of the mechanism. At last, in chapter 4 technical drawings of the mechanism have been drawn in order to manufacture the mechanism for industrial applications. Some conclusion and future works have been reported at the end of the thesis.

Chapter 1

The state of the art

1.1. Wool scouring methods

Wool is scoured mainly in two methods, aqueous and solvent scouring. This section presents brief information about these scouring methods.

1.1.1. Aqueous method

Aqueous or emulsion wool scouring is a traditional method, which is based on the aqueous solutions of soap and alkali. This method is most popular around the world [9]. The method has the benefit that, water soluble suint is easy to remove from the fiber, as it is dirt by agitation and squeezing. The most difficult of the contaminant groups to remove by this method is grease, which is removed by soda and soap mixture or detergents [10]. Agitation of the rakes or harrow help create an emulsion of grease in scouring liquor.

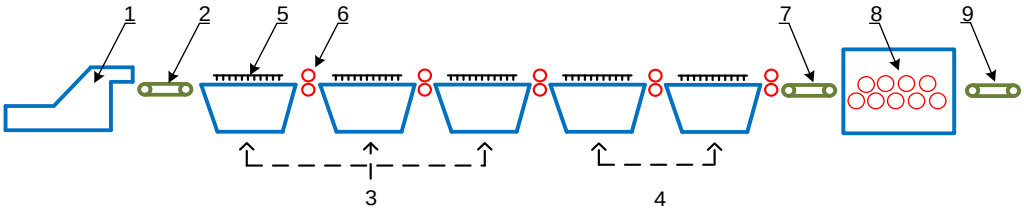

Figure 1.1. Conventional wool scouring line
1. Hopper feeder, 2, 7, 9. Belt conveyor, 3. Scouring bowls, 4. Rinsing bowls, 5. Wool transport mechanism, 6. Squeeze rollers, 8. Drying machine.

The conventional wool scouring machines operate based on the aqueous method. The line consists of 4-5 bowls (Figure 1.1). Three of them are filled with hot water and the other two bowls with pure cold or sometimes hot water for rinsing purposes. Each bowl has a wool transport mechanism and in between the bowls there are squeeze rollers. Raw wool is scoured, propelled, squeezed, and transferred to the next bowls by these mechanisms. At the last bowl, the scoured wool passes to the drier, which is located at the end of the scouring line. The drying machine dries the scoured wool and transfers it to the next stage of the process by conveyor or other ordinary ways.

Section 1.3 presents detailed information about the wool transport mechanisms.

1.1.2. Solvent method

Solvent scouring method is widely uses at some stages of the textile industry. The method appears to be alternative to aqueous scouring and particularly suitable for polyester and woollen goods [10].

In solvent scouring process wool fibers can be scoured more efficiently than aqueous method. In the solvent method entanglement associated with aqueous scouring are largely eliminated, wool grease recovery is much increased, suint recovery may be designed into the process, and aqueous effluent problems are avoided [11]. There are several clear advantages to be gained from solvent scouring, with only minor disadvantages – the necessity for solvent recovery, possible toxicity and fire hazards to be set against it [12]. Some detailed discussion of the solvent scouring can be found in the references [12, 13] as cited in [11]. According to [12], several different processes reached commercial prototype status during the 1950s–1970s without achieving significant commercial success.

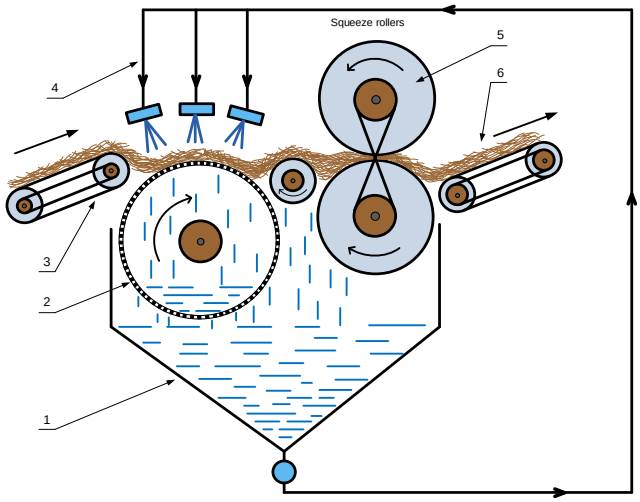

Figure 1.2. Jet scouring bowl (Adapted from [10])
1-hopper-bottomed bowl, 2-Suction drum, 3, 6- Conveyor, 4-jets, 5-squezze rollers

One of these machines is CSIRO jet scouring (Figure 1.2). In the jet scouring machines the wool is fed by a conveyor belt to the perforated drum and scouring liquor is sprayed on the fibre through low pressure jets [10] as shown in Figure 1.2. Solvent scouring is simple, robust, has a long working life and much more sophisticated than aqueous method, and requires a chemical process

engineering approach to its operation [4]. One of the disadvantages of the solvent scouring method is the use of harmful chemicals for human health.

1.2. Scouring systems

Wool can be scoured by several different scouring systems. Some of them is still using in wool processing. This section gives brief information about some scouring systems and their contribution on wool scouring process.

1.2.1. "WRONZ" comprehensive scouring system

Design of the individual scour bowls were continued until 1970. During the 1970s, in order to saving energy and pollution discharge, individual scour bowls became viewed in the context of a systems approach to wool scouring [4]. In 1972, the first comprehensive scouring system of the The Wool Research Organization of New Zealand (WRONZ) was installed at a new wool scour in Timaru, New Zealand [14, as cited in 4].

According to [4], the major outcomes of the system were to integrate the contaminant removal systems into the operation of the scour so that all heavy effluent received treatment before discharge. The treatment included removal of fibre, heavy solids, and recovery of wool grease. The scour bowls were discharged to drain from time to time, was replaced by a fully continuous discharging.

In this system (Figure 1.3), scouring liquor management was developed as bowl-to-bowl 'flowback' running countercurrent to the wool flow was used instead of bowl owerflow.

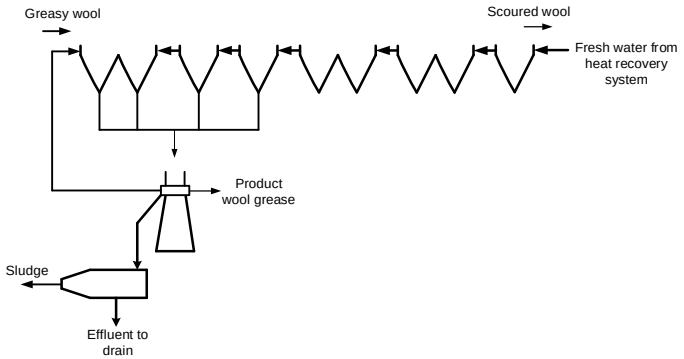

Figure 1.3. Simplified flow diagram of WRONZ comprehensive scouring system [4]

The heavy liquor draining was at a controlled rate that could be set manually or automatically via measurement of a particular property of the liquor (e.g. density or turbidity). Heat system was recovered from the flowdown and used to preheat fresh water being fed to the scour [4].

1.2.2. "Lo-Flo" and "Mini-Flo" scouring processes

In 1977, Commonwealth Scientific and Industrial Research Organization (CSIRO) released the Lo-Flo wool scouring process to industry [15, as cited in 4].

In the Lo-Flo process three mini bowls are used (Figure 1.4) in place of the first large bowl to effectively reduce water input and consumption [16].

In the Lo-Flo system, first one or two bowls of conventional scouring machine are replaced and wash plate bowls (Figure 1.5) are used instead [10].

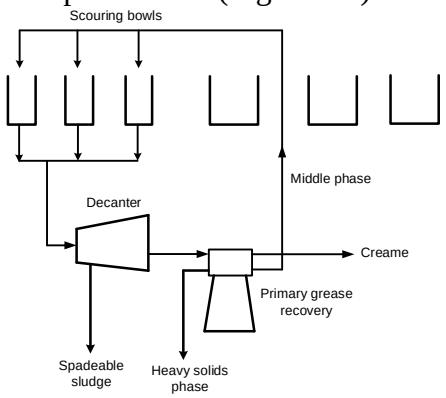

Figure 1.4. Contaminant recovery loop for Lo-Flo system [15].

The wool is washed down a perforated plate into the squeezing roller by jets or sprays of scouring liquor. According to [10], this is the shortest possible bowl, and it has a poor scouring efficiency. Lo Flo process mainly was used to recover grease and for pollution control purposes. In order to recovery the low rates of dirt removal of the wash plates, after two years of installation of the Lo-Flo process, Mini-Flo process was introduced [4].

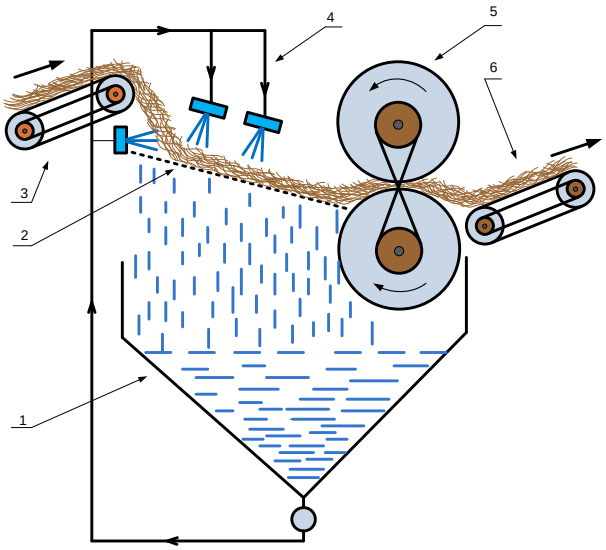

Figure 1.5. Washplate bowls used in Lo-Flo process (Adapted from [10])
1-hopper-bottomed bowl, 2-washpalte, 3, 6- conveyor, 4-jets, 5-squezze rollers

The Mini-Flo prototype used conventional bowls to remove dirt from wool after the wash plates, the commercial one used mini bowls for the purpose. But the results from the commercial prototype were promising, neither Mini-Flo nor Lo-Flo achieved continued commercial success [4]

1.2.3. "Siroscour" process

"Siroscour" is a technology package [17]. The system was designed by ANDAR wool scouring company in order to accommodate the different patterns of contaminant removing. The system highlighted the need for cleaner wool and better dirt recovery, which had been the biggest problems with Lo-Flo [4].

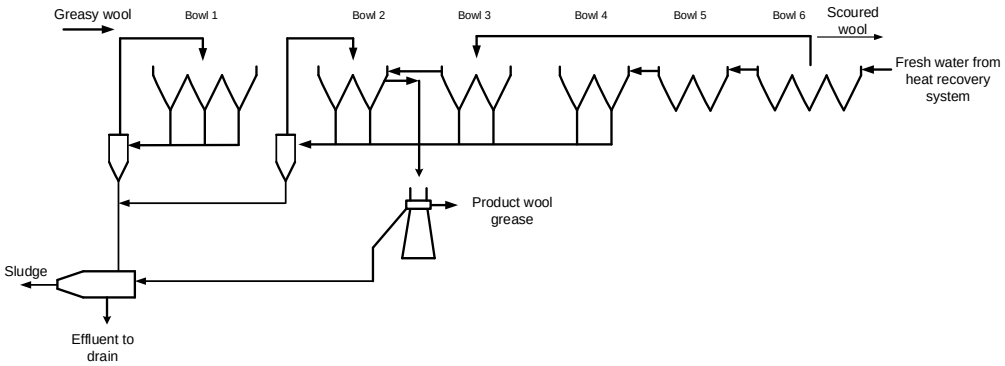

Figure 1.6. Simplified flow diagram of "Siroscour" system. [4]

The wool scours in the “Siroscour” system (Figure 1.6) through different stages. The first stage Bowl1 (Figure 1.6) removed only dirt by using a modified suint bowl. In the second stage (Bowls 2-4), easy to remove contaminants were removed. The third and final stage (Bowls 5-6) removed the hard to remove contaminants.

The reference [4] gives detailed information about scouring systems.

1.3. Wool transport mechanisms

Wool transport mechanisms are the main parts of the scouring machine. Mainly four types of wool transport mechanisms are used in scouring process. In this section all types of transport mechanisms are discussed.

1.3.1. Rake type mechanisms

In order to reduce the human labor, to produce good selling high-quality wool products and to increase the volume of the production, the initial wool scouring machines were created and installed in England [2].

In 1840, the initial single rake scouring machine was created by the firm “Mellet Freres” and later in 1853, the firm “Ien Petri&Taylor” created a developed wool scouring machine with multiple rakes, which called “Leviafan” [2]. Then, many wool scouring machines were created with several developed machine parts. Especially, F.Sargent, an American iron seeker and processor, and his family had a huge contribution [18, 19, 20, 21, and 22] on development of wool scouring machines. More than 100 inventions of brothers Sargents were patented. F.P.Pendleton, J.K Proctor [23, 24] and J.H.Knowles [25] are also well-known inventors who contributed on development of the wool scouring machines during the period of Sargents family achievements. These inventors carried out researches on developing the mechanisms of wool feeding, wool transportation, and scoured wool conveying.

Rake type mechanisms were consistently developed by several inventors during many years. One of the rake type machines created by F.G.Sargent in 1890 [26] is designed to move all rakes together as one by uniting the rakes placed in several rows. Each set of rakes consisted of four prongs fixed to a crossbar, and the machine had two sets of these rakes, where the first set was used for conveying, and the second for receiving and conveying to the next stage. This

machine was further developed by the same inventor and patented in 1892 [27]. According to this invention the rakes moving individually, were fixed to a bar which was placed in the center of the upper part of the machine and driven by four cranks mounted to one side of the machine. In order to achieve a smooth movement of the bar all cranks were rotated at the same velocity. The weights of the rakes were balanced by gears.

Following descriptions will give detailed information about the rake type wool scouring machines.

A swing rake machine is shown in Figure 1.6. In the figure, ***1*** represents the bowl or tank, forming the body or frame of the scouring machine, contains the scouring or scouring liquor ***2***, which is the soda-soap mixture for cleaning the wool. The greasy wool may be fed into it by feeding conveyor ***3***, driven by belts or gearing in any ordinary ways. As the greasy wool drops from the feeding conveyor into the bowl, the prongs ***b***, of the first rake ***6*** catches and immerses it into the scouring liquid and carrying it forward within the reach of the next rake. There may be two to six rakes in the rake machine. The rakes move the wool in the scouring liquor to clean it and pass it forward toward the squeeze rollers ***8***.

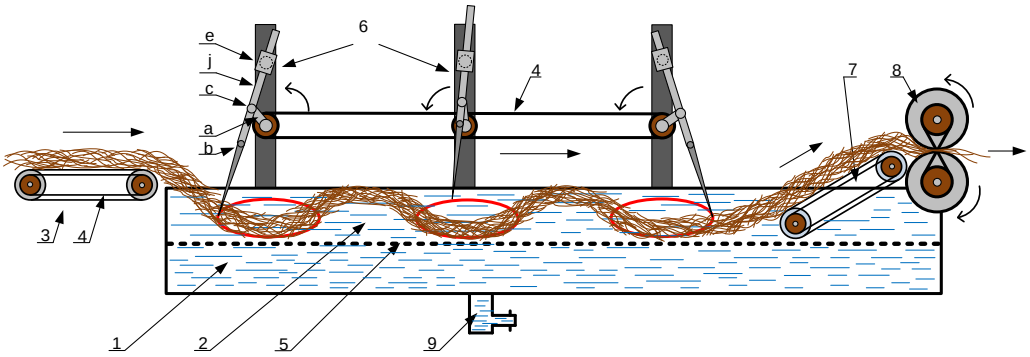

Figure 1.7. Swing rake type wool scouring machine

The rake ***6*** (Figure 1.7 and Figure 1.8.) moves by crank ***a***. Near the top of the rake there is a swivel joint ***e***, which allows the rake handle to move up and down through it and back and forth through the liquid, to suit the motion of the crank ***a***, and to properly guide it. By this arrangement the rake prongs ***b***, at their points will pass forward, and at the same time scour it by moving it through the liquid. At the end of the sweep, they move out of the liquid in a vertical position and return to the original position.

The output conveyor ***7*** receives the washed wool and carries it up to the squeeze rollers ***8***, which squeeze out the liquid from the wool, and liquid runs back

into the bowl. Squeeze rollers deliver the wool to the next scouring bowl. And scouring process continues in the next bowls.

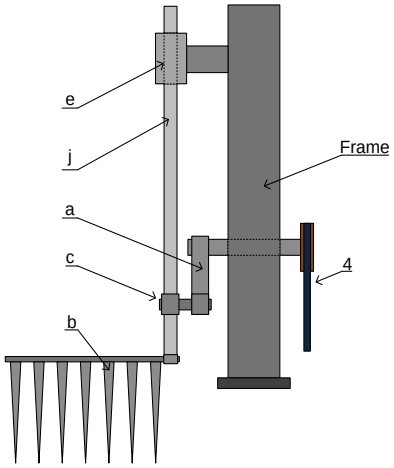

Figure 1.8. Rake type wool transport mechanism
a - prongs, b - crank, c-revolute joint, j-handle or shank, e-swivel joint

Near the bottom of the bowl ***1***, there is a perforated false bottom ***5***, through which the liquid may pass, but not the wool, and below this bottom, there should be a draw-off opening ***9***, for the sediment or emptying the bowl of the scouring liquor.

1.3.2. Harrow type mechanisms

The initial harrow type mechanisms were invented by the England inventors, John McNaught and William McNaught. Their inventions of harrow wool scouring machine were patented by Great Britain, France and Belgium in 1881-1882. The complete, clear and developed version of this invention was patented by the USA in 1888 [28].

According to this invention, the harrow type mechanism, where is hanged on columns mounted on the sides of the machine, is driven by the main shaft of the machine. Harrow type mechanism stays hanged with the support of the ropes. The motion of the Harrow is carried out by a cam mechanism. The inventors of this patent mentioned that the cam mechanism was used also their previous inventions [28]. In 1900 W.McNaught invented complexly developed harrow type wool scouring machine [29]. This invention is a developed version of the previous one, where harrow type mechanism stays fixed to the linkages instead of hanging with the support of the ropes. In addition, unlike previous inventions there is no small

harrow mechanism which was used for conveying the wool to the squeeze rollers. The wool can be propelled only by the main harrow mechanism. One of the most useful "Wool washing machine" of W.McNaught and T.Hawkins on harrow type mechanism is distinct by its peculiarities [30]. This invention was also focused developing the harrow type scouring machine, but it differs than others with the aspects that bowls are set on three floors. Wool is fed to the bowl on the 3rd floor. Then it is propelled by the harrow type mechanism to the squeeze rollers. Squeezed wool is fed to the 2nd floor by the feeder. This process will repeat in the all three floors. Harrow type mechanisms for all 3 floors are driven by single shaft with driving mechanisms such as linkages and cams. In an invention [31] offered after one year, in 1901, by F.G.Sargent, author of many patents on developing of the wool scouring machines, the harrow type mechanism was driven by oscillating driving mechanisms mounted to the sides of the machine. Later, in 1908 [32] and in 1909, [33] developed versions of wool transport mechanisms were proposed by F.G.Sargent. Currently, scouring machines developed on the basis of inventions [29] and [31] are widely used in many wool processing factories. Numerous researches have been conducted on developing feeding part, small harrow, and water supply to the machine and separation of waste materials from the used water for scouring. Including inventors Thomas Hawkins [30], Frederic G. Sargent [31, 32, 33], Allan C. Sargent [33], Friedrich Bernhard [34], Joseph Tillinghast [35] and Walter Oscar Milne [36] had significant contributions on developing the harrow type wool transport mechanisms.

Following descriptions will present detailed information about the harrow type wool scouring machines.

In the harrow type machine (Figure 1.9), as the swing rake machine in Figure 1.6, ***1*** represents the bowl or tank, forming the body or frame of the machine, contains the scouring or scouring liquor ***2***, raw or greasy wool may be fed into it by feeding conveyor ***3***, driven by belts or gearing in any ordinary ways. As the greasy wool drops from the feeding conveyor into the bowl. The prongs ***p***, which are all mounted on longitudinal girths ***h***, of harrow ***H***, catch and immerse the greasy wool into the scouring liquid and carrying it forward toward the output conveyor ***7***. On the wall of the bowl ***1***, secured columns ***j*** and ***j'***, provided at their upper ends with bearings for cross shafts O_2 and O_3. To each of cross shafts are secured two levers ***L*** and ***M*** respectively. ***L*** and ***M*** levers are being three armed levers. The arms ***l*** and ***m*** carry each weights ***i*** and ***i'***, said counterbalancing the weight of the harrow ***H***. And the arms ***l1*** and ***m1*** are connected by rods ***f*** and ***f',***

with the cross bars ***B*** and ***B′.*** While the ***l′*** and ***m′*** of the three armed levers ***L*** and ***M*** are connected together by the rod ***g***.

It is obvious that, when one of the cross shafts O_2 or O_3 is oscillated the other one will likewise be oscillated through the connecting rod ***g***, to impart to the harrow ***H*** the required rising and falling motion. This movement of the harrow required to and fro motion or sweep is imparted to harrow through the following mechanism, supported from the columns ***j*** and ***j′*** at the fed end of the bowl: there is rod ***e***, which is pivoted to the arm ***l*** of lever ***L***, the other end of rod ***e*** being pivoted to lever ***c***, that is fulcrumed at ***O4*** to an arm projecting rearwardly from the column ***j′***. The lever ***c*** carries near its right end roller ***d***, which rides on cam ***b***, secured to the shaft O_1. On the shaft ***O1*** also secured crank ***a***. The end of the crank is pivoted one end of the connecting rod ***k***, opposite end of the connecting rod ***k*** is pivoted to the cross bar ***B′***, secured to the longitudinal girths ***h*** of the harrow ***H***.

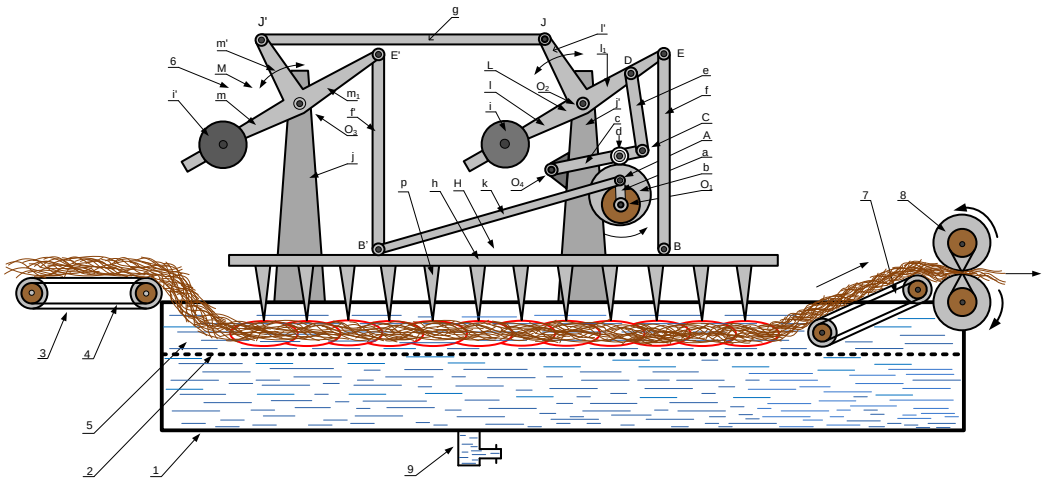

Figure 1.9. Conventional Harrow type wool scouring machine.

In the position of the harrow operating mechanism, the connecting rod ***k***, under the action of crank ***a***, is slowly moves the harrow ***H,*** toward the delivery end until said crank ***a*** is about to travel from its lower half circle to its upper half circle, and which time the cam ***b***, acting on rod ***e***, moves the arm ***l1*** of the lever ***L*** upward, thereby revolving shaft O_2 toward the left, which movement is communicated to lever ***M***, by connecting rod ***g***, thereon, whereby the harrow ***H*** is lifted out of the liquid ***5***. As said crank revolves through the upper half of its circle and in the upper portion of the slot in lever ***l′,*** the harrow will be moved backward at an increased speed and then downward back into the liquid.

As the swing rake machine in Figure 1.7, the output conveyor ***7*** receives the washed wool and carries it up to the squeeze rollers ***8***, which squeeze out the

scouring liquor from the wool, and liquor runs back into the bowl. Squeeze rollers deliver the wool to the next scouring bowl. And the scouring process continues in the next bowls.

Near the bottom of the bowl ***1***, there is a perforated false bottom ***2***, through which the liquor may pass, but not the wool, and below this bottom there should be a draw-off opening, ***9***, for the sediment or emptying the bowl of the scouring liquor.

1.3.3. Paddle type mechanisms

Besides the rake type and the harrow type, creating wool scouring machines with paddle type mechanisms also was subject to the researches. For instance, one of the initial paddle type mechanisms was proposed by an American inventor L.A.Peckham in 1896 [37]. The machine is specialised in washing as follows: raw wool is fed to the machine by feeder and propelled by paddle form ribbed surface cylinders which transfer the wool to the next paddles during rotation. Scoured wool is transferred to the squeeze rollers by a small harrow mechanism which is mounted on apron i.e. on the end of the machine. The main reason to propose this invention was the need to decrease the fibre damage and the fibre entanglement during scouring by rake and Harrow type mechanisms. In an invention [38] of another American inventor, Lund, the washing process takes place by the prongs which mounted to the two belt conveyors, where one of the conveyors is fully rotated under water and the second one half on the water surface and half under water, and wool is transported between these two conveyors. Another example for paddle type scouring machine invented by J.Keefe in 1902 [39] which differs from the invention [38] by only the conveyor surfaces. Conveyors of [38] have prongs and the ones [39] of have ribs on the surfaces. The main disadvantages of these inventions are that the working parts are always under water and causes these parts to get corroded. Additionally, the inventions of S.G.Sargent and Harrison [40], H.Walker [41], J.F.White at al [42], and W.W.Windle [43, 44] are focused on the developing of the paddle type machines. Differences between these inventions are the paddle forms and the location of paddles on the surface of the scouring liquor.

Following descriptions will give detailed information about the paddle type wool scouring machines.

In the paddle type scouring machine, the paddle action (Figure 1.10) gently swishes the wool along the bowl in which it has a longer period of immersion at a

much lower temperature than in the swing rake and harrow machines. As the swing rake and the harrow type machine in Figure 1.9, ***1*** represents the bowl or tank, forming the body or frame of the machine, contains the scouring or scouring liquor ***2***, which may be fed into it by feeding conveyor ***3***, driven by belts or gearing in any ordinary ways.

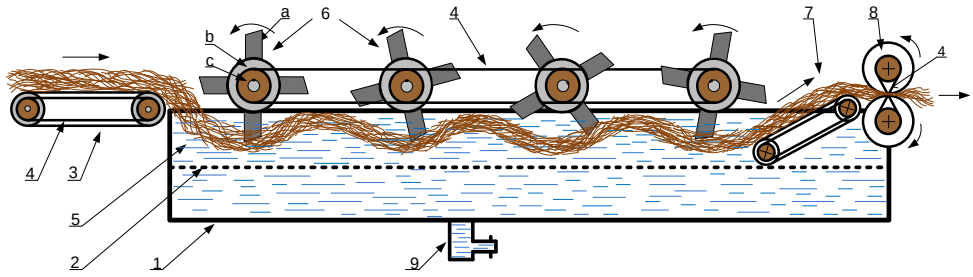

Figure 1.10. Paddle type wool scouring machine

As the wool drops from the feeding conveyor into the bowl, the blades or paddles ***a,*** which are all mounted on longitudinal cylinder ***b*** (Figure 1.10) of the first paddle cylinder ***6***, catch and immerse into the scouring liquid and carrying it forward toward the next paddle cylinders. The blades or paddles of the next paddle cylinders receive the wool and continue carrying forward toward the output conveyor. The paddle cylinders (Figure 1.11) secured in columns, driven by belts or gearing in any ordinary ways.

The output conveyor ***7*** receives the scoured wool and carries it up to the squeeze rollers ***8***, which squeeze out the liquid from the wool, and liquid runs back into the bowl. Squeeze rollers deliver the wool to the next scouring bowl and scouring process continues in the next bowls.

Near the bottom of the bowl ***1***, there is a perforated false bottom ***2***, through which the liquid may pass, but not the wool, and below this bottom there should be a draw-off opening, ***9***, for the sediment or emptying the bowl of the scouring liquor.

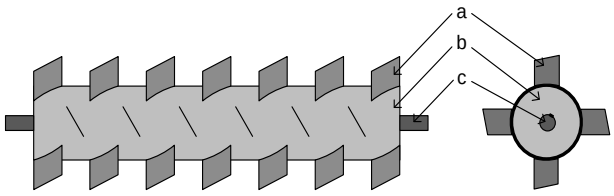

Figure 1.11. Paddle cylinder
a - blade or paddle, b-cylinder, c-shaft

In all the three types of the scouring machines, wool is scoured in bowls with perforated false bottoms, which permit the heavy impurities and sediments to escape, by setting into the compartment, at the bottom of the bowl. Side compartments are provided at the end of the bowl to receive the liquid from the squeezing rollers. As the dirt settles and the fats rise, the intermediate purer liquid may be fed back into the bowl for reuse.

1.3.4. Fleissner's suction drum

The raw wool also scoured by suction drum type machines [45] (as cited in [10]). During the 1960s Fleissner's suction drum was commercialized. In this type of machine loose wool is conveyed through the scouring bowl by a series of suction drum (Figure 1.12). The flow of scouring liquor through the raw wool and into the three suction drums is done by pumps through the perforated surface of the drum from outside to inside [10]. The efficiency of removing contaminants in Fleissner's suction drum is lesser than gentle scouring action and comparatively costlier than conventional wool scouring machines.

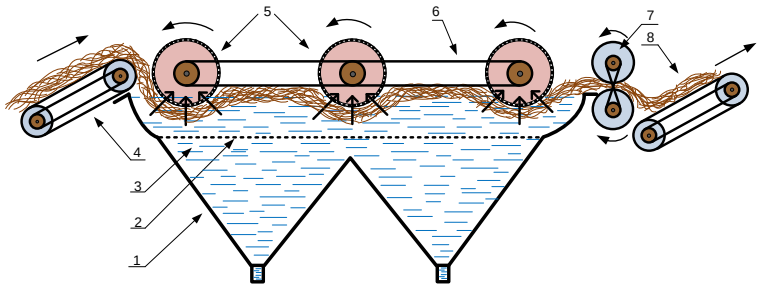

Figure 1.12. Fleissner's suction drum (Adapted from [10])

According to [10], the suction drum design has been successful for fine wool, on dirtier wools, product cleanliness become an issue. Later hybrid scour machines such as ANDAR hopper bottomed bowls installed by some mills with a selection of suction drum and rake bowls being fitted into the scouring bowl.

Chapter 2

Synthesis and analysis of a proposed mechanism

2.1. New scouring process

The wool fibres can be entangled during wool processing, mostly in opening and scouring processes by the mechanical agitations of the peg drums of wool opener and the prongs of the harrow mechanism [46]. As a result, in carding machine during the carding process, the entangled fibres can be broken and amount of waste materials will be increased. According to [46] there are four principal issues associated with wool scouring. These are:

- Effective contaminant removal;
- Minimal fibre entanglement;
- Product quality;
- Cost minimisation.

In the conventional Harrow type wool scouring machines the motion of the harrow is obtained by the crank and cam mechanisms. Changing of the cam profile can be obtained any desired trajectory of the Harrow motion. But manufacturing of cam mechanism is more costly than linkages.

During the working process of scouring machine, the prongs or teeth of the harrow type wool transport mechanisms pass forward with elliptical motion or sweep through the scouring liquor, and thus carry the wool forward, and at the same time scour it by moving through the liquor (Figure 2.1). The prongs catch and immerse the wool deeply into the scouring liquor and carrying it forward to the end of the bowl. As a result, fibre entanglement can be increased during washing process by wool transport mechanism.

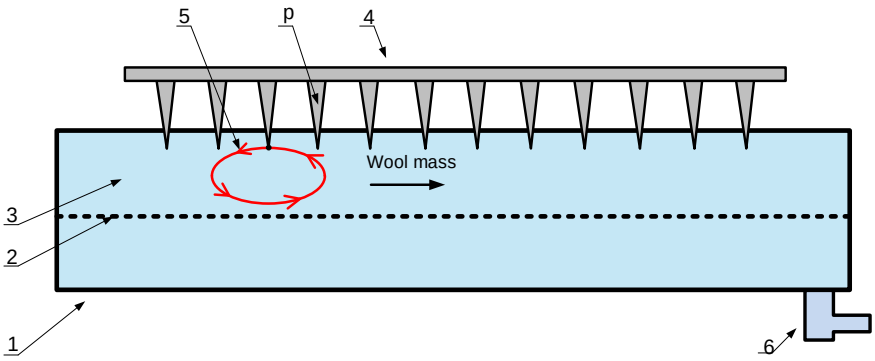

Figure 2.1. Trajectory of motion of the conventional Harrow mechanism
1-scouring bowl, 2-perforated false bottom, 3-scouring liquor, 4-harrow,
5-trajectory of motion of the prong, 6-sediment outlet

This thesis is focused on the design of a new wool transport mechanism in order to reduce fibre entanglement and damage based on the improving of motion of the mechanism by developing its topological structure. In order to reduce the mechanical agitation of the prongs to the fibres, the trajectory of the prongs was determined as an approximate straight line in certain length of rotation of the wool transport mechanism. In Figure 2.2, it can be seen that from point ***b*** to point ***c*** show the approximate straight line trajectory of the prong.

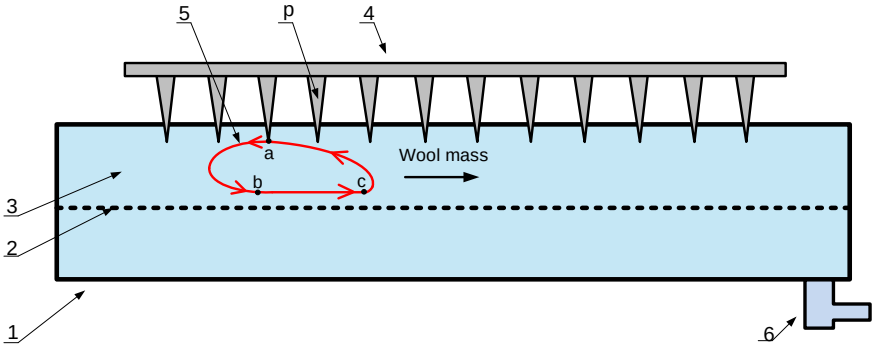

Figure 2.2. Trajectory of motion of the proposed wool transport mechanism
1-bowl or tank, 2-perforated false bottom, 3-scouring liquor, 4-harrow,
5-trajectory of the prong, 6-sediment outlet

Straight line mechanisms are divided into three categories [47]:
1. Exact straight line mechanisms.
2. Approximate straight line mechanisms.
3. Straight line copying mechanisms.

Straight line mechanisms are very important for some industrial applications. The first straight line mechanism invented and produced by James Watt in 1784 [48]. After Watt's straight line mechanism several new type straight line mechanisms were investigated by James White's hypocycloidal straight-line mechanism, about 1800, Freemantle straight-line linkage, later called the Scott

Russell linkage in 1803, an American pioneer Oliver Evans's "Columbian" engine, or "grasshopper" straight line linkage in 1813, Richard Robert's approximate straight line linkage in 1841, Sarrus's exact straight line linkage in 1853, Russian mathematician Pafnutiy Chebyshev's approximate straight line mechanism in 1867, Peaucellier exact straight-line linkage, in 1873, Hart's exact straight line mechanism in 1874 [49].

Another example of coupler curves of the four bar linkages has been investigated by Hrones and Nelson. They have completed approximately 7300 coupler curves of four bar linkages in their "Atlas of four bar coupler curves" [50]. It defines the linkage geometry for each of its Grashof's crank-rocker linkages. According to [51] these coupler curves was drawn to large scale and constitutes a very practical tool for the designer, who paging through, can find a shape and configuration suitable for a given application. It is a useful reference to provide a starting point for design and analysis.

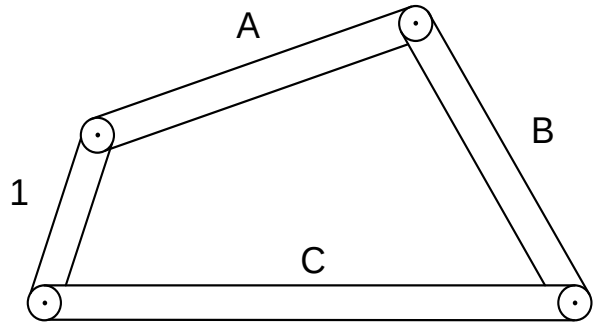

Figure 2.3. Four bar linkage [50]

According to [50] a four bar linkage is schematically shown in Figure 2.3. It consists of the four links having pin-to-pin lengths of 1, A, B, and C. The geometry of the linkage has been determined by the three ratios A/1, B/1, and C/1.

Up to this point the four-bar linkage has been represented as consisting of four lines. Actually, each member is a solid body which from purely theoretical aspects can be considered as being of indefinite extent. Each point of the body has been numbered as row and columns for the named of these points by the author of this thesis (Figure 2.4).

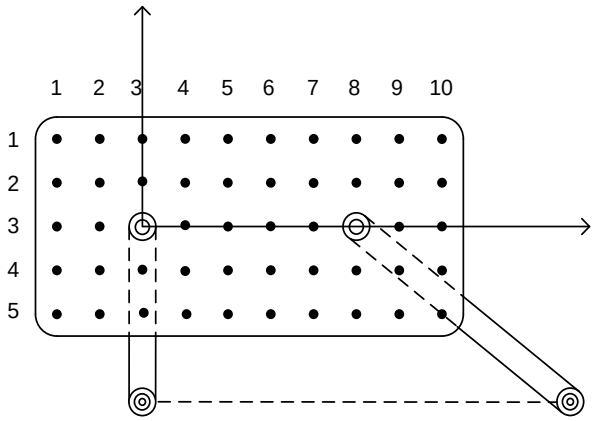

Figure 2.4. Behaviour of the points [50].

According to the geometry of the scouring bowl, the crank and the rocker have been chosen. The crank should be fixed on the upper sides of bowl and lever should be fixed side of the bowl. According to [51], when A=4.0, B=3.0 and C=4,5 (Figure 2.5) nearly between 5x6 and 5x7 points (Figure 2.4) will be drawn approximately straight line path.

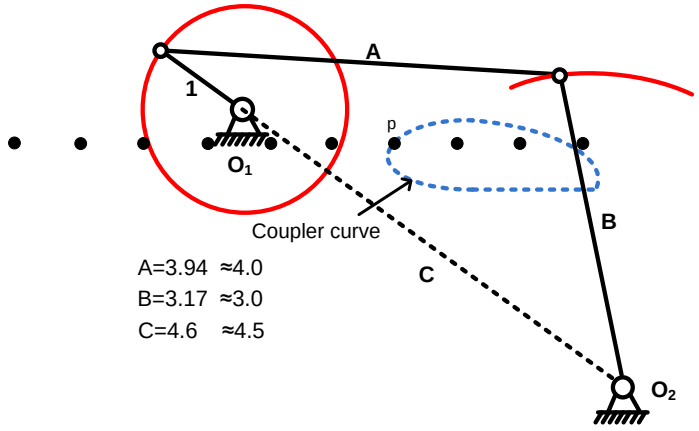

Figure 2.5. Trajectory of point ***p*** of the coupler A. When A=4.0; B=3.0 and C=4.5 (Adapted from [50], page 620).

Figure 2.5 represents a best solution for the desired trajectory of the harrow motion. In future works the point P has been connected to the two ends of the coupler A. The proposed four bar linkage is shown In Figure 2.6. The desired point has been found, when 1=250; A=985/250=3.9; B=793/250=3.2 and C=1150/250=4.6

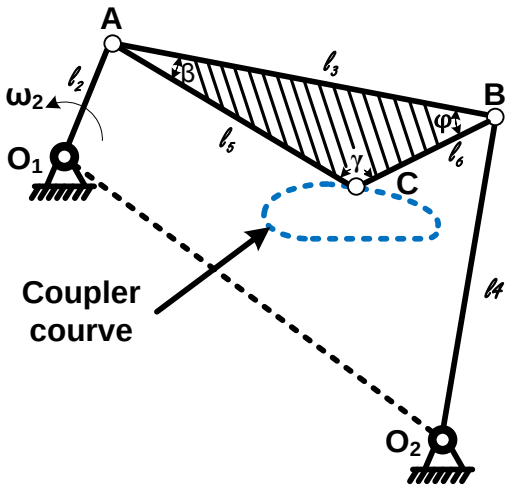

Figure 2.6. The proposed four bar linkage.

Referring to Figure 2.6, the point C can be imagined as connected to the longitudinal girth of the harrow by revolute joint. The longitudinal girth requires connection by revolute joints at least at two points in order to obtain full rotation. O_2BC dyad has been parallel replaced through connecting rods BE and CD. The whole proposed mechanism is shown in Figure 2.7.

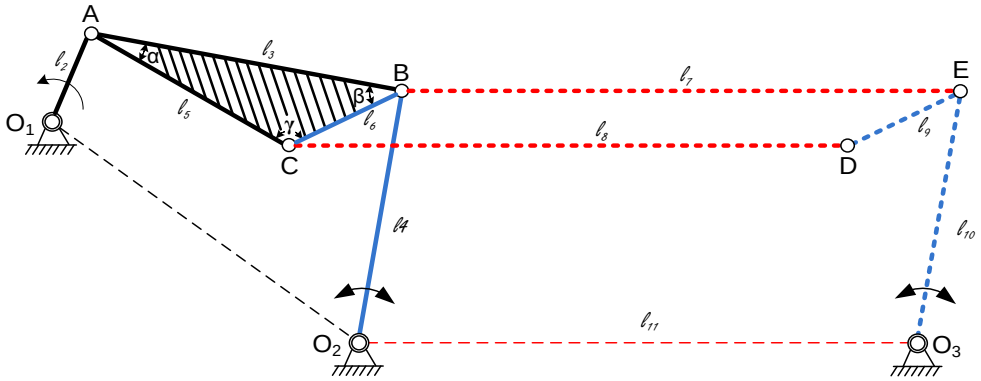

Figure 2.7. Proposed wool transport mechanism

The proposed mechanism consists of 8 links, and 10 lower kinematic pairs (Figure 2.7). Shafts ***O_1***, ***O_2***, and ***O_3*** are mounted on the frame of the proposed machine, ***O_1A*** is a crank, rotates 360^0 counterclockwise direction. ***ABC*** is a coupler**,** ternary link**,** ***BE***, ***CD*** and ***DE*** are connecting rods, ***O_2B*** and ***O_3E*** are levers, legs of the harrow that rotate with an oscillation motion.

Mobility of the proposed mechanism.
Number of links, n= 8;
Number of low pairs, j= 10;
Number of higher pairs, h= 0;

Mobility of the mechanism can be computed by Grubler's equation [47]:

$$DOF = 3(n-1) - 2j - 1h = 3(8-1) - 2 \cdot 10 - 1 \cdot 0 = 21 - 20 - 0 = 1;$$

In Figure 2.8, ***1*** represents the bowl or tank, forming the body or frame of the proposed machine that contains the scouring liquor ***2.*** Wool is fed into it by feeding conveyor ***3***, driven by belts 4, or gearing in any ordinary ways.

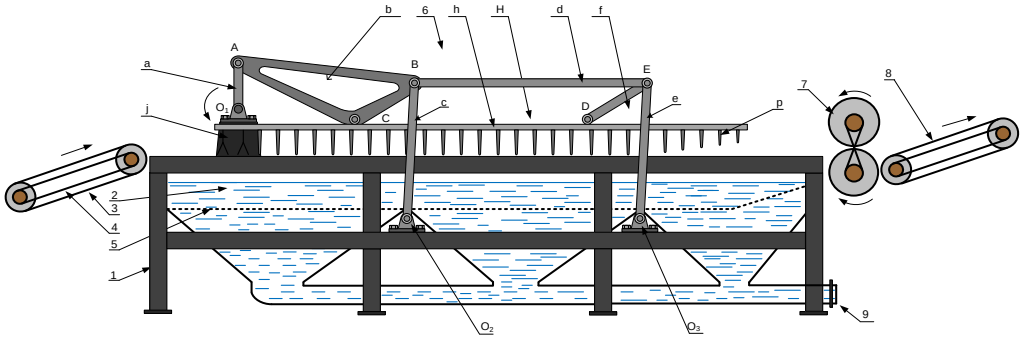

Figure 2.8. Proposed wool transport mechanism in the scouring machine

1- Bowl or tank, 2- Scouring liquor, 3- Feeding conveyor, 4- Belt, 5- Perforated false bottom, 6- Harrow mechanism: a- crank, b- coupler, c and e-levers, d -connecting rod, H-harrow platform: h- longitudinal girth, p-prongs, 7-Squeeze rollers, 8- Feeding conveyor, 9- Sediment outlet

The raw wool or greasy wool drops from the feeding conveyor ***3*** into the bowl ***1***, the prongs ***p,*** which are all mounted on longitudinal girths ***h,*** of the harrow***, H,*** catch and immerse into the scouring liquor and carrying it forward toward to the squeeze rollers **7.** Upon the side walls of the bowl ***1***, are secured standard or columns ***j***, provided at their upper end with bearing for cross shaft O_1 driven by belt drive from electromotor. On the shaft O_1 secured a crank ***a.*** The end of the crank is pivoted at one end of the coupler ***b*****;** one end of the coupler ***b*** is pivoted at a cross bar **C,** secured to the longitudinal girth ***h*** of the harrow ***H.*** One end of the coupler ***b*** is pivoted at a cross bar ***B.*** Besides of the bowl ***1,*** secured O_2**,** and O_3 shafts. O_2 and O_3 said cross shafts are secured two levers ***c*** and ***e.*** Lever ***c*** is pivoted at the upper end to the cross bar ***B.*** Lever ***e*** is pivoted at the upper end to the cross bar ***E*** respectively. Cross bars ***B*** and ***E*** connected together by a rod ***d.***

Cross bars ***D*** and ***E*** connected together by a rod ***f.*** Cross bar ***D*** secured to the longitudinal girth ***h*** of the harrow ***H*.**

In the position of harrow operating mechanism the coupler ***b***, under the action crank ***a***, is slowly moving the harrow ***H,*** toward the delivery end until said crank is about to travel from its upper to its lower half circle, whereby the harrow ***H*** is downward into the scouring liquor ***2***. The crank ***a*** revolves, levers ***c*** and ***e*** oscillate by the connecting rods.

The prongs of harrow pass the wool and carries forward to the squeeze rollers ***7***, which squeeze out the liquor from the wool. The dirty liquor returns to the bowl. The squeeze rollers deliver the wool to the next feeding conveyor ***8***. And scouring process continues in the next bowls.

Near the bottom of the bowl ***1***, there is a perforated false bottom ***5***, through which the liquor may pass, but not the wool, and below this bottom there should be a sediment outlet ***9***, for the sediment or emptying the bowl of the scouring liquor.

2.1.1. Dimensional synthesis of the proposed mechanism

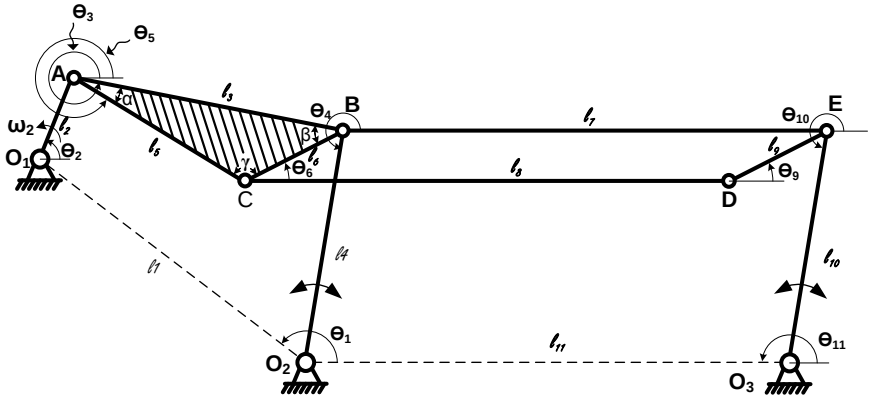

Figure 2.9. Geometry of the proposed wool transport mechanism

In Figure 2.9, l_1=1150 mm; distance between shafts O_1 and O_2; l_2=250 mm; length of the crank O_1A; l_3=985 mm; length of *AB* side of the coupler ABC or ternary link, l_5=671 mm; length of AC side of the coupler ABC, l_6=440 mm; length of *BC* side of the coupler ABC, l_4=793 mm; length of O_2B lever, l_7=2000 mm; length of BE connecting rod, l_8=2000 mm; length of CD connecting rod, l_9=440 mm; length of ED connecting rod, l_{10}=793 mm; length of O_3E lever, l_{11}=2000 distance between shafts O_2 and O_3.

Referring to the topology of the proposed mechanism (Figure 2.9), it can be seen, the proposed mechanism is constructed based on the four bar linkage.

2.2. Kinematic analysis of the proposed mechanism

2.2.1. Position analysis

The four bar of the whole proposed mechanism is shown in Figure 2.10. The crank O_1A is fixed on pivot O_1 which is located at the starting point of the coordinate system. The crank rotates counterclockwise with θ_2 angle about fixed pivot O_1. The point A of the coupler ABC rotates follows to the crank rotation. The rocker or lever O_2B move in oscillation motion with respect to the coupler motion. The output link of the mechanism is the harrow and it connects with its one end to the point C. The desired motion of the mechanism has been obtained by point C.

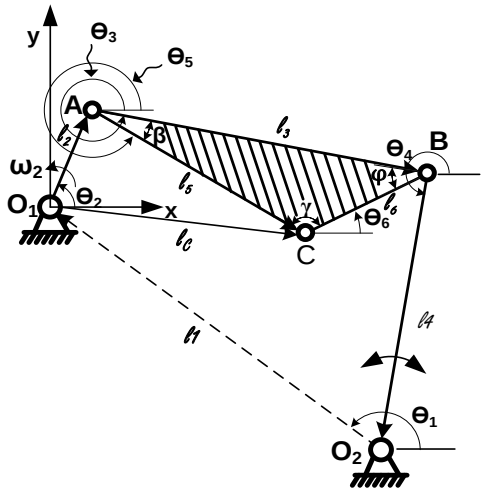

Figure 2.10. Vector representation of the four bar linkage

The position analysis of the four bar linkage starts from defining the coordinates of centers of the revolute joints in a coordinate system.

A reference system S1 (*x, y, O1*) with ***x*** axis or horizontal and the origin of the system at point O1, center of the revolute joint connecting links 1 and 2 are chosen. Coordinates of the pivots O_1 and O_2 are located the starting point of the coordinate system and can be written as follows:

$$O_1 = [x_{O_1}\ y_{O_1}] = [0\ 0]; \quad (2.1)$$

$$O_2 = [x_{O_2}\ y_{O_2}] = O_1 - l1[cos\theta_1\ sin\theta_1]; \quad (2.2)$$

The point A rotates about the origin of the coordinate system S1, its coordinates can be written as:

$$A = [x_A\, y_A] = O_1 + l_2[\, cos\theta_2\ sin\theta_2]; \tag{2.3}$$

Coordinates of point B:

Referring to Figure 2.10, if the coordinates of the points A and O_2 are known, the coordinates of the point B can be found by using the equation for circle as follows:

$$\left.\begin{matrix}\left(x_B - x_{O_2}\right)^2 + \left(y_B - y_{O_2}\right)^2 = l_4^2 \\ (x_B - x_A)^2 + (y_B - y_A)^2 = l_3^2\end{matrix}\right\} B(x_B\, y_B); \tag{2.4}$$

Equation (2.4) should be developed, simplified and one subtracted to the other as follows:

$$\left.\begin{matrix}x_B^2 - 2x_B x_{O_2} + x_{O_2}^2 + y_B^2 - 2y_B y_{O_2} + y_{O_2}^2 - l_4^2 = 0 \\ x_B^2 - 2x_B x_A + x_A^2 + y_B^2 - 2y_B y_A + y_A^2 - l_3^2 = 0\end{matrix}\right\} \tag{2.5}$$

$$-2x\left(x_{O_2} - x_A\right) + x_{O_2}^2 - x_A^2 - 2y\left(y_{O_2} - y_A\right) + y_{O_2}^2 - l_4^2 - y_A^2 + l_3^2 = 0; \tag{2.6}$$

Here is $x_B = x;\ y_B = y;$

$$x + y\frac{y_{O_2} - y_A}{x_{O_2} - x_A} = \frac{x_{O_2}^2 - x_A^2 + y_{O_2}^2 - y_A^2 + l_3^2 - l_4^2}{2\left(x_{O_2} - x_A\right)} = \frac{N(O_2)^2 - N(A)^2 + l_3^2 - l_4^2}{2\left(x_{O_2} - x_A\right)}; \tag{2.7}$$

Equation (2.7) can be simplified as:

$$\frac{y_{O_2} - y_A}{x_{O_2} - x_A} = A \tag{2.8}$$

$$\frac{N(O_2)^2 - N(A)^2 + l_3^2 - l_4^2}{2\left(x_{O_2} - x_A\right)} = B \tag{2.9}$$

The following simple equation can be obtained for $\boldsymbol{x}$:

$$x = -Ay + B; \tag{2.10}$$

Equation (2.10) can be inserted into the first line of Equation system (2.5) and can be written as follows:

$$A^2y^2 + B^2 - 2ABy + 2x_{O_2}Ay - 2x_{O_2}B + x_{O_2}^2 + y^2 - 2yy_{O_2} + y_{O_2}^2 - l_4^2 = 0; \tag{2.11}$$

$$(A^2 + 1)y^2 + \left(2x_{O_2}A - 2AB - 2y_{O_2}\right)y + \left(B^2 - 2x_{O_2}B + N(O_2)^2 - l_4^2\right) = 0; \tag{2.12}$$

$$a = (A^2 + 1); \tag{2.13}$$

$$b = \left(2x_{O_2}A - 2AB - 2y_{O_2}\right); \tag{2.14}$$

$$c = B^2 - 2x_{O_2}B + N(O_2)^2 - l_4^2; \tag{2.15}$$

$$ay^2 + 2by + c = 0; \tag{2.16}$$

$$y = \frac{-b \pm \sqrt{b^2 - ac}}{a}; \tag{2.17}$$

Coordinates of point C can be found as:

$$\overline{O_1C} = \overline{O_1A} + \overline{AC};$$

$$C = l_2(cos\theta_2 sin\theta_2) + l_5(\cos(\theta_3 - \beta)\ \sin(\theta_3 - \beta));$$

$$\left.\begin{aligned} X_C &= l_2 cos\theta_2 + l_5 cos(\theta_3 - \beta) \\ Y_C &= l_2 sin\theta_2 + l_5 sin(\theta_3 - \beta) \end{aligned}\right\} \tag{2.18}$$

Here is, $\beta = cos^{-1}\left[\frac{l_5^2 + l_3^2 - l_6^2}{2l_5 l_3}\right]$; (2.19)

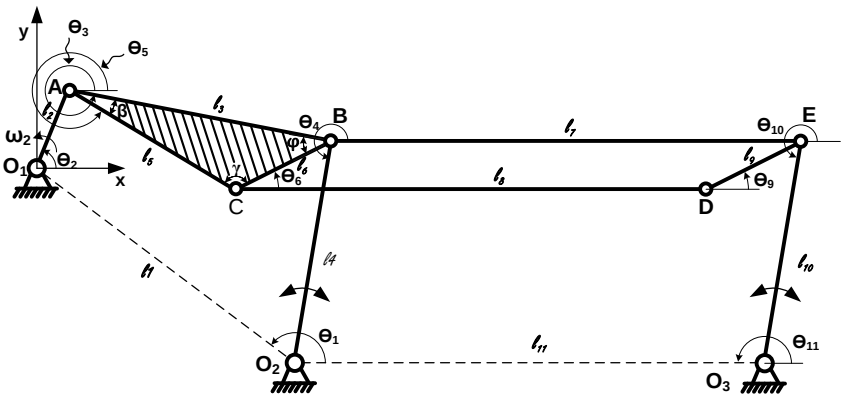

Figure 2.11. The position analysis of the proposed mechanism

Coordinates of pivot O_3 can be found as follow:

$$O_3 = \left[x_{O_3}\ y_{O_3}\right] = O_2 + l_{11}[cos\theta_{11}\ \sin\theta_{11}]; \tag{2.20}$$

Coordinates of point E:

$$E = B + l_7[\cos\theta_7\ \ sin\theta_7]; \tag{2.21}$$

Coordinates of point D:

$$D = C + l_8[\cos\theta_8\ \ sin\theta_8]; \tag{2.22}$$

Loop closure equations for four bar linkage can be written as follow:

$$\boldsymbol{l_2} + \boldsymbol{l_3} + \boldsymbol{l_4} + \boldsymbol{l_1} = 0; \tag{2.23}$$

Rewriting Equation (2.23) in its $\boldsymbol{x}$ and $\boldsymbol{y}$ axis component equations:

$$l_2 cos\theta_2 + l_3 cos\theta_3 + l_4 cos\theta_4 + l_1 cos\theta_1 = 0; \tag{2.24}$$

$$l_2 sin\theta_2 + l_3 sin\theta_3 + l_4 sin\theta_4 + l_1 sin\theta_1 = 0; \tag{2.25}$$

We know that θ_2 is known, and θ_1 is also known, constant. In order to eliminate θ_3, we first isolate it on one side of the Equations (2.24) and (2.25):

$$l_3 cos\theta_3 = -l_1 cos\theta_1 - l_4 cos\theta_4 - l_2 cos\theta_2; \tag{2.26}$$

$$l_3 sin\theta_3 = -l_1 sin\theta_1 - l_4 sin\theta_4 - l_2 sin\theta_2; \tag{2.27}$$

Both sides of the equations (2.26) and (2.27) should be squared, added and the result simplified using the trigonometric identity $sin^2\theta + cos^2\theta = 1$;

This gives:

$$l_3^2 = l_1^2 + l_2^2 + l_4^2 + 2l_1 l_4 (cos\theta_1 cos\theta_4 + sin\theta_1 sin\theta_4) -$$

$$-2l_1 l_2 (cos\theta_1 cos\theta_2 + sin\theta_1 sin\theta_2) - 2l_2 l_4 (cos\theta_2 cos\theta_4 + sin\theta_2 sin\theta_4); \tag{3.28}$$

Equation (2.28) gives θ_4 in terms of the given angle θ_2 (and constant angleθ_1), but not explicitly. To obtain explicit expression, Equation (2.28) should be simplified by combining the coefficients of $cos\theta_4$ and $sin\theta_4$ as follows:

$$Acos\theta_4 + Bsin\theta_4 + C = 0; \tag{2.29}$$

Where,

$$\left.\begin{aligned} A &= 2l_1 l_4 \cos\theta_1 - 2l_2 l_4 \cos\theta_2; \\ B &= 2l_1 l_4 \sin\theta_1 - 2l_2 l_4 \sin\theta_2; \\ C &= l_1^2 + l_2^2 + l_4^2 - l_3^2 - 2l_1 l_2 (\cos\theta_1 \cos\theta_2 + \sin\theta_1 \sin\theta_2) \end{aligned}\right\}; \tag{2.30}$$

To solve Equation (2.29), standard trigonometric identities can be used for half angles given in the following:

$$sin\theta_4 = \frac{2\tan(\theta_4/2)}{1+tan^2(\theta_4/2)}; \tag{2.31}$$

$$cos\theta_4 = \frac{1-tan^2(\theta_4/2)}{1+tan^2(\theta_4/2)}; \tag{2.32}$$

After substitution and simplification, the following equation can be obtained:

$$(C - A)t^2 + 2Bt + (A + C) = 0; \quad (2.33)$$

Where, $t = \tan\left(\frac{\theta_4}{2}\right)$;

Solving for *t* gives:

$$t = \frac{-2B+\sigma\sqrt{4B^2-4(C-A)(C+A)}}{2(C-A)} = \frac{-B+\sqrt{B^2-C^2+A^2}}{C-A}; \quad (2.34)$$

And $\theta_4 = 2\tan^{-1} t$; (2.35)

Equations (2.26) and (2.27) can now be solved for θ_3. Dividing Equation (2.27) by (2.26) and solving for θ_3 gives:

$$\theta_3 = \tan^{-1}\left[\frac{-l_4 sin\theta_4 - l_2 sin\theta_2 - l_1 sin\theta_1}{-l_4 cos\theta_4 - l_2 cos\theta_2 - l_1 cos\theta_1}\right]; \quad (2.36)$$

In equation (2.34) it is essential that the sign of the numerator and the denominator be maintained to determine the quadrant in which the angle θ_3 lies. This can be done directly by using ATAN2 function. The form of this function is:

$$ATAN2(\sin\theta_3, \cos\theta_3) = \tan^{-1}\left[\frac{sin\theta_3}{cos\theta_3}\right]; \quad (2.37)$$

Equations (2.35) - (2.37) give a complete and consistent solution to the position problem of the four bar linkage. For any values of $\boldsymbol{\theta_2}$, there are typically two values of $\boldsymbol{\theta_3}$ and $\boldsymbol{\theta_4}$, given the substituting $\sigma = +1$ and -1, respectively.

2.2.2. Velocity analysis

The velocity equations can be developed by differentiating Equation (2.23) as:

$$\dot{\boldsymbol{l}}_{\boldsymbol{2}} + \dot{\boldsymbol{l}}_{\boldsymbol{3}} + \dot{\boldsymbol{l}}_{\boldsymbol{4}} + \dot{\boldsymbol{l}}_{\boldsymbol{1}} = 0; \quad (2.38)$$

Rewriting Equations (2.38) in its $\boldsymbol{x}$ and $\boldsymbol{y}$ axis component is the same as that differentiating Equations (2.23) and (2.24). The resulting equations are:

$$-l_2 sin\theta_2\omega_2 - l_3 sin\theta_3\omega_3 - l_4 sin\theta_4\omega_4 - l_1 sin\theta_1\omega_1 = 0; \quad (2.39)$$

$$l_2 cos\theta_2\omega_2 + l_3 cos\theta_3\omega_3 + l_4 cos\theta_4\omega_4 + l_1 cos\theta_1\omega_1 = 0; \quad (2.40)$$

Since, θ_1 is constant, the angular velocity of link 2 ω_2 is known, the only new unknowns are ω_3 and ω_4 which are the angular velocities of link 3 and link 4 respectively. In matrix form, Equations (2.39) and (2.40) can be rearranged and rewritten as:

$$\begin{bmatrix} -l_3 sin\theta_3 & l_4 sin\theta_4 \\ l_3 cos\theta_3 & -l_4 cos\theta_4 \end{bmatrix} \begin{Bmatrix} \omega_3 \\ \omega_4 \end{Bmatrix} = \begin{Bmatrix} l_2 sin\theta_2 \omega_2 \\ -l_2 cos\theta_2 \omega_2 \end{Bmatrix}; \quad (2.41)$$

Solving these two equations in two unknowns yield:

$$\omega_4 = -\frac{l_2 sin\theta_2 \omega_2 - \frac{l_3 cos\theta_3 \cdot l_2 sin\theta_2 \omega_2}{l_3 sin\theta_3}}{l_4 sin\theta_4 - \frac{l_3 cos\theta_3 \cdot l_4 sin\theta_4}{l_3 sin\theta_3}}; \quad (2.42);$$

$$\omega_3 = -\frac{l_2 sin\theta_2 \omega_2 + l_4 sin\theta_4 \cdot \frac{l_2 sin\theta_2 \omega_2 - \frac{l_3 cos\theta_3 \cdot l_2 sin\theta_2 \omega_2}{l_3 sin\theta_3}}{l_4 sin\theta_4 - \frac{l_3 cos\theta_3 \cdot l_4 sin\theta_4}{l_3 sin\theta_3}}}{l_3 sin\theta_3}; \quad (2.43)$$

Velocity equations of coupler point C can be found by differentiating Equation (2.18) as:

$$\dot{C} = l_2 \omega_2 (-sin\theta_2 \ cos\theta_2) + l_5 \omega_3 (-sin(\theta_3 - \beta) \ cos(\theta_3 - \beta));$$

$$\left.\begin{matrix} \dot{X_C} = -l_2 sin\theta_2 \omega_2 - l_5 sin(\theta_3 - \beta)\omega_3 \\ \dot{Y_C} = l_2 cos\theta_2 \omega_2 + l_5 cos(\theta_3 - \beta)\omega_3 \end{matrix}\right\}; \quad (2.44)$$

3.2.3. Acceleration analysis

Since θ_1 is constant, the acceleration equations can be developed by differentiating Equation (2.38) as:

$$\ddot{\boldsymbol{l}}_{\boldsymbol{2}} + \ddot{\boldsymbol{l}}_{\boldsymbol{3}} - \ddot{\boldsymbol{l}}_{\boldsymbol{4}} = 0; \quad (2.45)$$

Rewriting Equation (2.45) in its $\boldsymbol{x}$ and $\boldsymbol{y}$ axis component equations is the same as that differentiating Equations (2.39) and (2.40). The resulting component equations are:

$$-l_2 sin\theta_2 \alpha_2 - l_2 cos\theta_2 \omega_2^2 - l_3 sin\theta_3 \alpha_3 - l_3 cos\theta_3 \omega_3^2 + l_4 sin\theta_4 \alpha_4 + l_4 cos\theta_4 \omega_4^2 = 0; \quad (2.46)$$

$$l_2 cos\theta_2 \alpha_2 - l_2 sin\theta_2 \omega_2^2 + l_3 cos\theta_3 \alpha_3 - l_3 sin\theta_3 \omega_3^2 - l_4 cos\theta_4 \alpha_4 + l_4 sin\theta_4 \omega_4^2 = 0; \quad (2.47)$$

These equations can also be represented in matrix form, where the terms associated with the known crank acceleration and the quadratic velocity terms are moved to the right-hand side as:

$$\begin{bmatrix} -l_3 sin\theta_3 & l_4 sin\theta_4 \\ l_3 cos\theta_3 & -l_4 cos\theta_4 \end{bmatrix} \begin{Bmatrix} \alpha_3 \\ \alpha_4 \end{Bmatrix} = \begin{Bmatrix} l_2(sin\theta_2\alpha_2 + cos\theta_2\omega_2^2) + l_3 cos\theta_3\omega_3^2 - l_4 cos\theta_4\omega_4^2 \\ -l_2(cos\theta_2\alpha_2 - sin\theta_2\omega_2^2) + l_3 sin\theta_3\omega_3^2 - l_4 sin\theta_4\omega_4^2 \end{Bmatrix}; \quad (2.48)$$

Solving first raw of these equations yield two unknowns as:

$$\alpha_4 = \frac{(l_2(sin\theta_2\alpha_2+cos\theta_2\omega_2^2)+l_3 cos\theta_3\omega_3^2-l_4 cos\theta_4\omega_4^2)-\frac{l_3 cos\theta_3 \cdot l_2(cos\theta_2\alpha_2-sin\theta_2\omega_2^2)+l_3 sin\theta_3\omega_3^2-l_4 sin\theta_4\omega_4^2}{l_3 sin\theta_3}}{l_4 sin\theta_4-\frac{l_3 cos\theta_3 \cdot l_4 sin\theta_4}{l_3 sin\theta_3}}; \quad (2.49)$$

$$\alpha_3 = \frac{l_2(sin\theta_2\alpha_2+cos\theta_2\omega_2^2)+l_3 cos\theta_3\omega_3^2-l_4 cos\theta_4\omega_4^2-l_4 sin\theta_4 \frac{(l_2(sin\theta_2\alpha_2+cos\theta_2\omega_2^2)+l_3 cos\theta_3\omega_3^2-l_4 cos\theta_4\omega_4^2)-\frac{l_3 cos\theta_3 \cdot l_2(cos\theta_2\alpha_2-sin\theta_2\omega_2^2)+l_3 sin\theta_3\omega_3^2-l_4 sin\theta_4\omega_4^2}{l_3 sin\theta_3}}{l_4 sin\theta_4-\frac{l_3 cos\theta_3 \cdot l_4 sin\theta_4}{l_3 sin\theta_3}}}{l_3 sin\theta_3}; \quad (2.50)$$

Acceleration equations of coupler point C can be found by differentiating Equation (2.44) as:

$$\left.\begin{aligned} \ddot{X}_C &= -l_2(\sin\theta_2\alpha_2 + \cos\theta_2\omega_2^2) - l_5(\sin\theta_5\,\alpha_3 + \cos\theta_5\omega_3^2) \\ \ddot{Y}_C &= l_2(\cos\theta_2\alpha_2 - \sin\theta_2\omega_2^2) + l_5(\cos\theta_5\,\alpha_3 - \sin\theta_5\omega_3^2) \end{aligned}\right\}; \quad (2.51)$$

Results of the kinematic analysis are shown in Figures 2.12-.

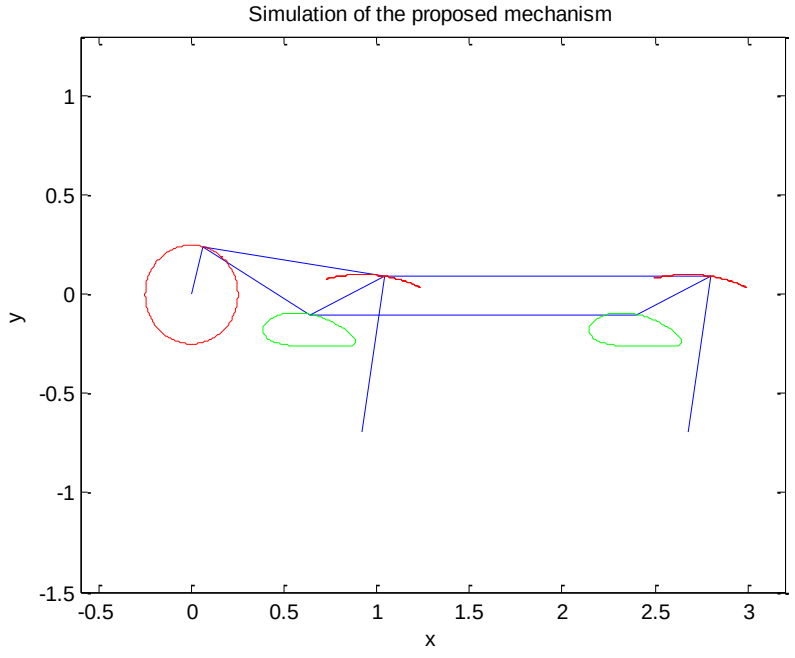

Figure 2.12. Simulation of the proposed mechanism

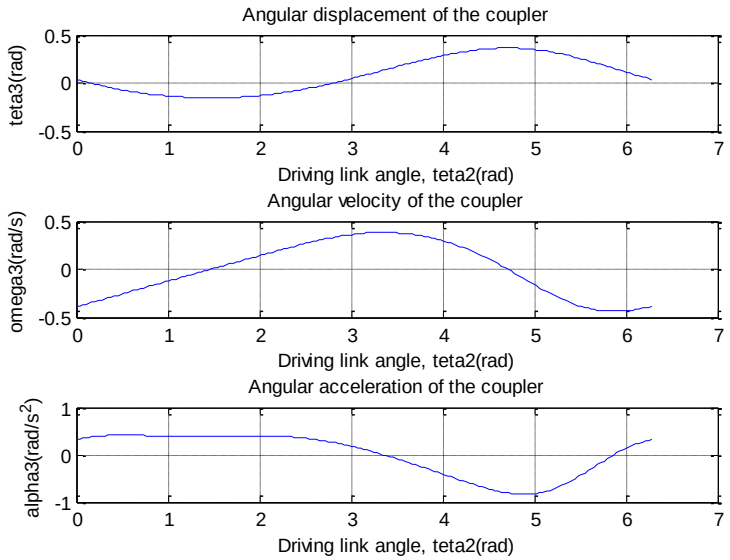

Figure 2.13. Angular displacement, velocity and acceleration of the coupler

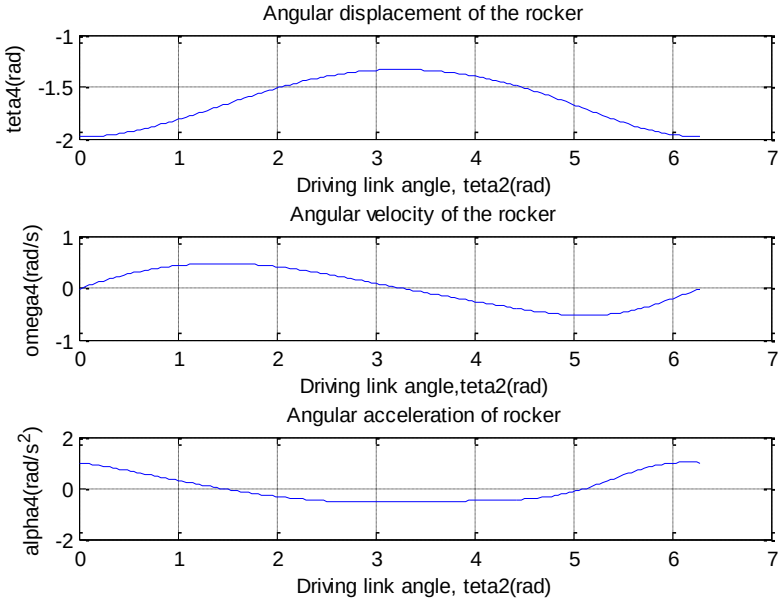

Figure 2.14. Angular displacement, velocity and acceleration of the rocker (link4).

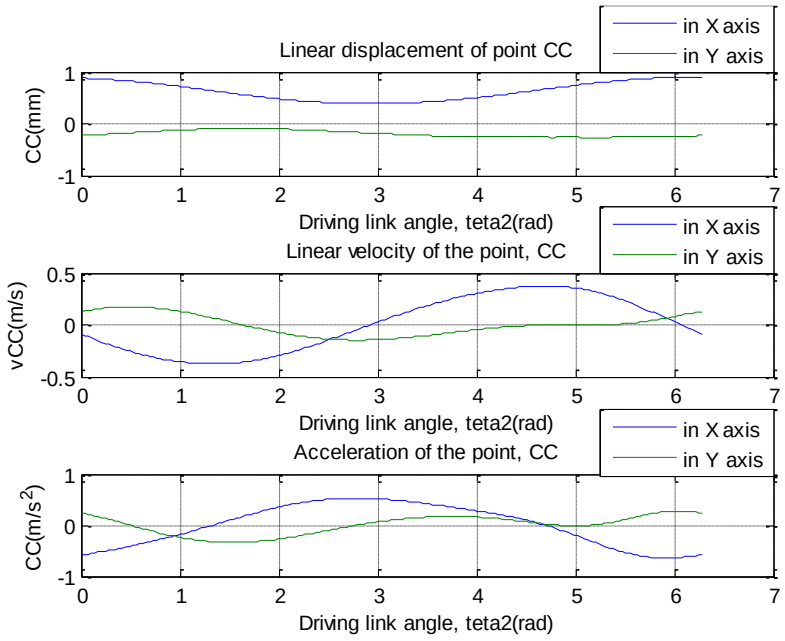

Figure 2.15. Linier displacement, velocity and acceleration of the point C.

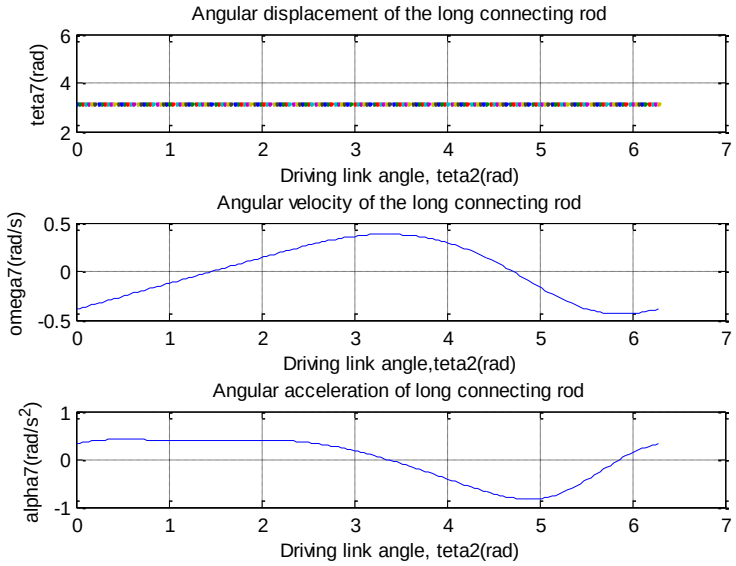

Figure 2.16. Angular displacement, velocity and acceleration of the long connecting rod (link5).

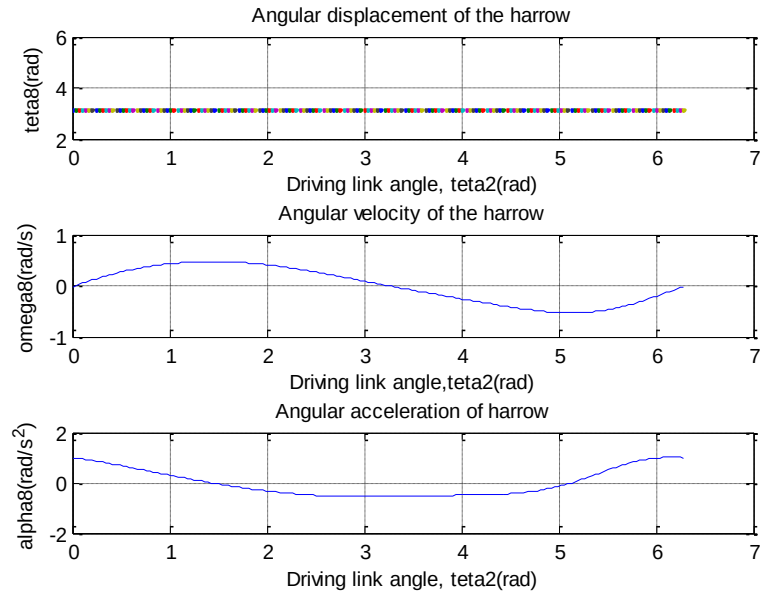

Figure 2.17. Angular displacement, velocity and acceleration of the harrow (link 6)

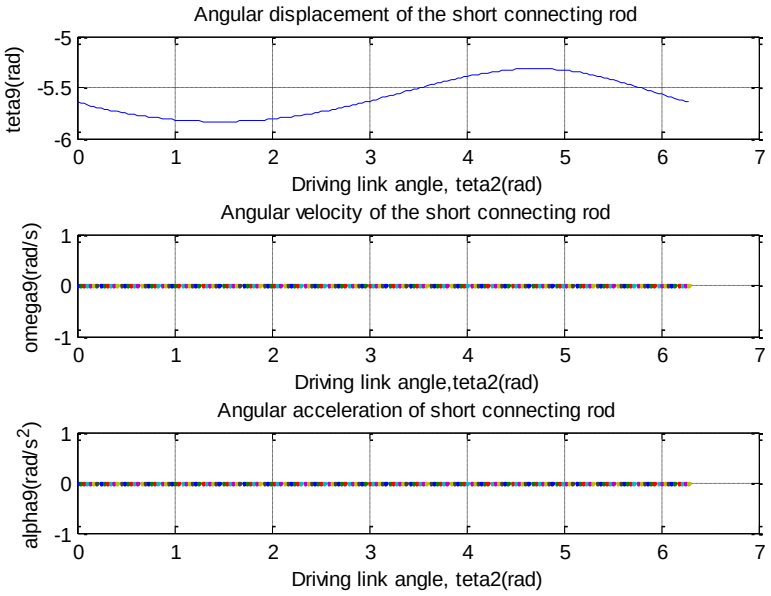

Figure 2.18.Angular displacement, velocity and acceleration of the short connecting rod (link7).

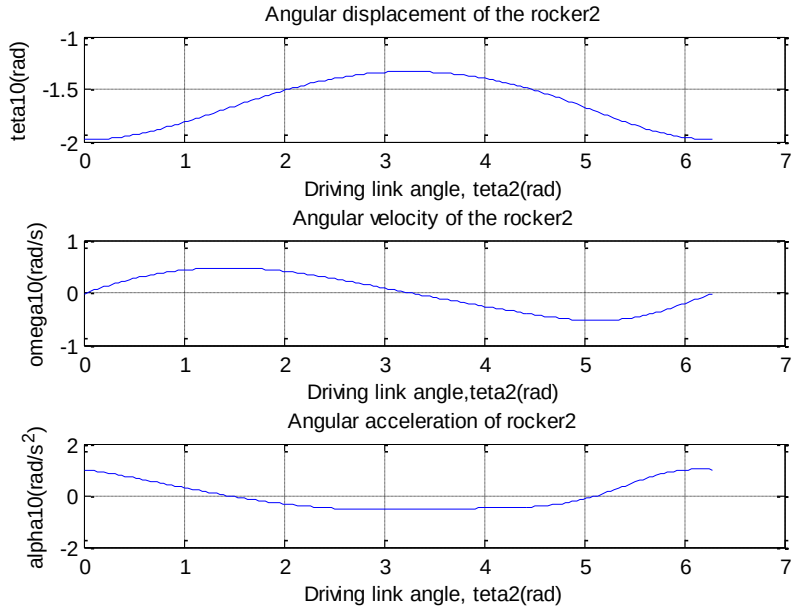

Figure 2.19. Angular displacement, velocity and acceleration of the rocker 2 (link 8).

2.3. Kinetostatic analysis of the proposed mechanism

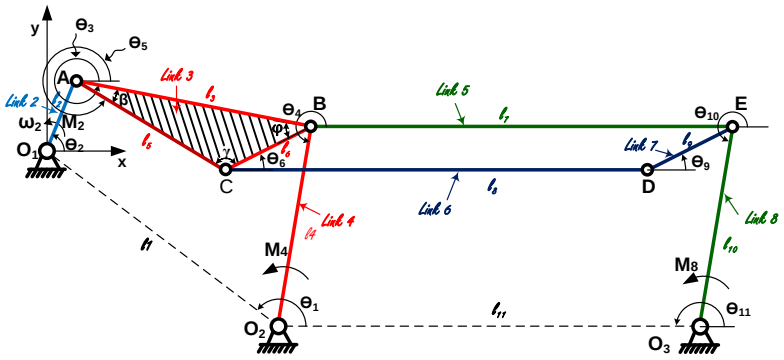

Figure 2.20. Dyad representation of proposed mechanism

Referring to Figure 2.20, the proposed wool transport mechanism is a one degree-of-freedom mechanism, and it contains 7 moving links. In order to determine the magnitudes and the directions of the reaction forces and the applied forces/torques, the free body diagrams and the static equilibrium equations should be written for each moving links.

2.3.1 Free body diagrams and static equilibrium equations

The analyses starts from link 2 (crank). In the following forces F_{12x} and F_{12y} represent the *x* and *y* component respectively of the reaction forces of link 1 on link 2. The forces F_{32x} and F_{32y} represent the *x* and *y* component respectively of the reaction forces of link 3 on link 2. m_2 is the mass of link 2. a_{G2x} and a_{G2y} represent the x and y component respectively linear acceleration of link 2. I_{G_2} is the inertia moment with respect to the center of mass of link 2. α_2 is the angular acceleration of link 2. M_2 is the driving torque of link 2. The vectors r_{12} and r_{32} define the position of the center of mass G2. Their *x* and *y* components are r_{12x}, r_{12y}, r_{32x} and r_{32y} respectively. l_2 is the length of link 2.

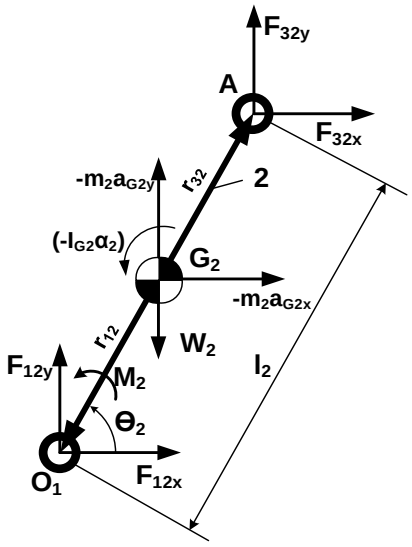

Figure 2.21. Free body diagram of link2 (crank)

Vectors can be defined as follows:

$r_{12} = G_2O_1 = \frac{l_2}{2}$; $\quad r_{12x} = -\frac{l_2}{2}cos\theta_2$; $\quad r_{12y} = -\frac{l_2}{2}sin\theta_2$;

$r_{32} = G_2A = \frac{l_2}{2}$; $\quad r_{32x} = \frac{l_2}{2}cos\theta_2$; $\quad r_{32y} = \frac{l_2}{2}sin\theta_2$;

$W_2 = m_2g$;

Static equilibrium equations for link 2 (Moments about centre of mass G_2):

$\sum F_x = F_{12x} + F_{32x} + (-m_2a_{G2x}) = 0$;

$$\sum F_y = F_{12y} + F_{32y} + (-m_2 a_{G2y}) - m_2 g = 0;$$

$$\sum M = M_2 + \left(r_{12x}F_{12y} - r_{12y}F_{12x}\right) + \left(r_{32x}F_{32y} - r_{32y}F_{32x}\right) + \left(-I_{G_2}\alpha_2\right) = 0;$$

The link 2 is connected to the one part of the ternary link. The next analysis can be performed for link 3 or ternary link. In the following forces F_{23x} and F_{23y} represent the *x* and *y* component respectively of the reaction forces of link 2 on link 3. On the joint B, three links 3, 4 and 5 are connected, the forces F_{3Bx} and F_{3By} represent the *x* and *y* component respectively of the reaction forces of link 3 on joint *B*. m_3 is the mass of link 3. a_{G3x} and a_{G3y} represent the *x* and *y* component respectively linear acceleration of link 3. I_{G_3} is the inertia moment with respect to the center of mass of link 3. α_3 is the angular acceleration of link 3. The vectors r_a , r_b and r_c define the position of the center of mass G3. Their *x* and *y* components are r_{ax}, r_{ay}, r_{bx} r_{by} , r_{cx} and r_{cy}respectively. l3, l5 and l6 are the lengths between joints A, B and C as shown in Figure 2.22.

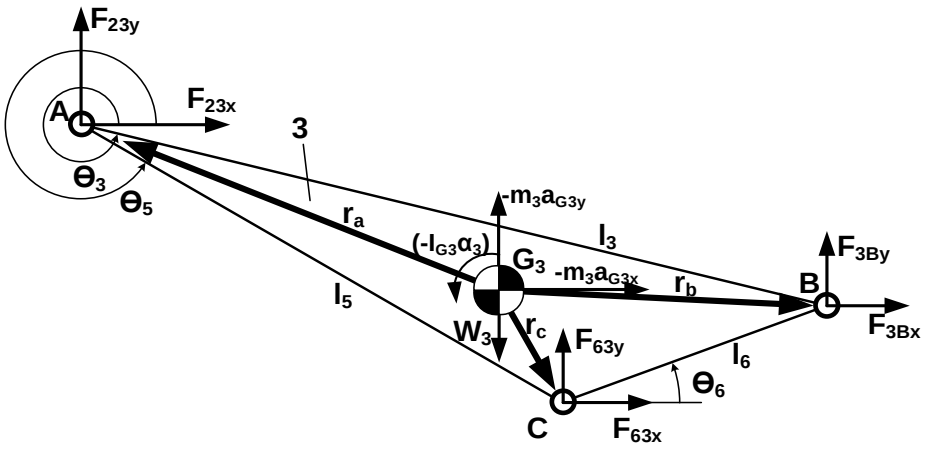

Figure 2.22. Free body diagram of link3 (ternary link)

Referring to free the body diagram of link 3, the center of mass G_3 can be found from following equation: $G_{3xy} = \frac{A_{xy}+B_{xy}+C_{xy}}{3}$; and the vectors can be defined as follows:

$$r_a = G_3A = A - G_3; \qquad r_{a_x} = A_x - G_{3x}; \qquad r_{a_y} = A_y - G_{3y};$$

$$r_b = G_3B = B - G_3; \qquad r_{b_x} = B_x - G_{3x}; \qquad r_{b_y} = B_y - G_{3y};$$

$$r_c = G_3C = C - G_3; \qquad r_{c_x} = C_x - G_{3x}; \qquad r_{c_y} = C_y - G_{3y};$$

The weight of the link 3, equals mass times gravitational acceleration of the link 3:

$$W_3 = m_3 g;$$

The static equilibrium equations for link 3 (Moments about centre of mass G_3):

$$\sum F_x = F_{23x} + F_{3Bx} + F_{63x} + (-m_3 a_{G3x}) = 0;$$

$$\sum F_y = F_{23y} + F_{3By} + F_{63y} + \left(-m_3 a_{G3y}\right) - m_3 g = 0;$$

$$\sum M = \left(r_{a_x} F_{23y} - r_{a_y} F_{23x}\right) + \left(r_{c_x} F_{63y} - r_{c_y} F_{63x}\right) + \left(r_{b_x} F_{3By} - r_{b_y} F_{3Bx}\right) + \left(-I_{G_3} \alpha_3\right) = 0;$$

The ternary link is connected with its one end to the link 4 and with other end to the link 5 respectively as shown in Figure 2.22. Force analysis can be continued for link 4, because the link 4 is a one part of the four bar linkage. In the following forces F_{14x} and F_{14y} represent the *x* and *y* component respectively of the reaction forces of link 1 on link 4. The forces F_{4Bx} and F_{4By} represent the *x* and *y* component respectively of the reaction forces of link 4 on joint B. m_4 is the mass of link 4. a_{G4x} and a_{G4y} represent the *x* and *y* component respectively linear acceleration of t link 4. I_{G_4} is the inertia moment with respect to the center of mass of link 4. α_4 is the angular acceleration of link 4. The vectors r_{14} and r_{34} define the position of the center of mass G4. Their *x* and *y* components are r_{14x}, r_{14y}, r_{34x} and r_{34y} respectively. l_4 is the length of link 4.

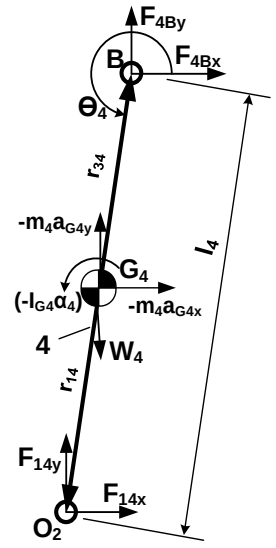

Figure 2.23. Free body diagram of link4 (lever1)

Vectors can be defined as follow:

$r_{14} = G_4O_2 = \frac{l_4}{2}$; $\quad r_{14x} = \frac{l_4}{2}cos\theta_4$; $\quad r_{14y} = \frac{l_4}{2}sin\theta_4$;

$r_{34} = G_4B = \frac{l_4}{2}$; $\quad r_{34x} = -\frac{l_4}{2}cos\theta_4$; $\quad r_{34y} = -\frac{l_4}{2}sin\theta_4$;

Weight of the link: $W_4 = m_4g$;

Referring to the free body diagram of the link 4, F_{4B} is a redundant force, and its components in Cartesian coordinate system are:

$F_{4Bx} = -F_{3Bx} - F_{5Bx}$; $\quad F_{4By} = -F_{3By} - F_{5By}$;

The static equilibrium equations for link 4 (Moments about centre of mass G_4):

$\sum F_x = F_{14x} + (-F_{3Bx} - F_{5Bx}) + (-m_4a_{G4x}) = 0$;

$\sum F_y = F_{14y} + (-F_{3By} - F_{5By}) + \left(-m_4a_{G4y}\right) - m_4g = 0$;

$\sum M = (r_{14x}F_{14y} - r_{14y}F_{14x}) + (r_{34_x}\left(-F_{3By} - F_{5By}\right) - r_{34_y}(-F_{3Bx} - F_{5Bx})) + \left(-I_{G_4}\alpha_4\right) = 0$;

Next analysis can be performed for the link 5. In the following forces F_{5Bx} and F_{5By} represent the *x* and *y* component respectively of the reaction forces of link 5 on joint B. On the joint E, three links 5, 7 and 8 are connected. The forces F_{5Ex} and F_{5Ey} represent the *x* and *y* component respectively of the reaction forces of link 5 on joint B. m_5 is the mass of link 5. a_{G5x} and a_{G5y} represent the x and y component respectively linear acceleration of link 5. I_{G_2} is the inertia moment with respect to the center of mass of link 5. α_5 is the angular acceleration of link 5. The vectors r_{35} and r_{85} define the position of the center of mass G5. Their *x* and *y* components are r_{35x}, r_{35y}, r_{85x} and r_{85y} respectively. l_7 is the length of link 5.

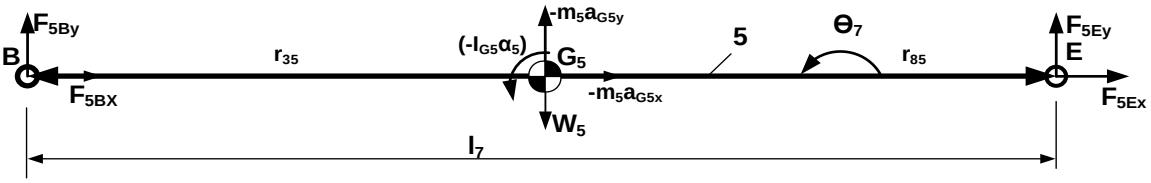

Figure 2.24. Free body diagram of the link 5 (long connecting rod)

Vectors can be defined as follow:

$r_{35} = G_5B = \frac{l_7}{2}$; $\quad r_{35x} = \frac{l_7}{2}cos\theta_7$; $\quad r_{35y} = \frac{l_7}{2}sin\theta_7 = 0$; $\quad \theta_7 = 180^0$;

$r_{85} = G_5E = \frac{l_7}{2}$; $r_{85x} = -\frac{l_7}{2}cos\theta_7$; $r_{85y} = -\frac{l_7}{2}sin\theta_7 = 0$;

Weight of the link: $W_5 = m_5 g$;

Referring to the free body diagram of the link 4, F_{5E} is a redundant force, and its components in Cartesian coordinate system are:

$F_{5Ex} = -F_{7Ex} - F_{8Ex}$; $F_{5Ey} = -F_{7Ey} - F_{7Ey}$;

The static equilibrium equations for link 5 (Moments about centre of mass G_5):

$\sum F_x = F_{5Bx} + (-F_{7Ex} - F_{8Ex}) + (-m_5 a_{G5x}) = 0$;

$\sum F_y = F_{5By} + (-F_{7Ey} - F_{8Ey}) + (-m_5 a_{G5y}) - m_5 g = 0$;

$\sum M = r_{35x}F_{5By} + r_{85x}(-F_{7Ey} - F_{8Ey}) + (-I_{G_5}\alpha_5) = 0$;

Next analysis can be done for the link6. In the following forces F_{36x} and F_{36y} represent the *x* and *y* component respectively of the reaction forces of link 3 on link 6. The forces F_{76x} and F_{76y} represent the *x* and *y* component respectively of the reaction forces of link 7 on link 6. m_6 is the mass of link 6. a_{G6x} and a_{G6y} represent the x and y component respectively linear acceleration of link 6. I_{G_6} is the inertia moment with respect to the center of mass of link 6. α_5 is the angular acceleration of link 6. The vectors r_{36} and r_{76} define the position of the center of mass G6. Their *x* and *y* components are r_{36x}, r_{36y}, r_{76x} and r_{76y} respectively. l_8 is the length of link 6.

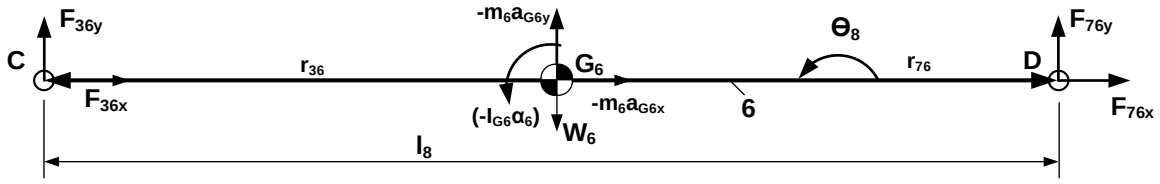

Figure 2.25. Free body diagram of the link6 (harrow)

Vectors can be defined as follows:

$r_{36} = G_6C = \frac{l_8}{2}$; $r_{36x} = \frac{l_8}{2}cos\theta_8$; $r_{36y} = \frac{l_8}{2}sin\theta_8 = 0$; $\theta_8 = 180^0$;

$r_{76} = G_6D = \frac{l_8}{2}$; $r_{76x} = -\frac{l_8}{2}cos\theta_8$; $r_{76y} = -\frac{l_8}{2}sin\theta_8 = 0$;

The weight of the link: $W_6 = m_6 g$;

The static equilibrium equations for link 6 (Moments about centre of mass G6):

$\sum F_x = F_{36x}+F_{76x} + (-m_6 a_{G6x}) = 0;$

$\sum F_y = F_{36y} + F_{76y} + (-m_6 a_{G6y}) - m_6 g = 0;$

$\sum M = r_{36x}F_{36y} + r_{76x}F_{76y} + \left(-I_{G_6}\alpha_6\right) = 0;$

Analysis of the link 7 or short connecting rod.

In the following forces F_{67x} and F_{67y} represent the *x* and *y* component respectively of the reaction forces of link 6 on link 7. The forces F_{7Ex} and F_{7Ey} represent the *x* and *y* component respectively of the reaction forces of link 7 on joint E. m_7 is the mass of link 7. a_{G7x} and a_{G7y} represent the x and y component respectively linear acceleration of link 7. I_{G_7} is the inertia moment with respect to the center of mass of link 7. α_7 is the angular acceleration of link 7 The vectors r_{67} and r_{57} define the position of the center of mass G7. Their *x* and *y* components are r_{67x}, r_{67y}, r_{57x} and r_{57y} respectively. l_9 is the length of link 7.

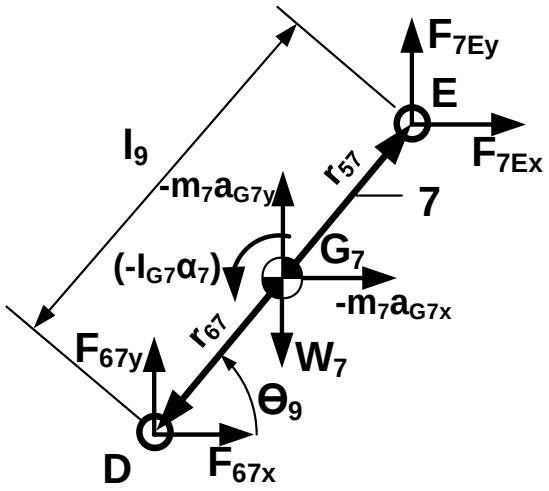

Figure 2.26. Free body diagram of link 7 (short connecting rod)

Vectors can be defined as follows:

$r_{67} = G_7D = \frac{l_9}{2};$ $r_{67x} = -\frac{l_9}{2}cos\theta_9;$ $r_{67y} = -\frac{l_9}{2}sin\theta_9;$

$r_{57} = G_7E = \frac{l_9}{2};$ $r_{57x} = \frac{l_9}{2}cos\theta_9;$ $r_{57y} = \frac{l_9}{2}sin\theta_9;$

The weight of the link: $W_7 = m_7 g;$

The static equilibrium equations for link 7 (Moments about centre of mass G7):

$\sum F_x = F_{67x} + F_{7Ex} + (-m_7 a_{G7x}) = 0;$

$\sum F_y = F_{67y} + F_{7Ey} + (-m_7 a_{G7y}) - m_7 g = 0;$

$\sum M = (r_{67x} F_{67y} - r_{67y} F_{67x}) + (r_{57x} F_{7Ey} - r_{57y} F_{7Ex}) + \left(-I_{G_7} \alpha_7\right) = 0;$

Analysis of the link 8. In the following forces F_{8Ex} and F_{8Ey} represent the *x* and *y* component respectively of the reaction forces of link 8 on joint E. The forces F_{18x} and F_{18y} represent the *x* and *y* component respectively of the reaction forces of link 1 on link 8. m_8 is the mass of link 8. a_{G8x} and a_{G8y} represent the x and y component respectively linear acceleration of link 8. I_{G_8} is the inertia moment with respect to the center of mass of link 8. α_8 is the angular acceleration of link 5. The vectors r_{58} and r_{18} define the position of the center of mass G8. Their *x* and *y* components are r_{58x}, r_{58y}, r_{18x} and r_{18y} respectively. l_8 is the length of link 8.

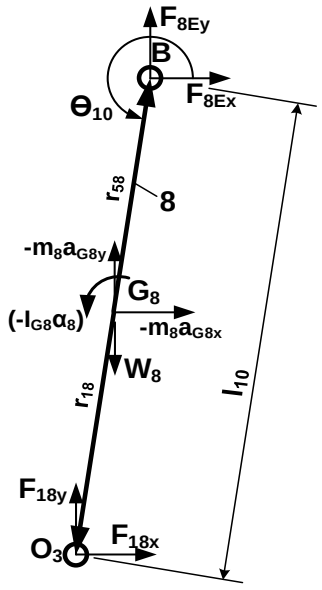

Figure 2.26. Free body diagram of link 8 (lever3)

Vectors can be defined as follows:

$r_{18} = G_8 O_3 = \frac{l_{10}}{2};$ $r_{18x} = -\frac{l_{10}}{2} cos\theta_{10};$ $r_{18y} = -\frac{l_{10}}{2} sin\theta_{10};$

$r_{58} = G_8 E = \frac{l_{10}}{2};$ $r_{58x} = \frac{l_{10}}{2} cos\theta_{10};$ $r_{58y} = \frac{l_{10}}{2} sin\theta_{10};$

Weight of the link 8: $W_8 = m_8 g$;

The static equilibrium equations for link 8 (Moments about centre of mass G8):

$\sum F_x = F_{18x} + F_{8Ex} + (-m_8 a_{G8x}) = 0;$

$\sum F_y = F_{18y} + F_{8Ey} + (-m_8 a_{G8y}) - m_8 g = 0;$

$\sum M = (r_{18x} F_{18y} - r_{18y} F_{18x}) + (r_{58x} F_{8Ey} - r_{58y} F_{8Ex}) + \left(-I_{G_8} \alpha_8\right) = 0;$

2.3.2. Dynamic equilibrium equations

In previous section, 3 linier equations has been obtained for 7 links. These 21 equations can be written as a set of linear equations ($Ax = B$) and solved for the 21 unknowns as follows:

$$\begin{bmatrix}
1 & 0 & 1 & 0 & 0 & 0 & 0 & 0 & 0 & 0 & 0 & 0 & 0 & 0 & 0 & 0 & 0 & 0 & 0 & 0 & 0 \\
0 & 1 & 0 & 1 & 0 & 0 & 0 & 0 & 0 & 0 & 0 & 0 & 0 & 0 & 0 & 0 & 0 & 0 & 0 & 0 & 0 \\
-r_{12y} & r_{12x} & -r_{32y} & r_{32x} & 0 & 0 & 0 & 0 & 0 & 0 & 0 & 0 & 0 & 0 & 0 & 0 & 0 & 0 & 0 & 0 & 1 \\
0 & 0 & -1 & 0 & 1 & 0 & 1 & 0 & 0 & 0 & 0 & 0 & 0 & 0 & 0 & 0 & 0 & 0 & 0 & 0 & 0 \\
0 & 0 & 0 & -1 & 0 & 1 & 0 & 1 & 0 & 0 & 0 & 0 & 0 & 0 & 0 & 0 & 0 & 0 & 0 & 0 & 0 \\
0 & 0 & r_{ay} & -r_{ax} & -r_{by} & r_{bx} & -r_{cy} & r_{cx} & 0 & 0 & 0 & 0 & 0 & 0 & 0 & 0 & 0 & 0 & 0 & 0 & 0 \\
0 & 0 & 0 & 0 & -1 & 0 & 0 & 0 & 1 & 0 & -1 & 0 & 0 & 0 & 0 & 0 & 0 & 0 & 0 & 0 & 0 \\
0 & 0 & 0 & 0 & 0 & -1 & 0 & 0 & 0 & 1 & 0 & -1 & 0 & 0 & 0 & 0 & 0 & 0 & 0 & 0 & 0 \\
0 & 0 & 0 & 0 & r_{34y} & -r_{34x} & 0 & 0 & -r_{14y} & r_{14x} & r_{34y} & -r_{34x} & 0 & 0 & 0 & 0 & 0 & 0 & 0 & 0 & 0 \\
0 & 0 & 0 & 0 & 0 & 0 & 0 & 0 & 0 & 0 & 1 & 0 & 0 & 0 & -1 & 0 & 0 & 0 & -1 & 0 & 0 \\
0 & 0 & 0 & 0 & 0 & 0 & 0 & 0 & 0 & 0 & 0 & 1 & 0 & 0 & 0 & -1 & 0 & 0 & 0 & -1 & 0 \\
0 & 0 & 0 & 0 & 0 & 0 & 0 & 0 & 0 & 0 & 0 & r_{35x} & 0 & 0 & 0 & -r_{85x} & 0 & 0 & 0 & -r_{85x} & 0 \\
0 & 0 & 0 & 0 & 0 & 0 & -1 & 0 & 0 & 0 & 0 & 0 & 1 & 0 & 0 & 0 & 0 & 0 & 0 & 0 & 0 \\
0 & 0 & 0 & 0 & 0 & 0 & 0 & -1 & 0 & 0 & 0 & 0 & 0 & 1 & 0 & 0 & 0 & 0 & 0 & 0 & 0 \\
0 & 0 & 0 & 0 & 0 & 0 & 0 & -r_{36x} & 0 & 0 & 0 & 0 & r_{76x} & 0 & 0 & 0 & 0 & 0 & 0 & 0 & 0 \\
0 & 0 & 0 & 0 & 0 & 0 & 0 & 0 & 0 & 0 & 0 & 0 & -1 & 0 & 1 & 0 & 0 & 0 & 0 & 0 & 0 \\
0 & 0 & 0 & 0 & 0 & 0 & 0 & 0 & 0 & 0 & 0 & 0 & 0 & -1 & 0 & 1 & 0 & 0 & 0 & 0 & 0 \\
0 & 0 & 0 & 0 & 0 & 0 & 0 & 0 & 0 & 0 & 0 & 0 & r_{67y} & -r_{67x} & -r_{57y} & r_{57x} & 0 & 0 & 0 & 0 & 0 \\
0 & 0 & 0 & 0 & 0 & 0 & 0 & 0 & 0 & 0 & 0 & 0 & 0 & 0 & 0 & 0 & 1 & 0 & 1 & 0 & 0 \\
0 & 0 & 0 & 0 & 0 & 0 & 0 & 0 & 0 & 0 & 0 & 0 & 0 & 0 & 0 & 0 & 0 & 1 & 0 & 1 & 0 \\
0 & 0 & 0 & 0 & 0 & 0 & 0 & 0 & 0 & 0 & 0 & 0 & 0 & 0 & 0 & 0 & -r_{18y} & r_{18x} & -r_{58y} & r_{58x} & 0
\end{bmatrix}$$

$$\begin{Bmatrix}
F_{12x} \\ F_{12y} \\ F_{32x} \\ F_{32y} \\ F_{3Bx} \\ F_{3By} \\ F_{63x} \\ F_{63y} \\ F_{14x} \\ F_{14y} \\ F_{5Bx} \\ F_{5By} \\ F_{76x} \\ F_{76y} \\ F_{7Ex} \\ F_{7Ey} \\ F_{18x} \\ F_{18y} \\ F_{8Ex} \\ F_{8Ey} \\ M_2
\end{Bmatrix} = \begin{Bmatrix}
m_2 a_{G2x} \\ m_2(a_{G2y} + g) \\ I_{G_2}\alpha_2 \\ m_3 a_{G3x} \\ m_3(a_{G3y} + g) \\ I_{G_3}\alpha_3 \\ m_4 a_{G4x} \\ m_4(a_{G4y} + g) \\ I_{G_4}\alpha_4 \\ m_5 a_{G5x} \\ m_5(a_{G5y} + g) \\ I_{G_5}\alpha_5 \\ m_6 a_{G6x} \\ m_6(a_{G6y} + g) \\ I_{G_6}\alpha_6 \\ m_7 a_{G7x} \\ m_7(a_{G7y} + g) \\ I_{G_7}\alpha_7 \\ m_8 a_{G8x} \\ m_8(a_{G8y} + g) \\ I_{G_8}\alpha_8
\end{Bmatrix} \quad (2.52)$$

In the above system of linear equations($Ax = B$), ***A*** matrix contains geometric information, and ***B*** vector contains dynamic information of the mechanism. The vector ***x*** contains unknown forces and the moments should be determined.
The system of linear equations (2.52) can be written separately for dyads as shown in Figures 2.28, 2.30, 2.32, 2.34. The proposed mechanism has three RRR dyads. Dyads can be obtained from the end or output link of the mechanism. First RRR dyad is a couple of link 6 and link 7 (Figure 2.28). The results of the reaction forces and torque have been presented in Figures 2.29, 2.31, 2.33 and 2.35
1. Separated linear equations starts from link 6 and link 7. For dyad link 6 and link 7 linear equations has been written in Equation 2.53. These each lines of the equation has been separated from Equation 2.52.

Figure 2.28. RRR dyad 1 (links 6 and 7).

$$\begin{bmatrix} -1 & 0 & 1 & 0 & 0 & 0 \\ 0 & -1 & 0 & 1 & 0 & 0 \\ 0 & -r_{36x} & 0 & r_{76x} & 0 & 0 \\ 0 & 0 & -1 & 0 & 1 & 0 \\ 0 & 0 & 0 & -1 & 0 & 1 \\ 0 & 0 & r_{67y} & -r_{67x} & -r_{57y} & r_{57x} \end{bmatrix} \begin{Bmatrix} F_{63x} \\ F_{63y} \\ F_{76x} \\ F_{76y} \\ F_{7Ex} \\ F_{7Ey} \end{Bmatrix} = \begin{Bmatrix} m_6 a_{G6x} \\ m_6(a_{G6y} + g) \\ I_{G_6}\alpha_6 \\ m_7 a_{G7x} \\ m_7(a_{G7y} + g) \\ I_{G_7}\alpha_7 \end{Bmatrix} \quad (2.53)$$

$$[\mathrm{A}_{67}]\{v_{67}\} = \{b_{67}\}$$

In equation (2.53), the 6 unknowns F63x, F63y, F76x, F76y, F7Ex and F7Ey can be determined by using the inverse matrix as follow and calculate by MATLAB program:

$$\{\mathrm{v}_{67}\} = [\mathrm{A}_{67}]^{-1}\{\mathrm{b}_{67}\}$$

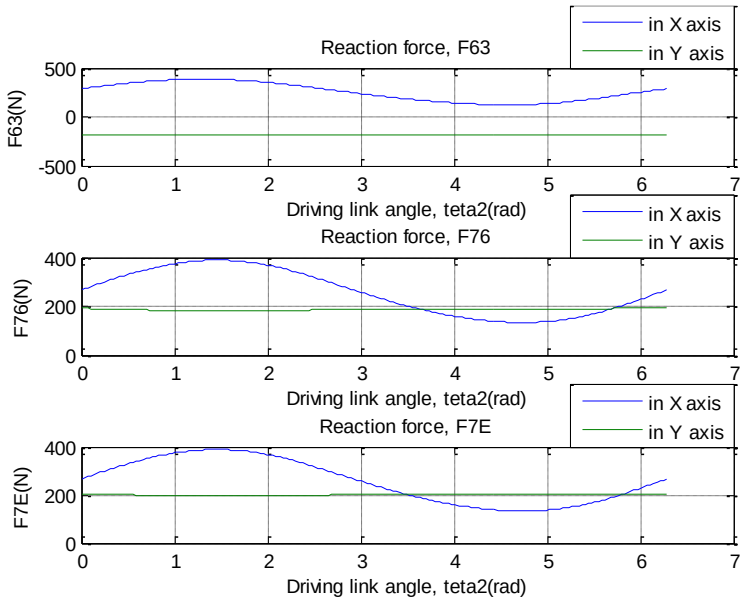

Figure 2.29. Plot of the reaction forces F63x, F63y, F76x, F76y, F7Ex and F7Ey.

2) Next RRR dyad is shown in Figure 2.30 for link 5 and link 8. Figure 2.30 represents the 6 unknowns F5Bx, F5By, F8Ex, F8Ey, F18x and F18y, and their linear equations are shown in Equation (2.54). The linear equations (2.54) has been obtained by separating the 7th, 8th, 13th, 14th, 15th and 16th linear equations of the Equation (2.52).

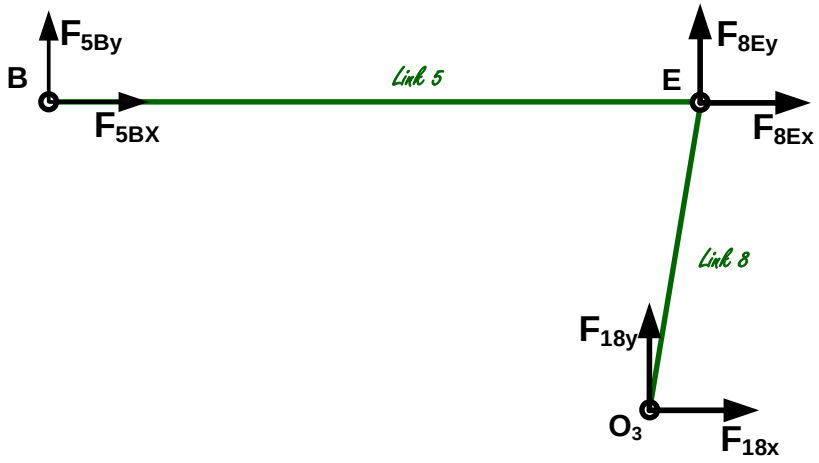

Figure 2.30. RRR dyad 2 (links 5 and 8).

$$\begin{bmatrix} 1 & 0 & 0 & 0 & -1 & 0 \\ 0 & 1 & 0 & 0 & 0 & -1 \\ 0 & r_{35x} & 0 & 0 & 0 & -r_{85x} \\ 0 & 0 & 1 & 0 & 1 & 0 \\ 0 & 0 & 0 & 1 & 0 & 1 \\ 0 & 0 & -r_{18y} & r_{18x} & -r_{58y} & r_{58x} \end{bmatrix} \begin{Bmatrix} F_{5Bx} \\ F_{5By} \\ F_{18x} \\ F_{18y} \\ F_{8Ex} \\ F_{8Ey} \end{Bmatrix} = \begin{Bmatrix} m_5 a_{G5x} + F_{7Ex} \\ m_5(a_{G5y} + g) + F_{7Ey} \\ I_{G_5}\alpha_5 + r_{85x}F_{7Ey} \\ m_8 a_{G8x} \\ m_8(a_{G8y} + g) \\ I_{G_8}\alpha_8 \end{Bmatrix} \quad (2.54)$$

$$[\mathrm{A}_{58}]\{v_{58}\} = \{b_{58}\}$$

In above linear equation (2.53), the unknowns F5Bx, F5By, F18x, F18y, F8Ex and F8Ey can be determined by using the inverse matrix by MATLAB program as follow:

$$\{\mathrm{v}_{58}\} = [\mathrm{A}_{58}]^{-1}\{\mathrm{b}_{58}\}$$

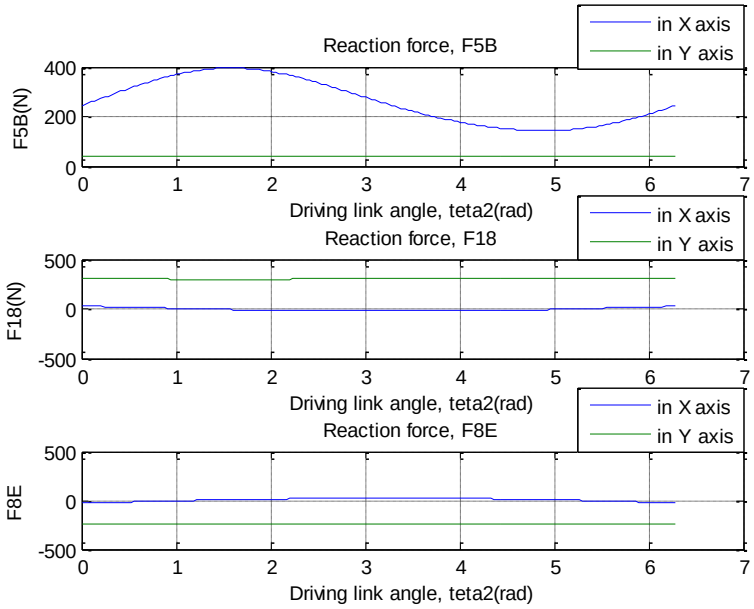

Figure 2.31. Plot of the reaction forces F5Bx, F5By, F18x, F18y, F8Ex and F8Ey.

3) Next RRR dyad is shown in Figure 2.32 for link 3 and link 4. Figure 2.32 represents 6 unknowns F23x, F23y, F4Bx, F4By, F14x and F14y, and their linear equations are shown in Equation (2.55). The 11th, 12th, 17th, 18th, 19th and 10th linear equations have been separated from the Equation (2.52)

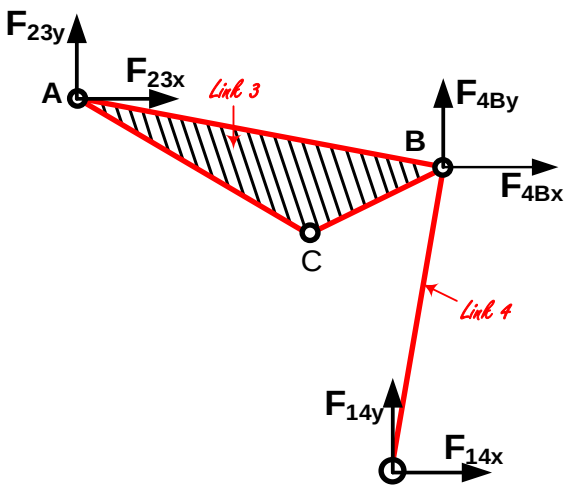

Figure 2.32. RRR dyad 3 (links 3 and 4).

$$\begin{bmatrix} -1 & 0 & 1 & 0 & 0 & 0 \\ 0 & -1 & 0 & 1 & 0 & 0 \\ r_{ay} & -r_{ax} & -r_{by} & r_{bx} & 0 & 0 \\ 0 & 0 & -1 & 0 & 1 & 0 \\ 0 & 0 & 0 & -1 & 0 & 1 \\ 0 & 0 & r_{34y} & -r_{34x} & -r_{14y} & r_{14x} \end{bmatrix} \begin{Bmatrix} F_{32x} \\ F_{32y} \\ F_{3Bx} \\ F_{3By} \\ F_{14x} \\ F_{14y} \end{Bmatrix} = \begin{Bmatrix} m_3 a_{G3x} - F_{63x} \\ m_3(a_{G3y} + g) - F_{63y} \\ I_{G_3}\alpha_3 + r_{cy}F_{63x} - r_{cx}F_{63y} \\ m_4 a_{G4x} + F_{5Bx} \\ m_4(a_{G4y} + g) + F_{5By} \\ I_{G_4}\alpha_4 - r_{34y}F_{5Bx} + r_{34x}F_{5By} \end{Bmatrix} \quad (2.55)$$

$$[\mathrm{A}_{34}]\,\{v_{34}\} = \{b_{34}\}$$

In Equation (2.55), the 6 unknowns F32x, F32y, F3Bx, F3By, F14x and F14y can be determined by using the inverse matrix by MATLAB program as follow:

$$\{\mathrm{v}_{34}\} = [\mathrm{A}_{34}]^{-1}\{\mathrm{b}_{34}\}$$

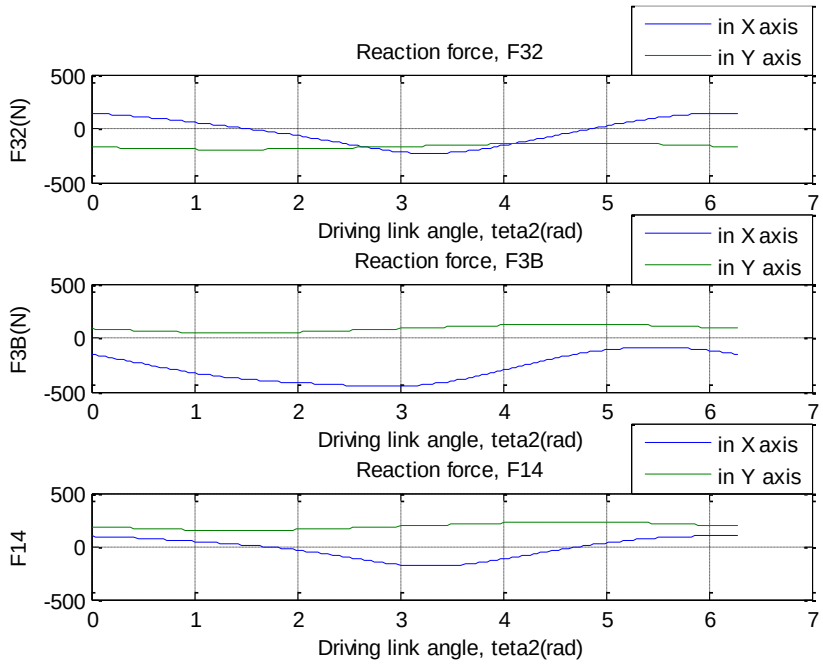

Figure 2.33. Plot of the reaction forces F32x, F32y, F3Bx, F3By, F14x and F14y.

4) The last link, the crank is shown in Figure 2.34. The crank has 5 unknowns F32x, F32y, F12x F12y, and input torque M2. In Equation (2.56) has been written only for reaction forces F12x F12y and input torque M2. Because the reaction forces F32x and F32y are known from the linear Equation (2.55) and equal to reaction forces F23x, F23y.

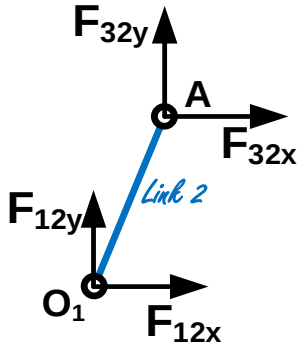

Figure 2.34. Driver link, crank.

$$\begin{bmatrix} 1 & 0 & 0 \\ 0 & 1 & 0 \\ -r_{12y} & r_{12x} & 1 \end{bmatrix} \begin{Bmatrix} F_{12x} \\ F_{12y} \\ M_2 \end{Bmatrix} = \begin{Bmatrix} m_2 a_{G2x} - F_{32x} \\ m_2(a_{G2y} + g) - F_{32y} \\ I_{G_2}\alpha_2 + r_{32y}F_{32x} - r_{32x}F_{32y} \end{Bmatrix} \quad (2.56)$$

$$[\mathrm{A}_2]\{v_2\} = \{b_2\}$$

In Equation (2.56), 3 unknowns F12x, F12y and M2 can be determined by using the inverse matrix by MATLAB program as follow:

$$\{\mathrm{v}_2\} = [\mathrm{A}_2]^{-1}\{\mathrm{b}_2\}$$

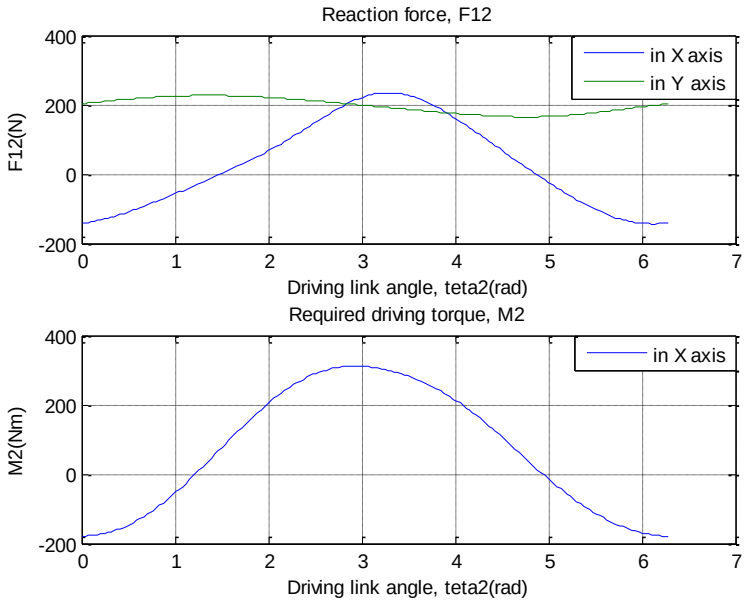

Figure 2.35. Plot of the reaction forces F12x, F12y and input torque M2.

Chapter 3

Structural design of the new mechanism

3.1. Stress analysis of the proposed mechanism

When the wool is dropping into the bowl, the prongs of the transport mechanism immerse it into the scouring liquor and propel forward toward the apron of the scouring bowl. According to [52] the motion of the moving body is resisted by the drag force or resistant force which acts in the direction opposite to motion. Drag force of the liquid to the harrow is shown in Figure 3.1. It is considered that the harrow has 20 lines of the cross bars. On the each cross bar 13 pieces of prongs are mounted. Each line of the prongs moves a portion of the total wool (Figure 3.1). At the same time the several portions of the wool move in a certain distance.

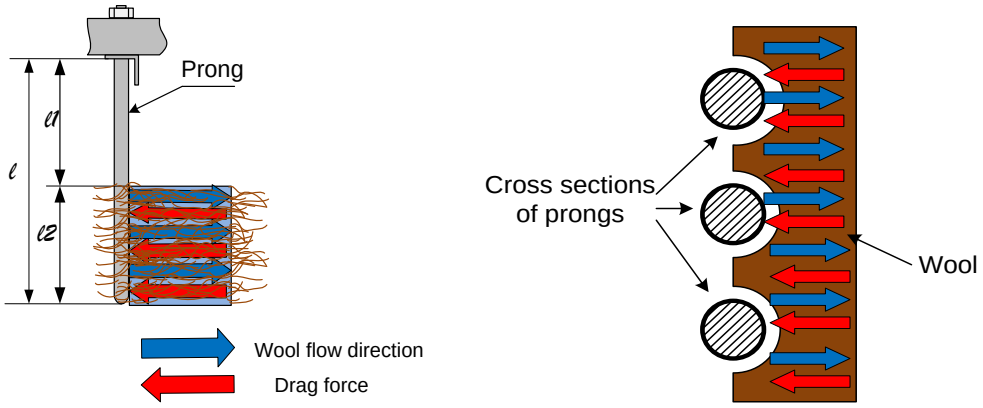

Figure 3.1. The forces between the prongs, wool and the fluid
a) side-view of the prong, b) cross sections of the prongs

Drag force which acts on the whole harrow can be found by the following formula [52]:

$$F_D = A \cdot C_D \cdot \rho \cdot \frac{v^2}{2}; \qquad (3.1)$$

The magnitude of the drag force depends on three quantities: the frontal area of the moving body, the drag coefficient and the density of liquid.

In equation 3.1, A represents a frontal area of the floating object. The frontal area of the immersed part of the prong varies during rotation of the machine. The shape of the prong is cylindrical. The frontal area of the cylinder can be found as a product of height and diameter of the cylinder.

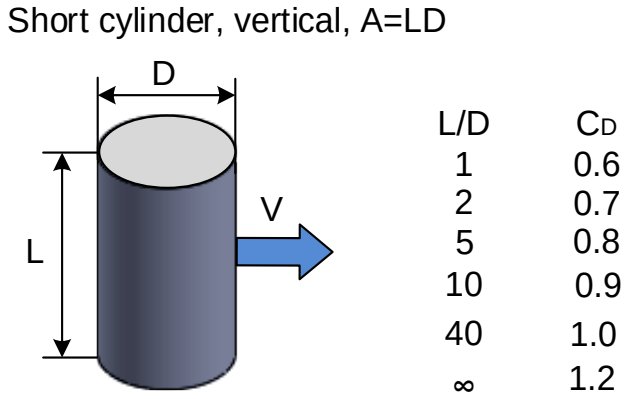

Figure 3.2. The drag force for short cylinder (Adapted from [52])

In the Figure 3.2, ***D*** represents the diameter of the prong, and ***L*** represents the height of the body. ***D*** is a constant, height ***L*** varies respect to the crank rotation. It is considered that, the range of height of the body equals to $L = 0.012m \div 0.11m$; The range of the frontal area is tabulated in Table 3.1.

C_D - drag coefficient, is a dimensionless quantity that is used to quantify the drag force [51]. Drag coefficient for short cylinder depends on the relationship between the height and the diameter of the cylinder as shown in Figure 3.2.

Drag coefficient C_D can be varied as follows: if, L=0.012m and each distance equals to 0.01m. The results of the drag coefficient C_D for short and long immersed positions of the prong are shown in Table 3.1.

Table 3.1. The range of the frontal area A and the drag coefficient C_D for the different immersed parts of the prong

L	D	L/D	C_D	$A=LD$
0.01	0.012	0.83	≈0.6	0.00012
0.02	0.012	1.66	≈0.65	0.00024
0.03	0.012	2.5	≈0.7	0.00036
0.04	0.012	3.33	≈0.75	0.00048
0.05	0.012	4.16	≈0.8	0.00060
0.06	0.012	5	≈0.8	0.00072
0.07	0.012	5.83	≈0.8	0.00084
0.08	0.012	6.66	≈0.8	0.00096
0.09	0.012	7.5	≈0.8	0.00108
0.10	0.012	8.33	≈0.85	0.00120
0.11	0.012	9.16	≈0.9	0.00132

The Figure 3.3 represents the different positions of the prong in the scouring liquor. If the frontal area increases, the drag coefficient increases respectively.

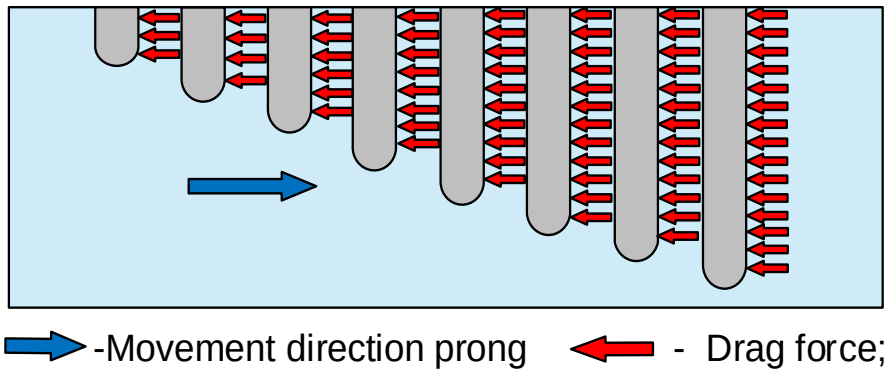

Figure 3.3. The range of the immersed part of the prong

ρ – Density of water. The bowl is filled with raw wool. Density of wool equals to 1310 kg/m3. It is considered that, density of scouring liquor will wary between 1000 $^{kg}/_{m^3}$ and 1310 $^{kg}/_{m^3}$ during rotation of the machine.

v – is a velocity of the moving body. Velocity of the moving body is equals to the velocity of the harrow. Velocity of the harrow is known from equation 2.44 in Chapter 2, as follows:

$$\dot{C} = l_2\omega_2(-sin\theta_2\ cos\theta_2) + l_5\omega_3(-sin(\theta_3 - \beta)\ cos(\theta_3 - \beta));$$

Drag force has been calculated by MATLAB program. The drag force varies with respect to the motion of the crank. Each variables has been calculated with respect to the crank rotation. Plot of the drag force is shown in Figure 3.4.

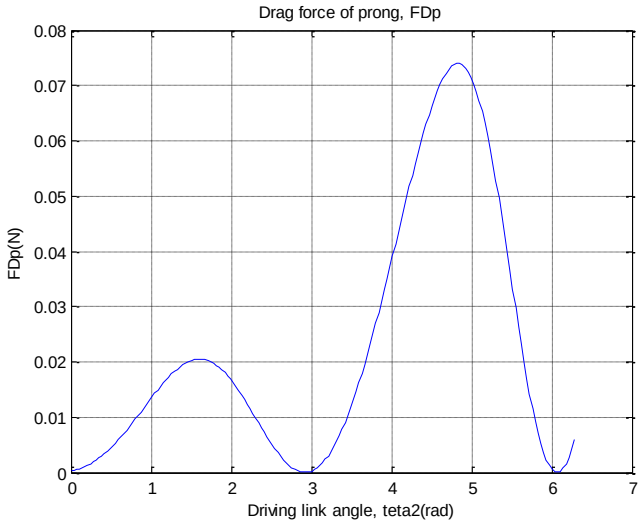

Figure 3.4. The range of the drag force

During rotation of the harrow, the drag force acts on the all prongs of the harrow (Figure 3.5). In order to determine the total drag force which acts on the total number of prongs, the drag force should be multiplied by the number of prongs. It is considered that, one cross bar has 13 prongs, there may be 20 pieces of cross bars in harrow as mentioned above. In this case, the total drag force can be calculated as follows:

$$F_D = F_{D_p} * 13 * 20;\ N \qquad (3.2)$$

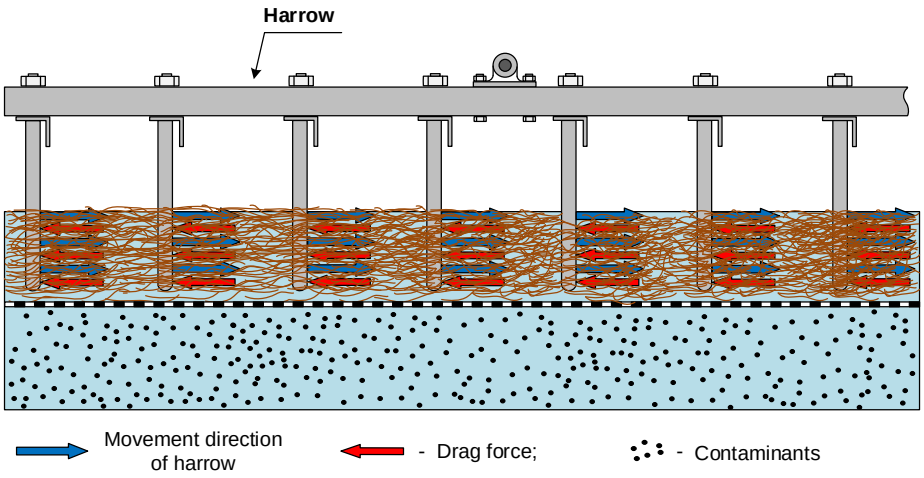

Figure 3.5. The drag force which is acting on a several lines of the prongs

The plot of the total drag force is shown in Figure 3.6.

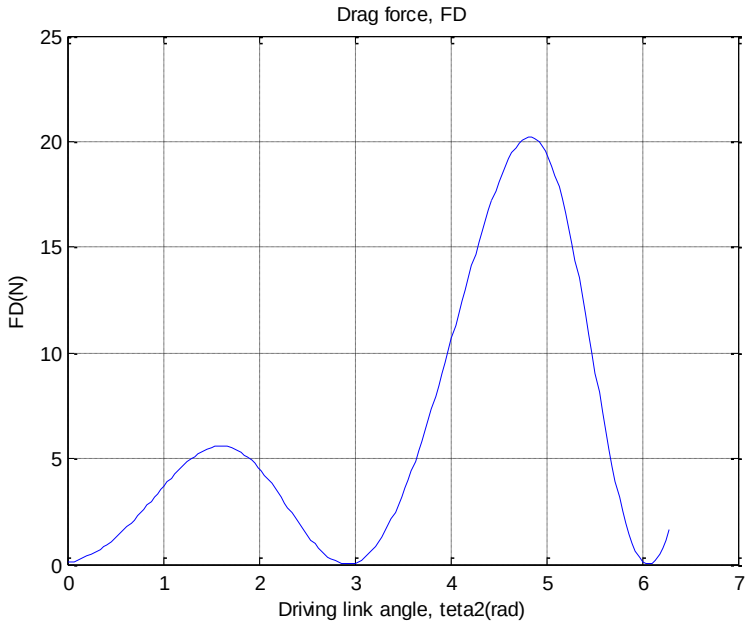

Figure 3.6. The plot of the total drag force.

While, the drag force is acts on the prong (Figure 3.5), it causes the bending of the prong. In order to design any parts of the machine, stress analysis of the parts should be determined.

1. Material selection for prong.

The material selection is one of the important stages of the design. The proper material can be extended the working life of the machine. Wool transport mechanisms operate in the aquatic environment. The raw wool contains grease, suint, dirt and vegetable matters as mentioned in Introduction section. Suint is a dried perspiration of sheep and rich in the potassium salts. The temperature of the scouring liquor is about 50-70^{0}C. The salty water and steam rust the metallic materials. Figure 3.7 represents the wool scouring machine. It can be seen, the bowl, the longitudinal bars and the cross bars are corroded. Only the prongs are not corroded. The material of the prong should be selected by corrosion resistant.

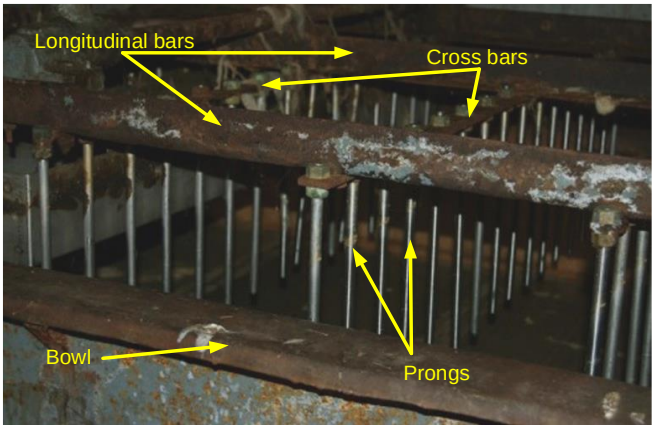

Figure 3.7. Corroded parts of the scouring machine [53].

The most corrosion resistant materials which are used in machine design are stainless steel and aluminium. Stainless steel S31600 has been selected for the prong. Its density equals to $\rho_d = 8000 kg/m^3 = 8\ g/cm^3$ [54];

2. Calculation of volume of the prong.

The prong has three different parts. They are the threaded shank, cylindrical body, and semi sphere form tip. Each part should be calculated separately. The prong is shown in Figure 3.8.

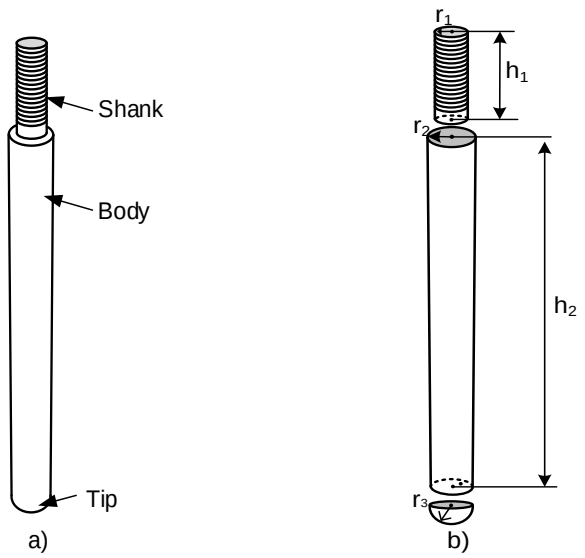

Figure 3.8. The sketch of the prong.

Dimensions of the prong:

Radius of the shank, $r_1 = 5mm\ or\ 0.5cm$;

Lengths of the shanks, $h_1 = 1.6\ cm\ and\ 4.2\ cm$

Upper radius of the cylindrical body, $r_2 = 6\ mm\ or\ 0.6cm$;

Length of the body $h_2 = 250mm\ or\ 25\ cm$;

Bottom radius of the cylindrical body and also radius of the tip, $r_3 = 6mm = 0.6cm$;

In the whole harrow mechanism, the two different lengths of prongs can be used in terms of the positions of the components.

They depend on the length of the threaded shank and denoted that short and long prong. The short prong is used for mounting on the cross bars (Figure 3.9.a). The long prong is used for mounting on cross bars and together with longitudinal bar (Figure 3.9.b). Their threaded shanks should be calculated separately.

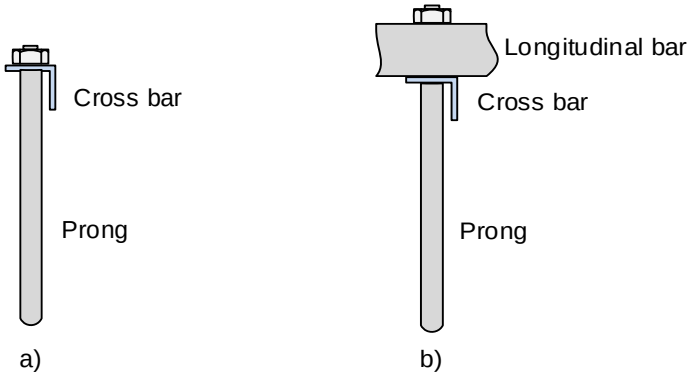

Figure 3.9. The prong and its mounting on the cross bar and the longitudinal bar;
a) Short prong is mounted on cross bar, b) Long prong is mounted on cross bar with together longitudinal bar.

2a. The volume of the threaded shank is calculated as following standard formula for cylinder (thread is neglected):

The volume of the short prong: $V_{t.sh.} = \pi \cdot r_1^2 \cdot h_1 = 3.14 \cdot 0.5^2 \cdot 1.6 = 1.25 cm^3$;

The volume of the long prong: $V_{t.m.} = \pi \cdot r_1^2 \cdot h_1 = 3.14 \cdot 0.5^2 \cdot 4.2 = 3.29 cm^3$;

2 b. The volume of the cylindrical body is calculated as following standard formula for cylinder:

$V_b = \pi \cdot r_2^2 \cdot h_2 = 3.14 \cdot 0.6^2 \cdot 24.4 = 27.6 cm^3$;

2 c. The volume of the hemisphere form tip of the prong is calculated as following standard formulas:

$V_{ss} = \frac{2}{3} \cdot \pi \cdot r_0^3 = \frac{2}{3} \cdot 3.14 \cdot 0.4^3 = 0.45 cm^3$;

2 d. The total volume of the prong can be calculated as follows

The volume of the short prong:

$V_{sh.p} = V_{t.sh.} + V_{sc} + V_{ss} = 1.25 + 27.6 + 0.45 = 29.3 cm^3$;

The volume of the long prong:

$V_{mid.p} = V_{t.m.} + V_{sc} + V_{ss} = 3.29 + 27.6 + 0.45 = 31.34 cm^3$;

3. Calculation of mass of the prong.

The mass of the prong is a product of the volume and the density of the material and it can be calculated as follows:

3 a. The mass of the short prong:

$m_{sh.p} = V_{sh.p} \cdot \rho_d = 29.3cm^3 \cdot 8\ g/cm^3 = 234.4g = 0.234kg;$

3 b. The mass of the long prong:

$m_{l.p} = V_{l.p} \cdot \rho_d = 31.34cm^3 \cdot 8\ g/cm^3 = 250.7g = 0.25kg;$

4. Calculation of weight of the prong.

4 a. The weight of the short prong:

$W_{sh.p} = m_{sh.p} \cdot g = 0.234kg \cdot 9.81m/c^2 = 2.3\ N$

4 b. The weight of the long prong:

$W_{l.p} = m_{l.p} \cdot g = 0.25kg \cdot 9.81m/c^2 = 2.45\ N$

5. Stress analysis of the prong:

The dimensions of the prong are known from Chapter 2 as follows:

$l_p = 0.25m;\ l_{p1} = 0.14m;\ l_{p2} = 0.11m;$

It is assumed that, the prong is a cantilever beam. The drag force acts on the certain length l_{p2} of the prong such as s uniformly distributed load (Figure 3.10). In order to find the magnitude of the distributed load, the drag force divides by the length under the distributed load as follows:

$$qp = \frac{F_{Dp}}{l_{p2}} N/m; \qquad (3.3)$$

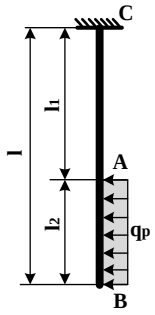

Figure 3.10. The cantilever beam under distributed load on the free end

5 a. Calculation of reactions.

In order to determine the reaction forces and the moments, the free body diagram of the beam should be drawn (Figure 3.11). During working of the machine the several forces and the moments act on the prongs.

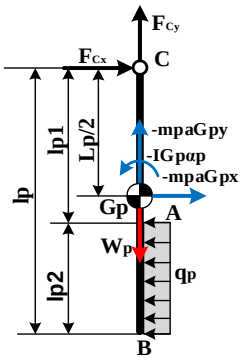

Figure 3.11. The free body diagram of the prong

In the Figure 3.11, the weight of the prong $\boldsymbol{W_p}$, the reaction forces $\boldsymbol{F_{Cx}}$ and $\boldsymbol{F_{Cy}}$ at support $\boldsymbol{C}$, uniformly distributed load $\boldsymbol{q_p}$, the inertia forces $\boldsymbol{mpaGx}$, $\boldsymbol{mpaGy}$ and the mass moment of inertia $\boldsymbol{IGp\alpha p}$ are represented.

The reaction forces and the moments can be determined by applying the static equilibrium equations as follows:

$+\uparrow \sum Fx = 0;$ $\qquad F_{Cx} = mp \cdot aGpx + qp \cdot l_{p2};\quad N;$

$+\uparrow \sum Fy = 0;$ $\qquad F_{Cy} = mp \cdot aGpy + Wp;\quad N;$

$+\circlearrowleft \sum M = 0;$ $\qquad M_B = mp \cdot aGpx \cdot \frac{l_p}{2} + IGp\alpha p \cdot \frac{l_p}{2} - qp \cdot (\frac{l_p - l_{p1}}{2})^2;\ Nm;$

5 b. Calculation of shear force and bending moment.

Shear force and bending moment are calculated by cross sections of the cantilever beam (Figure 3.14a). Stress analysis of the cantilever beam starts from the free end of the beam.

Free body diagram of section I:

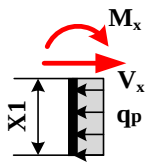

Figure 3.12. Free body diagram of section I.

Static equilibrium equations of section I can be written as follows:

$+\rightarrow \sum Fx = 0; \qquad V_x = qp \cdot x;$

$\circlearrowleft + \sum M = 0; \qquad M_x = -qp\frac{x^2}{2};$

For section I the following assumptions can be written: $0 \leq x \leq l_{p2};$

If, $x = 0;$	$V_{x1} = 0;$	$M_{x1} = 0;$
If, $x = \frac{l_{p2}}{2};$	$V_{x2} = qp \cdot \frac{l_{p2}}{2};$	$M_{x2} = -qp\frac{\frac{l_{p2}{}^2}{2}}{2};$
If, $x = l_{p2};$	$V_{x3} = qp \cdot l_{p2};$	$M_{x3} = -qp\frac{l_{p2}{}^2}{2};$

Free body diagram of section II:

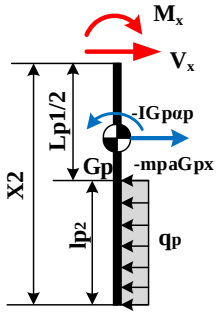

Figure 3.13. Free body diagram of section II.

Static equilibrium equations of section II can be written as follows:

$+\rightarrow \sum Fx = 0; \qquad V_x = mp \cdot aGpx \cdot x + qp \cdot l_p;$

$+\circlearrowleft \sum M = 0;$ $\quad M_x = mp \cdot aGpx \cdot x + IGp\alpha p \cdot x - qp \cdot l_p(\frac{x-\frac{lp_1}{2}}{2});$

For section II the following assumptions can be written: $\frac{l_{p2}}{2} \leq x \leq lp_1;$

$If, x = l_{p2} + \frac{l_{p1}}{2};$ $\quad V_{x4} = mpaGpx \cdot (l_{p2} + \frac{l_{p1}}{2}) +;$

$$M_{x4} = IGp\alpha p \cdot (l_{p2} + \frac{l_{p1}}{2}) + mpaGpx \cdot (l_{p2} + \frac{l_{p1}}{2}) - qp \cdot \frac{{l_{p2}}^2}{2};$$

$If, x = l_p;$ $\quad V_{x5} = mpaGpx \cdot l_p + qp \cdot l_{p2};$

$$M_{x6} = IGp\alpha p \cdot l_p + mpaGpx \cdot l_p - qp \cdot \frac{{l_{p2}}^2}{2};$$

The shear force and the bending moment have been calculated by MATLAB program and their diagrams are shown in Figure 3.14 b, c.

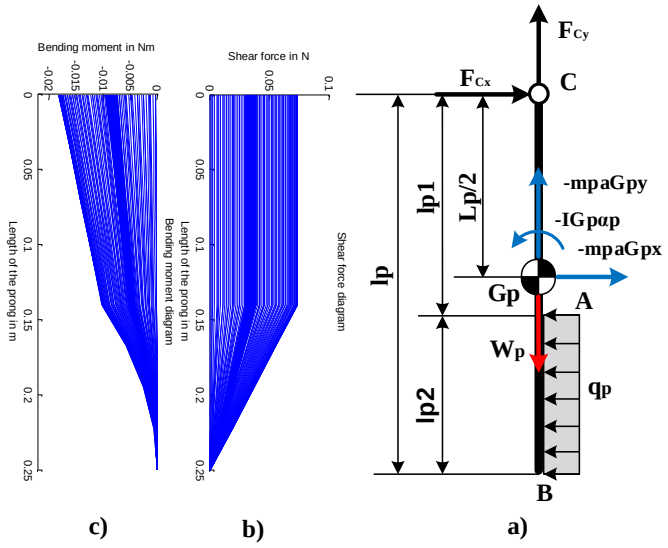

Figure 3.14. Stress analysis of the cantilever beam
a) cross sections of the beam, b) shear force diagram, c) bending moment diagram

Bending strength can be calculated as following equation:

$$\delta = \frac{M_b^{max}}{S}; \qquad (3.4)$$

Here, M_b^{max} - maximum bending moment. Maximum bending moment value has been taken from MATLAB results and equals to $M_b^{max} = 0.0183\text{Nm};$

S – Section modulus;

Section modulus for solid circular shape - $S = \frac{\pi \cdot d^3}{32} = 0.1 \cdot d^3$;

The actual bending stress should be small or equals to allowable bending stress:

$\delta \leq [\delta]$;

Here, $[\delta]$ is the allowable stress of the material.

Stainless steel AISI 314L has been selected for prong. Mechanical properties of the selected material was tabulated in Section 3.2. Allowable stress for cylindrical shape:

$[\delta] = 0.61 * 314 = 191 MPa$;

Equation (3.4) can be rewritten as follows:

$\frac{M_b^{max}}{0.1 \cdot d^3} \leq [\delta]$;

$\frac{M_b^{max}}{0.1 \cdot d^3} = \frac{0.0183 Nm}{0.1 \cdot 12^3 mm^3} = \frac{0.0183 Nm}{172.8 \cdot 10^{-9} m^3} = \frac{105902.77 N}{m^2} = 0.11 MPa$;

Comparison of the actual and allowable stress:

$\delta < [\delta] = 0.11 < 191$;

The result is acceptable.

Stress analysis of the cross bar

It is considered that, square angle bar can be selected for cross bar (Figure 3.15). In order to find the proper dimensions of the angle bar, it can be selected the nearly dimensions for the shank diameter of the prong from the standard catalogues of materials.

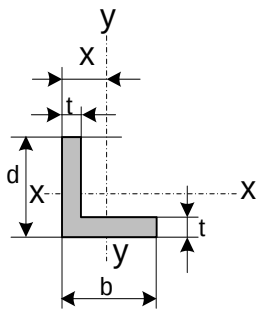

Figure 3.15. The shape of the cross bar

The smallest size of the square end angle has been selected from the table – "Square end angles - equal legs" [55].

Table 3.2. Mechanical properties of selected square end angle

Designation	d in	b in	Thickness, t, in	Area A, in^2	I_{xx} In^4	I_{yy} In^4	S_{xx} In^3	S_{yy} In^3
$1x1x\frac{1}{8}$	1.000	1.500	0.125	0.234	0.0217	0.0217	0.309	0.309

1. Material selection for cross bar.

Cross bars also require corrosion resistant material. Aluminium 6061-T6 can be selected for cross bar. Its density is equals to $\rho_{st} = 2700kg/m^3 = 2.7\ g/cm^3$ [54];

2. Calculation of volume of the cross bar.

The cross bar is shown in Figure 3.16. The shape of the cross bar is a square equal length angle, and it contains 13 of holes for mounting the prongs.

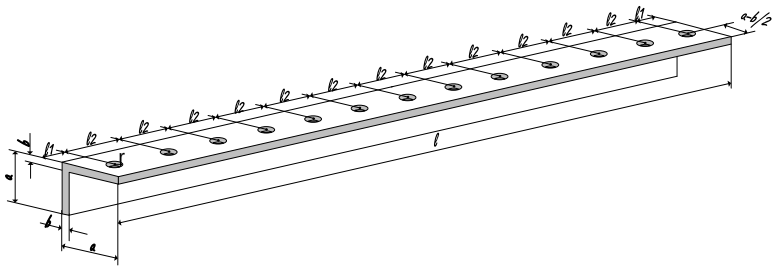

Figure 3.16. The cross bar

Referring to Figure 3.16, the lengths $l = 112cm = 1.12m$; $l_1 = 2cm = 0.2m$; $l_2 = 9cm = 0.9m$; and the thickness $b = 0.3175cm = 0.003175m$; are the same in both sections, only the widths of the sections depend as follows: the width of the angle bar of section 1: $a_1 = 1in = 2.54cm\ or\ 0.0254m$; the width of the angle bar of section 2: $a_2 = a_1 - b = 2.22cm\ or\ 0.0222m$;

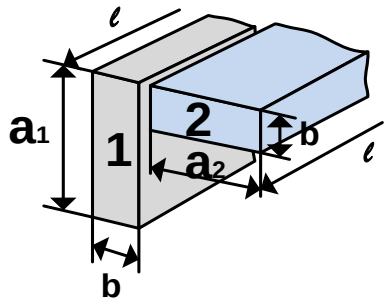

Figure 3.17. Two separate parts of the cross bar

In order to find the volume of the angle bar, it can be divided by two sections (Figure 3.17), and can be calculated separately.

2 a. The volumes of the sections can be calculated as follows:

$V_1 = a_1 \cdot b \cdot l = 2.54 \cdot 0.3175 \cdot 112 = 90.32cm^3$;

$V_2 = a_2 \cdot b \cdot l = 2.22 \cdot 0.3175 \cdot 112 = 79.03cm^3$;

2 b. The total volume of the cross bar is:

$V_{c.b} = V_1 + V_2 = 90.32cm^3 + 79.03cm^3 = 169.35cm^3$;

3. Calculation of mass of the cross bar.

The mass of the cross bar is a product of the volume and the material density. The density of Aluminium 6061-T6 equals to:

$\rho_{st} = 2700kg/m^3 = 2.7\ g/cm^3$; [54]

The mass of the cross bar can be found as follows:

$m_{c.b} = V_{c.b} \cdot \rho_{st} = 169.35cm^3 \cdot 2.7g/cm^3 = 457.25\ g = 0.457kg;$

4. Calculation of weight of the cross bar.

The weight of the cross bar is: $W_{c.b} = m_{c.b} \cdot g = 0.457kg \cdot 9.81m/s^2 = 4.49\ N$

It is considered that, 13 pieces of prongs mount on the cross bar. And, the cross bar mounts on the two locations of the longitudinal bars. Figure 3.18 shows the cross bar with mounted prongs.

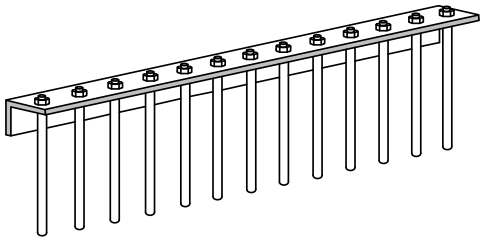

Figure 3.18. The cross bar with mounted prongs

The dimensions of the cross bar equal to:

$l_{cb1} = 0.29\ m;\quad l_{cb2} = 0.54\ m;\quad l_{cb} = 1.12\ m;$

The total weight of the cross bar with mounted prongs can be calculated as follows:

$W_{tcb} = W_{cb} + 13 \cdot W_{shp} = 4.49N + 13 \cdot 2.3N = 34.39N;$

In order to find the magnitude of the uniformly distributed load during working of machine, the total weight of the cross bar and inertia forces can be divided by entire length of the cross bar as follows:

$$q_{cb} = \frac{W_{tcb} + m_{cb} a G_{cby}}{l_{cb}}; \qquad (3.5)$$

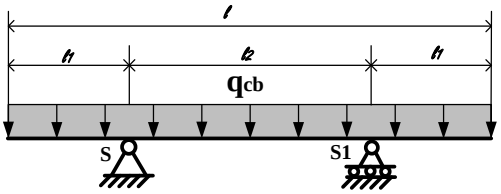

Figure 3.19. Distributed load of the cross bar.

The shear force and the bending moment of the cross bar can be determined in vertical plane. Because, in horizontal plane only x components of the inertia forces act on the cross bar. Their magnitudes are too small than magnitudes of the vertical loads. Figure 3.20 shows the load diagram of the cross bar. In the vertical plane, the weight of the cross bar, the total weight of the mounted prongs and ***y*** component of the inertia force act on the cross bar as a uniformly distributed load.

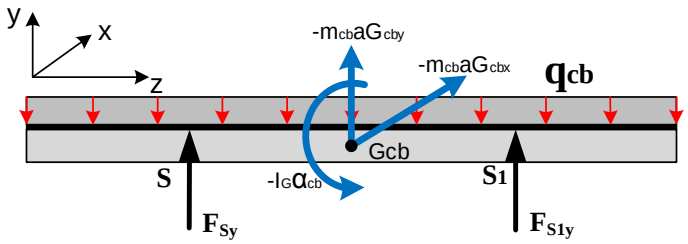

Figure 3.20. Load diagram of the cross bar.

5. Calculation of reactions.

The free body diagram of the beam is shown in Figure 3.20. During working of the machine, the several forces and the moments act on the prongs. In the Figure 3.20, the reaction forces $\boldsymbol{F_{Sy}}$ and $\boldsymbol{F_{S1y}}$ at supports ***S*** and ***S1,*** uniformly distributed load $\boldsymbol{q_{cb}}$, the inertia forces $\boldsymbol{m_p a_{Gcbx}}$ and $\boldsymbol{m_p a_{Gcby}}$ and the mass moment of the inertia $\boldsymbol{IG_{cb}\alpha_{cb}}$ are represented.

5 a. Determination of the reaction forces and the moments.

The reaction forces can be calculated by dividing the uniformly distributed load by equal because the symmetry of applied load as follows:

$$F_S = F_{S1} = \frac{q_{cb} \cdot l_{cb}}{2}; \qquad (3.6)$$

5 b. The shear force and the bending moment can be calculated by dividing the cross sections as shown in Figure 3.21 and Figure 3.22.

Free body diagram of section I:

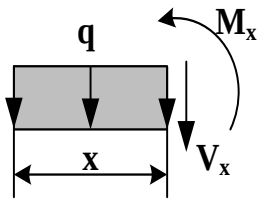

Figure 3.21. Free body diagram of section I.

Static equilibrium equations of the section I can be written as follows:

$+\uparrow \sum Fy = 0 \qquad V_x = -q_{cb} \cdot x;$

$+\circlearrowleft \sum M = 0 \qquad M_x = -q_{cb} \frac{x^2}{2};$

For section I, following assumptions can be written: $0 \leq x \leq l_1;$

If, $x = 0; \qquad V_x = 0; \qquad M_x = 0;$

If, $x = l_{cb1}; \qquad V_x = -q_{cb} \cdot l_{cb1}; \qquad M_x = -q_{cb} \cdot \frac{l_{cb1}^2}{2};$

Free body diagram of section II:

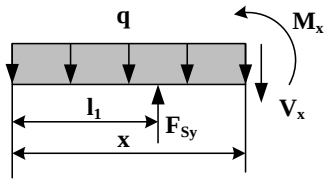

Figure 3.22. Free body diagram of section II.

Static equilibrium equations of section II can be written as follows:

$+\uparrow \sum F_y = 0; \qquad V_x = F_{Sy} - q_{cb} \cdot x;$

$+\circlearrowleft \sum M_x = 0; \qquad M_x = \frac{q_{cb} \cdot l_{cb}}{2} \cdot (x - l_{cb1}) - \frac{q_{cb} \cdot x^2}{2};$

For section II the following assumptions can be written: $l_1 \leq x \leq l_2;$

If, $x = l_{cb1}; \qquad V_x = F_{Sy} - q_{cb} \cdot l_{cb1}; \qquad M_x = \frac{q_{cb} \cdot l_{cb}}{2} \cdot (x - l_{cb1}) - \frac{q_{cb} \cdot x^2}{2};$

If, $x = l_{cb1} + \frac{l_{cb2}}{2}$; $V_x = \frac{q_{cb} \cdot l_{cb}}{2} - q_{cb} \cdot \left(l_{cb1} + \frac{l_{cb2}}{2}\right)$; $M_x = \frac{q_{cb} \cdot l_{cb}}{2} \cdot \frac{l_{cb2}}{2} - q_{cb} \cdot \frac{\left(lcb_1 + \frac{l_{cb2}}{2}\right)^2}{2}$;

If $x = l_{cb1} + l_{cb2}$; $V_x = \frac{q_{cb} \cdot l_{cb}}{2} - q_{cb} \cdot (l_{cb1} + l_{cb2})$; $M_x = \frac{q_{cb} \cdot l_{cb}}{2} \cdot l_2 - \frac{q(l_{cb1} + l_{cb2})^2}{2}$;

The shear force and the bending moment diagrams are shown in 3.23.

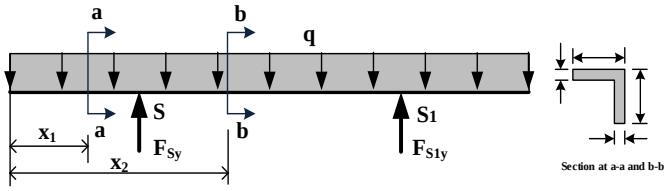

Figure 3.22. Reaction forces at supports S and S1.

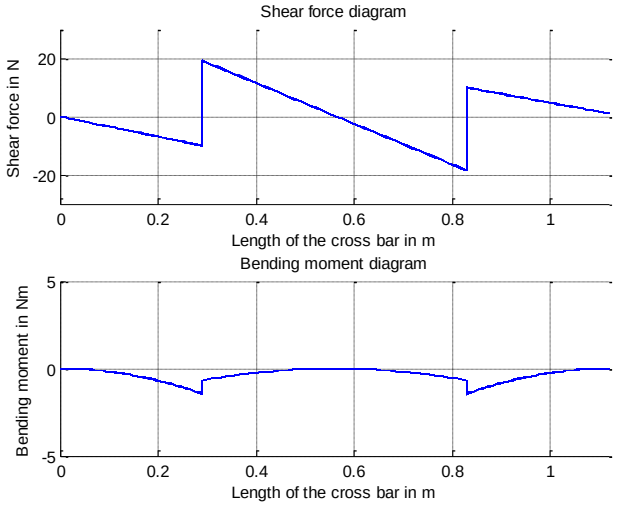

Figure 3.23. Shear stress and bending moment diagrams

Bending strength can be calculated as following equation:

$$\delta = \frac{M_{max}}{S} \leq [\delta]; \qquad (3.7)$$

Here, M_{max} - maximum bending moment; Maximum bending moment value has been taken from MATLAB results and equals to $M_b^{max} = 1.43$ Nm;

S - Section modulus; Section modulus has been taken from the Table 3.2 for xx axis, and equals to $S_{xx} = 0.309\text{in}^3$;

$[\delta]$ - Allowable stress;

$[\delta] = \frac{1.30F_{ty}}{n_y} = \frac{1.30 \cdot 276}{1.65} = 217.45\text{MPa} = 217.45 \cdot 10^6 \frac{N}{m^2}$;

Here, F_{ty}- is the tensile yield strength of the Aluminium 6061-T6, and n_y is a coefficient of safety factor for angle shapes [55].

Bending strength of the cross bar can be found as follows:

$\delta = \frac{M_{max}}{S_{xx}} = \frac{1.43Nm}{0.309\text{in}^3} = \frac{1.43 \cdot Nm}{0.00000506m^3} = 282608.69 \frac{N}{m^2} = 0.283MPa$;

The result is accepted when compared to the allowable stress:

$\delta < [\delta] = 0.283 < 217.45$;

Stress analysis of the longitudinal bar.

It is considered that, the shape of the longitudinal bar is a hollow rectangular as shown in Figure 3.24.

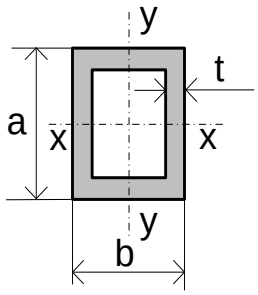

Figure 3.24. The shape of the longitudinal bar

1. Material selection for cross bar.

Longitudinal bars also require corrosion resistant material. Steam of the hot scouring liquor can be rusted the material. Aluminium 6061-T6 can be selected for longitudinal bar. Its density is equals to $\rho_{st} = 2700kg/m^3 = 2.7\ g/cm^3$;

It can be also selected nearly dimensions to the width of the cross bar from the table – "Rectangular tubes" [55].

Figure 3.24. Mechanical properties of selected rectangular tube

Designation	d in, cm	b in, cm	Thickness, t, in, cm	Area A, in^2, cm^2	I_{xx} In^4, cm^4	I_{yy} In^4, cm^4	S_{xx} In^3, cm^3	S_{yy} In^3, cm^3
$1x1\frac{1}{2}x\frac{1}{8}$	1000	1500	0.125	0.563	0.0811	0.159	0.162	0.212
	2.54	4.445	0.3175	1.43	0.206	0.404	0.411	0.538

2. Calculation of volume of the longitudinal bar.

The shape of the longitudinal bar is a hollow rectangular. There are two longitudinal bars in harrow. One of them is shown in Figure 3.25. It is considered that, 20 pieces of cross bars mount on 2 longitudinal bars.

2 a. The dimensions of the longitudinal bar are:

$l = 3080\,mm = 308cm;\ l_1 = 20mm = 2cm;\ \ l_2 = 152mm = 15.2cm;$

$h_1 = 1.905cm;\ h_2 = 2.54cm;\ \ b_1 = 3.175cm;\ \ \ b_2 = 3.81cm;$

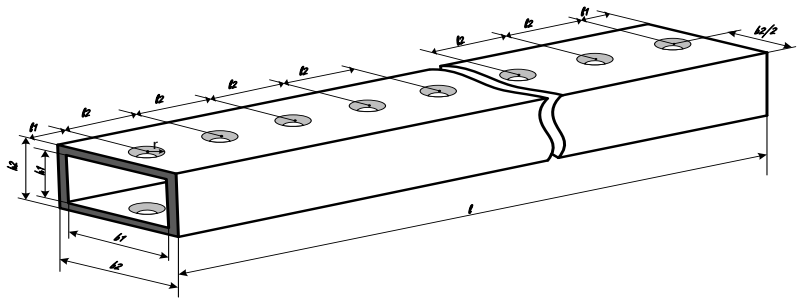

Figure 3.25. The longitudinal bar.

2 a. The volume of the outer rectangular prism:

$V_{outer.l.b} = l \cdot b_2 \cdot h_2 = 308 \cdot 3.81 \cdot 2.54 = 2980.6cm^3;$

2 b. The volume of inner rectangular prism:

$V_{inner.l.b} = l \cdot b_1 \cdot h_1 = 308 \cdot 3.175 \cdot 1.905 = 1862.8cm^3$;

Subtracting the volume of the inner rectangular prism from the volume of the outer rectangular prism gives real volume of the longitudinal bar as follows:

$V_{l.b.r} = V_{outer.l.b} - V_{inner.l.b} = 2980.6 - 1862.8 = 1117.8cm^3$;

3. Calculation of the mass $m_{l.b}$ and the weight W_{lb} of the cross bar.

Mass of the longitudinal bar is a product of the volume and the material density. The density of Aluminium 6061-T6 equals to:

$\rho_{st} = 2700kg/m^3 = 2.7\ g/cm^3$; [54]

$m_{l.b} = V_{l.b.r} \cdot \rho_{st} = 1117.8cm^3 \cdot \frac{2.7\ g}{cm^3} = 3018.1\ g = 3.01kg$;

$W_{lb} = m_{l.b} \cdot g = 3.01kg \cdot 9.81\frac{m}{s^2} = 29.6N$;

4. Calculation of the total load.

It is considered that, 21 pieces of cross bars mount on the harrow. Each cross bar has 13 pieces of prongs. The total mass is a product of mass of the total cross bars and prongs as follow:

$m_{20cb} = (21 \cdot m_{c.b}) + (273 \cdot m_{sh.p}) = 9.59 + 63.8 = 73.39kg$;

The weight of the total cross bars with mounted prongs is:

$W_{20cb} = m_H \cdot g = 73.39kg \cdot 9.81m/s^2 = 720$N;

The total weight of the cross bars acts on the two longitudinal bars as a uniformly distributed load. Stress analysis can be performed for one longitudinal bar. Figure 3.26 shows a longitudinal bar with following dimensions:

$$l_{lb1} = 0.684\ m; \quad l_{lb2} = 1.672\ m; \quad l_{lb} = 3.08\ m;$$

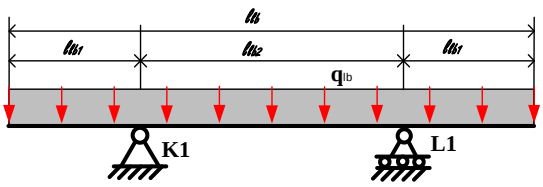

Figure 3.26. Simply supported beam

In order to find the magnitude of the uniformly distributed load, the total load which acts on the longitudinal bar should be determined. And then, obtained magnitude can be divided by entire length of the longitudinal bar as follows:

$$W_{tlb} = \frac{W_{tcb}}{number\ of\ longitudinal\ bars} = \frac{720\text{N}}{2} = 360N;$$

In order to find the magnitude of the uniformly distributed load during working of machine, the total weight of the cross bars, inertia forces and weight of the longitudinal bar can be divided by entire length of the longitudinal bar as follows:

$$q_{lb} = \frac{W_{tlb}+m_{lb}aG_{lby}+W_{lb}}{l_{lb}}; \qquad (3.8)$$

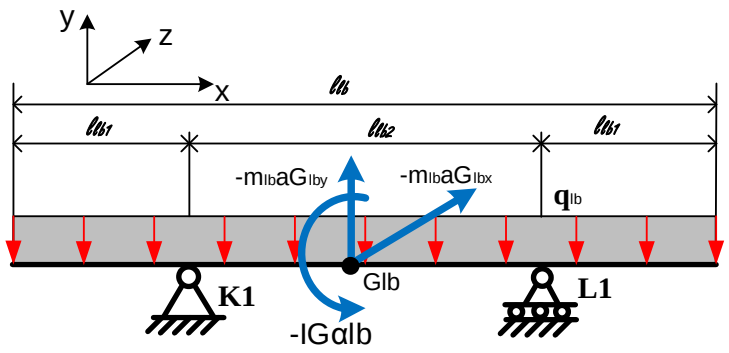

Figure 3.27. Load diagram of the cross bar.

4 a. Calculation of the reaction forces.

The reaction forces of the beam are shown in Figure 3.27. Because the symmetry of forces reaction forces are half of the total load as follow:

$$F_{K1} = F_{L1} = \frac{q_{lb}\cdot l_{lb}}{2}; \qquad (3.9)$$

4 b. Calculation of shear force and bending moment.

The shear force and the bending moment can be calculated by dividing cross sections of the beam as shown in Figure 3.30.

Free body diagram of section I:

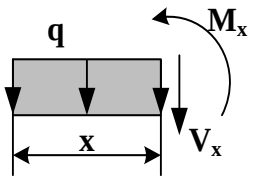

Figure 3.28. Free body diagram of section I.

Static equilibrium equations of section I:

$+\uparrow \sum Fy = 0 \qquad V_x = -q_{lb} \cdot x;$

$+\circlearrowleft \sum M = 0 \qquad M_x = -q_{lb} \frac{x^2}{2};$

For section I following assumptions can be written: $0 \leq x \leq l_1;$

If, $x = 0; \qquad V_x = 0; \qquad M_x = 0;$

If, $x = l_1; \qquad V_x = -q_{lb} \cdot l_{lb1}; \qquad M_x = -q_{lb} \cdot \frac{l_{lb1}^2}{2};$

Free body diagram of section II:

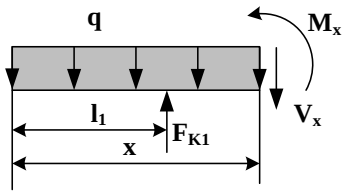

Figure 3.29. Free body diagram of section II.

Static equilibrium equations of section II:

$+\uparrow \sum F_y = 0; \qquad V_x = \frac{q_{lb} \cdot l_{lb}}{2} - q_{lb} \cdot x;$

$+\circlearrowleft \sum M_x = 0; \qquad M_x = \frac{q_{lb} \cdot l_{lb}}{2} \cdot (x - l_{lb1}) - \frac{q_{lb} \cdot x^2}{2};$

For section II the following assumptions can be written: $l_{lb1} \leq x \leq l_{lb2};$

If, $x = l_{lb1}; \qquad V_x = \frac{q_{lb} \cdot l_{lb}}{2} - q_{lb} \cdot l_{lb1}; \qquad M_x = -\frac{q_{lb} \cdot l_{lb1}^2}{2};$

If, $x = l_{lb1} + \frac{l_{lb2}}{2}$; $V_x = \frac{q_{lb} \cdot l_{lb}}{2} - q_{lb}\left(l_{lb1} + \frac{l_{lb2}}{2}\right)$; $M_x = \frac{q_{lb} \cdot l_{lb}}{2} \cdot \frac{l_{lb2}}{2} - \frac{q_{lb}\left(l_{lb1} + \frac{l_{lb2}}{2}\right)^2}{2}$;

If $x = l_{lb1} + l_{lb2}$; $V_x = \frac{q_{lb} \cdot l_{lb}}{2} - q_{lb}(l_{lb1} + l_{lb2})$; $M_x = \frac{q_{lb} \cdot l_{lb}}{2} \cdot l_{lb2} - \frac{q_{lb}(l_{lb1} + l_{lb2})^2}{2}$;

The shear force and the bending moment diagrams are shown in Figure 3.31.

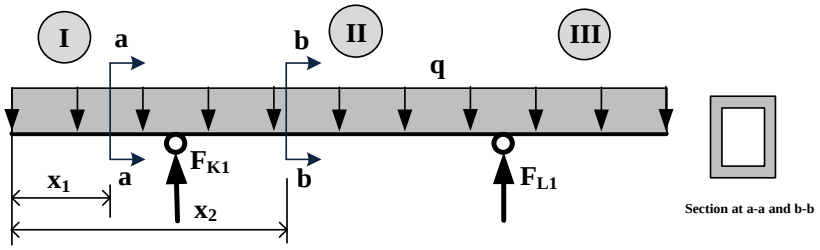

Figure 3.30. Reaction forces in supports K1 and L1.

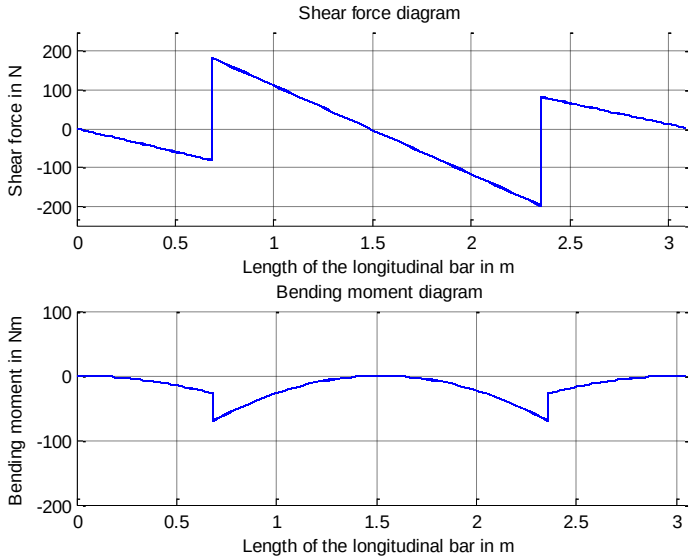

Figure 3.31. Shear force and bending moment diagrams

Actual stress of the longitudinal bar can be found by following formulas:

$$\delta = \frac{M_{max}}{S} \leq [\delta]; \qquad (3.10)$$

Here, M_{max} is a maximum bending moment of the longitudinal bar. Maximum value of the bending moment has been taken from the MATLAB calculation. $M_{max} = 81.4Nm$

S is a cross section of the hollow rectangular shape, and its values depend on different axis as shown in Table 3.3. In this example value of *S* can be selected for xx axis and equals to $S_{xx} = 0.162\text{in}^3$

$$[\delta] = \frac{F_{ty}}{n_y} = \frac{241}{1.65} = 146.6\text{MPa}; \qquad (3.11)$$

Here, F_{ty}- is the tensile yield strength of the Aluminium 6061-T6, and n_y is a coefficient of safety factor for hollow rectangular shapes [54].

$$\delta = \frac{M_{max}}{S_{xx}} = \frac{81.4Nm}{0.162\text{in}^3} = \frac{81.4 \cdot Nm}{0.0000026547m^3} = 30662598.41\frac{N}{m^2} = 30.66MPa;$$

$\delta < [\delta] = 30.66 < 146.6;$ The result is acceptable.

Stress analysis of the shaft 2

It is considered that the shaft 1 and the shaft 2 mount at the two locations on the longitudinal bars. The total weight of the harrow are hanged on the shafts. It is considered that dimensions of the shafts can be determined according to the bowl dimensions. Stress analysis has been performed for shaft 2. Dimensions has been computed respect to the machine capacity. In Figure 3.32, section 1 represents the location of the female end rod bearing, which is connected with its threaded hole part to the short connecting rods. The section 2 represents the location of the pillow block bearing. The pillow block bearings mount on the longitudinal bars.
The diameters of the bearing locations have been selected 20 mm for end rod bearing, and 25 mm for pillow block bearing.
1. Material selection for shaft 2.
Carbon plane steel AISI 1045 [54] has been selected for shaft 2. Section 3.2 gives detailed information about selected material.

2. Calculation of the volume of the shaft 2.
The sketch of the shaft 2 is shown in Figure 3.32. It can be selected as a step shaft, because there are four bearings mount on the shaft 2.

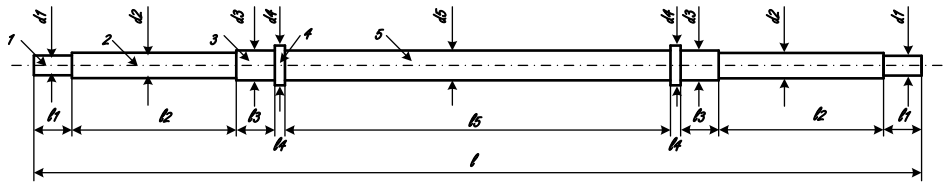

Figure 3.32. The sketch of the shaft 2

The dimensions of the shaft 2 has been selected as follows:

$l = 0.94m;\quad l_1 = 0.03m;\quad l_2 = 0.15m;\quad l_3 = 0.04m;\quad l_4 = 0.01m;\quad l_5 = 0.48m;$
$d_1 = 0.02m;\quad d_2 = 0.024m;\quad d_3 = 0.025m;\quad d_4 = 0.03m;\quad d_5 = 0.025m;$

The volume of the shaft 2 can be calculated as following standard formula for circular solid bar separately for each steps of the shaft. In the following volumes V1 for section 1, V2 for section 2 and V3, V4 and V5 are for sections 3, 4 and 5 respectively.

$V_1 = \pi \cdot r_1^2 \cdot l_1 = 3.14 \cdot 0.01^2 \cdot 0.03 = 0.00000942m^3;$

$V_2 = \pi \cdot r_2^2 \cdot l_2 = 3.14 \cdot 0.012^2 \cdot 0.15 = 0.0000678m^3;$

$V_3 = \pi \cdot r_3^2 \cdot l_3 = 3.14 \cdot 0.0125^2 \cdot 0.04 = 0.0000196m^3;$

$V_4 = \pi \cdot r_4^2 \cdot l_4 = 3.14 \cdot 0.015^2 \cdot 0.01 = 0.00000706m^3;$

$V_5 = \pi \cdot r_5^2 \cdot l_5 = 3.14 \cdot 0.0125^2 \cdot 0.48 = 0.000235m^3;$

2 a. The total volume of the shaft 2 is:

$V_t = 2V_1 + 2V_2 + 2V_3 + 2V_4 + V_5 = 0.00034m^3;$

3. Calculation of mass of the shaft 2.

The mass of the shaft 2 can be calculated as follows:

$m_{sh3} = V_t \cdot \rho = 0.00034m^3 \cdot \frac{7850kg}{m^3} = 2.67$ kg;

Here, ρ- density of carbon plane steel AISI 1045, it is equals to $7850\ \frac{kg}{m^3}$; [54].

4. Calculation of weight of the shaft 2.

The weight of the shaft 2 equals mass times gravitational acceleration as follows:

$W_{sh2} = m_{sh} \cdot g = 2.67 \cdot 9.81 = 26.18\ N;$

It is known that from the stress analysis of the longitudinal bar, the total weight of the harrow is 747.3 N. The shaft 1 and the shaft 2 mount on the longitudinal bars. In order to find the total load which acting on the each shaft, the total weight of the harrow can be divided by equals as follows:

$$F_{sh1} = F_{sh2} = \frac{W_{20cb}+W_{lb}}{2} = \frac{747.3}{2} = 373.65\text{N};$$

The inertia forces and the weight of the shaft act on the shaft as a uniformly distributed load as follow:

$$q_{sh2} = W_{sh2} + m_{sh2}aG_{sh2y}; \qquad (3.12)$$

The shear force and the bending moments of the shafts can be determined for shaft 2. Because, the total load acts symmetrically on the both shafts and their magnitudes are equal. It is considered that, a simply beam is supported at points O_{51} and O_{52}. The vertical loads $F_{D_{1y}}$ and $F_{D_{2y}}$ are acting on the ends of the beam (Figure 3.33). The dimensions of the beam are: $l_{sh1} = 0.2\ m;\ \ l_{sh2} = 0.54\ m;\ \ l_{sh} = 0.94\ m;$

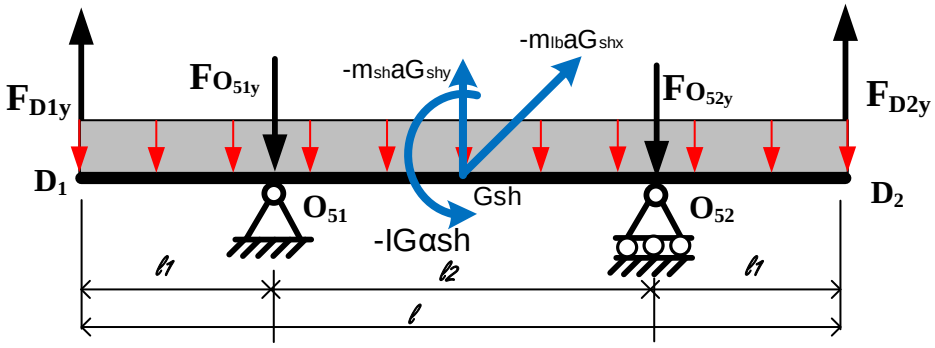

Figure 3.33. Simply supported beam

The free body diagram and the cross sections of the beam is shown in Figure 3.36. In order to determine the reaction forces at supports, the static equilibrium equations of the beam can be written as follows:

$+\uparrow \sum Fy = 0; \quad F_{D1y} - F_{O51y} - F_{O52y} + F_{D2y} = 0;$

$F_{D1y} + F_{D2y} = F_{O51y} + F_{O52y};$

$F_{D1y} = F_{D2y} = \frac{F_{sh2}+q_{sh2}}{2};$

From the symmetry of the supports, the reaction forces are equal to the total loads, and they can be represented as follows:

$$F_{O51y} = F_{O52y} = F_{D1y} = F_{D2y};$$

$\circlearrowleft + \sum M = 0;$ $\qquad M = F_{D2y}(l_{sh2} + l_{sh1}) - F_{O52y} \cdot l_{sh2} - F_{D1y} \cdot l_2;$

The shear force and the bending moment of the shaft can be determined dividing by cross sections (Figure 3.36).

Free body diagram of section I:

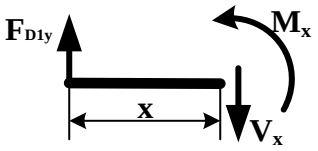

Figure 3.34. Free body diagram of section I.

Static equilibrium equations for section I, can be written as follows:

$+\uparrow \sum Fy = 0;$ $\qquad V_x = F_{D1y};$

$\circlearrowleft + \sum M = 0;$ $\qquad M_x = F_{D1y} \cdot x;$

For section I, the following assumptions can be written: $0 \le x \le l_1;$

If $x = 0;$ $\qquad V_x = F_{D1y};$ $\qquad M_x = 0;$

If $x = l_{sh1};$ $\qquad V_x = F_{D1y};$ $\qquad M_x = F_{D1y} \cdot l_{sh1};$

Free body diagram of section II:

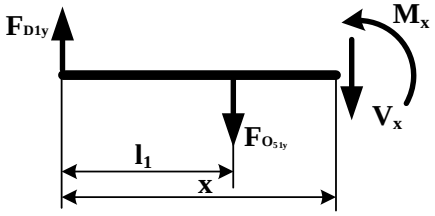

Figure 3.35. Free body diagram of section II.

Static equilibrium equations for section II, can be written as follows:

$+\uparrow \sum Fy = 0;$ $\qquad V_x = F_{O51y} - F_{D1y};$

$\circlearrowleft + \sum M = 0;$ $\qquad M_x = F_{D1y} \cdot x - F_{O51y} \cdot (x - l_{\mathrm{sh1}});$

For section II, for following assumptions can be written: $l_{sh1} \le x \le l_{sh2};$

If $x = l_{sh1} + \frac{l_{sh2}}{2};$ $\qquad V_x = F_{D1y} - F_{O51y};$ $\qquad M_x = F_{D1y} \cdot (l_{sh1} + \frac{l_{sh2}}{2}) - F_{O51y} \cdot \frac{l_{sh2}}{2};$

If $x = l_{sh1} + l_{sh2}$; $V_x = F_{O51y} - F_{O52y} - F_{D1y}$; $M_x = F_{D1y} \cdot (l_{sh1} + l_{sh2}) - F_{O51y}(l_{sh2})$;

The shear force and the bending moment diagrams are shown in Figure 3.37.

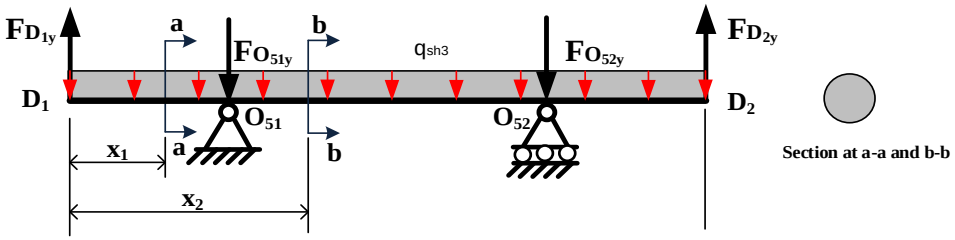

Figure 3.36. Reaction forces of the beam

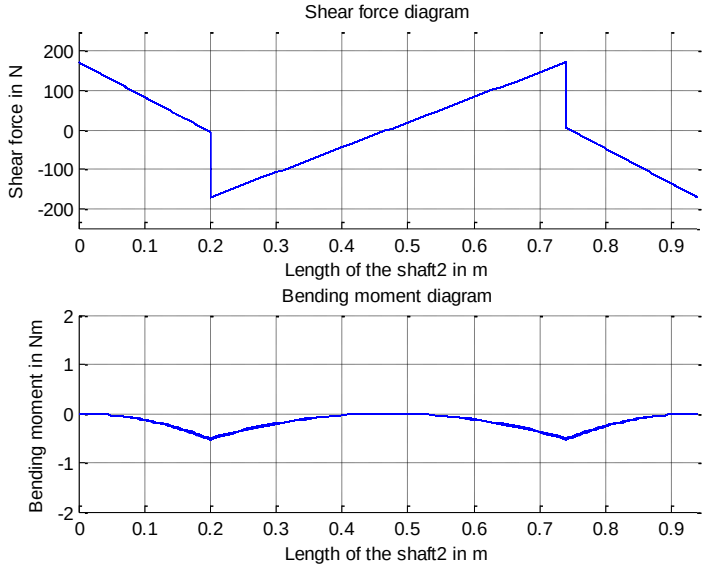

Figure 3.37. Shear force and bending moment diagrams

5. Determination of actual stress of the shaft 2.

Actual stress of the shaft 2 can be determined by following formulas:

$$\delta = \frac{M_b^{max}}{S}; \qquad (3.13)$$

Here, M_b^{max}- maximum bending moment. Maximum value of the bending moment has been taken from the MATLAB calculation. $M_{max} = 0.5374Nm$

S – Section modulus; section modulus for solid circular shape – $S = \frac{\pi \cdot d^3}{32} = 0.1 \cdot d^3$;

d - Diameter of the shaft.

The bending stress of the shaft 2 should be smaller than allowable bending stress as follows: $\delta \leq [\delta]$;

$[\delta]$ - Allowable stress of circular cross section,

$[\delta] = 0.60\text{Fty} = 0.60 \cdot 310 = 186\text{MPa}$

Here, Fty - is the tensile yield strength of the steel AISI 1045.

Equation (3.13) can be rewritten as follows:

$$\frac{M_b^{max}}{0.1 \cdot d^3} \leq [\delta];$$

It is considered that the small diameter of the shaft at location 1 equals to 20 mm. Actual stress can be calculated as follows:

$\delta = \frac{M_b^{max}}{\frac{\pi \cdot d^3}{32}} = \frac{0.5374Nm}{0.1 \cdot 20^3\, mm^3} = \frac{0.5374Nm}{800 \cdot 10^{-9} m^3} = 671750N/m^2 = 0.671MPa;$

$\delta < [\delta] = 0.671 < 186;$ The result is accepted.

Stress analysis of the short connecting rod

The short connecting rods connect to the shaft 2 and upper shaft 2 by their two ends. It is considered that, both ends of the short connecting rods are the threaded shank and connect to the shafts with female end rod bearings. Sketch of the short connecting rod is shown in Figure 3.38.

It is considered that, the shape of the cross section of the short connecting rod is a circular form. The inner diameter of the end rod bearings should be equals to the small diameter of the shaft 2. The small diameter of the shaft 2 is known from the previous stress analysis and equals to 20mm or 0.02 m. End rod bearing DIN ISO 12240-4 (DIN 648 E series) has been selected from the MBO catalogue [58]. The inner diameter of the selected bearing equals to 20 mm. The diameter of the

threaded hole equals M20x1.5. From the center of the inner diameter of the bearing to the end equals 77 mm. The depth of the threaded hole equals to 40 mm. The difference between these lengths equals to 37 mm. The total difference of two bearings equal 74 mm. The distance between centers of the mounted bearings known from the position analysis of the proposed machine and equals to 440 mm or 0.44m. The section 3.3 gives detailed information about selected bearings.

In order to find the real length l of the short connecting rod (Figure 3.38), the total differences of the bearings should be subtracted from the distance of the bearing centers as follow:

$$l = 440 - 74 = 366mm = 0.366m;$$

$$l_1 = l - 2 * l_2 = 366 - 2 * 40 = 286mm = 0.286m;$$

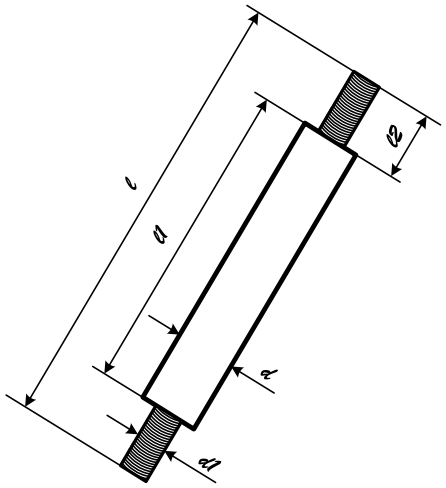

Figure 3.37. The sketch of the short connecting rod.

The selected dimensions of the short connecting rod:

$l = 366mm = 0.366m; \quad l_1 = 286mm = 0.286m; \quad l_2 = 40mm = 0.04m;$
$d = 25mm = 0.025m; \quad d_1 = 20mm = 0.02m;$

The volume, the mass and the weight of the rod can be calculated as following equations:

Radius of the rod: $r = \frac{d}{2} = \frac{25}{2} = 12.5mm = 0.0125m;$

$V = \pi \cdot r^2 \cdot l = 3.14 \cdot 0.0125^2 \cdot 0.366 = 0.000179m^3;$

The mass of the connecting rod can be calculated as product of volume and density of material. Carbon plane steel AISI 1045 has been selected for short connecting rod. The density of the selected material equals to $7850\ \frac{kg}{m^3}$;

$m_{cr3} = V_t \cdot \rho = 0.000179 m^3 \cdot \frac{7850 kg}{m^3} = 1.4$ kg;

The weight of the connecting rod is a product of the mass and the gravity force:

$W_{cr3} = m_{cr3} \cdot g = 1.4 \cdot 9.81 = 13.79\ N;$

According to the kinetostatic analysis (Section 2.3) of the proposed machine, tension forces act on the short connecting rod (Figure 3.39). Medium carbon steel AISI 1045 has been selected for short connecting rod.

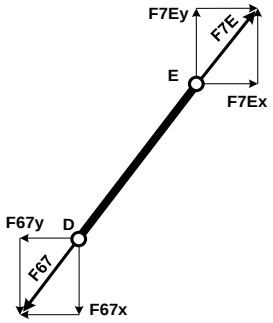

Figure 3.39. Reaction forces of short connecting rod.

In order to determine the maximum tensile stress of the short connecting rod, the reaction forces, the inertia forces and the mass moments of inertia should be taken into consideration.

Tensile stress of the short connecting rod can be calculated as follows:

$$\sigma_t = \frac{P}{A}; \qquad (3.14)$$

Where, σ_t – tensile stress, (N/mm^2);

P- External force (N); $P = F_{67x} + F_{67y} = F_{67}$; $F_{67} = F_{7E}$;

A- Cross sectional area (mm^2);

Maximum stress should be small or equals to the allowable stress as follows:

$\sigma_t = \frac{P}{A} \leq [\sigma_t]$;

$[\delta]$ - Allowable stress of circular cross section,

$[\delta] = 0.60\text{Fty} = 0.60 \cdot 310 = 186\text{MPa}$

Here, Fty - is the tensile yield strength of the medium carbon steel AISI 1045.

Actual stress of the short connecting rod has been calculated by MATLAB program. The plot of the actual stress is shown in Figure 3.40. The maximum tensile stress compares with allowable stress in order to verify diameter of the short connecting rod.

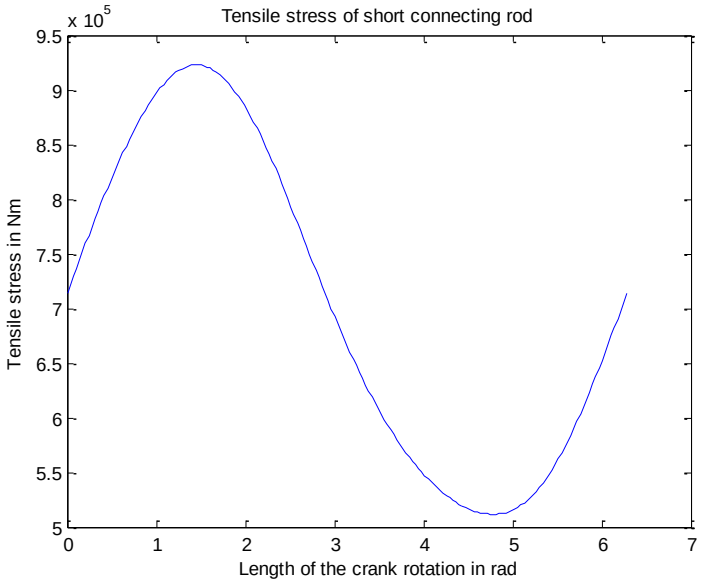

Figure 3.40. Plot of the tensile stress of the short connecting rod.

Maximum value of the tensile stress has been taken from the MATLAB calculation:

$\sigma_t = 922800.06 \frac{N}{m^2} = 0.922\ Mpa$;

$\sigma_t \leq [\delta] = 0.885 < 186$

The result is acceptable.

Stress analysis of the long connecting rod.

According to the position analysis of the proposed mechanism (Section 2.2.1), the two pieces of the long connecting rods connect to the two upper shafts. Both connecting rods are supported at their two ends by end rod bearings. In the previous stress analysis of the short connecting rod, the diameter of the end rod bearings has been found, it is equals 20 mm. The diameter of end rod bearings of the long connecting rods location should be bigger than previous. Because, the end rod bearings of the long connecting rods locate near the centre of the shaft. It is known that, the diameters of bearings location of the step shafts diminish from centre to end of the shaft. End rod bearing DIN ISO12240-4 (DIN 648 E series) has been selected for long connecting rods from the MBO catalogue [58]. The inner diameter of the selected bearing equals to 25 mm. The diameter of the threaded hole equals M24x2. From the center of inner diameter of the bearing to the end equals 94 mm. The depth of the threaded hole equals to 48 mm. The difference between these lengths equals to 46 mm. The total difference of two bearings equal 92 mm. The distance between centers of the mounted bearings known from the position analysis of the proposed machine and equals to 1672 mm or 1.672m. The depth of the threaded hole equals to 48 mm. The section 3.3 gives detailed information about selected bearings.

In order to find the real length l of the long connecting rod (Figure 3.41), the total differences of the bearings should be subtracted from the distance of the bearing centers as follow:

$$l = 1672 - 92 = 1580mm = 1.58m;$$

$$l_2 = l - 2 * l_1 = 1580 - 2 * 48 = 1484\ mm = 1.484m$$

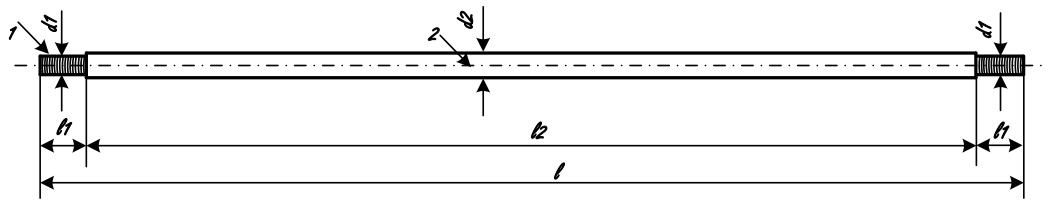

Figure 3.41. The sketch of the connecting rod

The selected dimensions of the long connecting rod equal to:

$l = 1.58m; \quad l_1 = 0.048m; \quad l_2 = 1.484m; \quad d_1 = 0.024m; \quad d_2 = 0.03m;$

2. Calculation of the volume, mass end weight of the long connecting rod.

The volume of the long connecting rod can be calculated as following standard formula for circular solid bar separately for two different parts:

$V_1 = \pi \cdot r_1^2 \cdot l_1 = 3.14 \cdot 0.012^2 \cdot 0.048 = 0.0000217m^3;$

$V_2 = \pi \cdot r_2^2 \cdot l_2 = 3.14 \cdot 0.015^2 \cdot 1.484 = 0.00105m^3;$

The total volume of the long connecting rod:

$V_t = 2V_1 + 2V_2 = 2 \cdot 0.0000217 + 0.00105 = 0.0011m^3;$

The mass of the long connecting rod can be calculated as product of volume and density of material. Carbon plane steel AISI 1045 has been selected for long connecting rod. Density of the selected material equals to $7850\ \frac{kg}{m^3}$;

$m_{lcr} = V_t \cdot \rho = 0.0011m^3 \cdot \frac{7850kg}{m^3} = 8.96$ kg;

The weight of the long connecting rod is a product of the mass and the acceleration of gravity:

$W_{lcr1} = m_{lcr} \cdot g = 8.96 \cdot 9.81 = 87.9\ N;$

In order to find the magnitude of the uniformly distributed load, the weight of the connecting rod times inertia force are divided by entire length of the connecting rod as follows:

$$q_{lcr} = \frac{W_{lcr} \cdot m_5 a_{G5y}}{length\ of\ connecting\ rod}; \qquad (3.15)$$

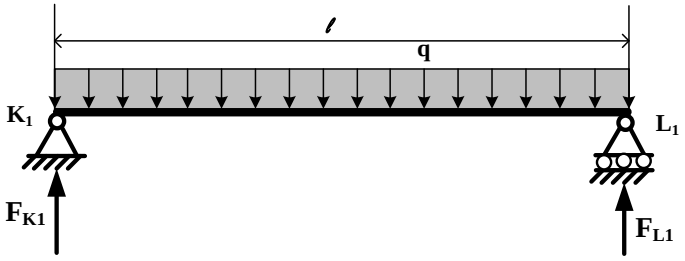

Figure 3.42. The uniformly distributed load which is acting on the long connecting rod.

3. Calculation of the reaction forces.

The reaction forces of the beam are shown in Figure 3.39. Reaction forces can be calculated by dividing the distributed load by equal because the symmetry of forces as follows:

$$F_{K1} = F_{L1} = \frac{q_{lcr} \cdot l_{lcr}}{2};$$

4. Calculation of the shear force and the bending moment.

The shear force and the bending moment can be calculated by dividing the cross sections as shown in Figure 3.45.

Free body diagram of section I:

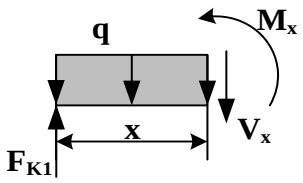

Figure 3.43. Free body diagram of the cross section I.

$+\uparrow \sum Fy = 0;$ $\qquad V_x = q_{lcr} \cdot x - F_{K1};$

$\circlearrowleft + \sum M = 0;$ $\qquad M_x = F_{K1} \cdot x - q_{lcr} \cdot \frac{x^2}{2};$

For section I following assumptions can be written: $0 \leq x \leq \frac{q_{lcr}}{4};$

If, $x = 0;$ $\qquad V_x = 0;$ $\qquad M_x = 0;$

If, $x = \frac{l}{4}$; $V_x = q_{lcr} \cdot \frac{l_{lcr}}{4} - F_{K1}$; $M_x = F_{K1} \cdot \frac{l_{lcr}}{4} - q_{lcr} \cdot \frac{(\frac{l_{lcr}}{4})^2}{2}$;

Free body diagram of section II:

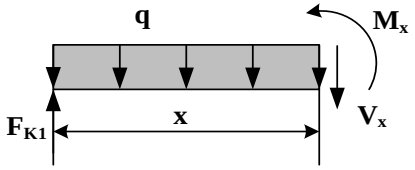

Figure 3.44. Free body diagram of the cross section II.

$+\uparrow \sum Fy = 0$; $V_x = q_{lcr} \cdot x - F_{K1}$;

$\circlearrowleft + \sum M = 0$; $M_x = F_{K1} \cdot x - q_{lcr} \cdot \frac{x^2}{2}$;

For section II the following assumptions can be written: $\frac{q_{lcr}}{4} \leq x \leq \frac{q_{lcr}}{2}$;

If, $x = \frac{l_{lcr}}{3}$; $V_x = q_{lcr} \cdot \frac{l_{lcr}}{3} - F_{K1}$; $M_x = F_{K1} \cdot \frac{l_{lcr}}{3} - q_{lcr} \cdot \frac{(\frac{l_{lcr}}{3})^2}{2}$;

If, $x = \frac{l_{lcr}}{2}$; $V_x = q_{lcr} \cdot \frac{l_{lcr}}{2} - F_{K1}$; $M_x = F_{K1} \cdot \frac{l_{lcr}}{2} - q_{lcr} \cdot \frac{(\frac{l_{lcr}}{2})^2}{2}$;

The shear force and the bending moment diagrams are shown in Figure 3.46.

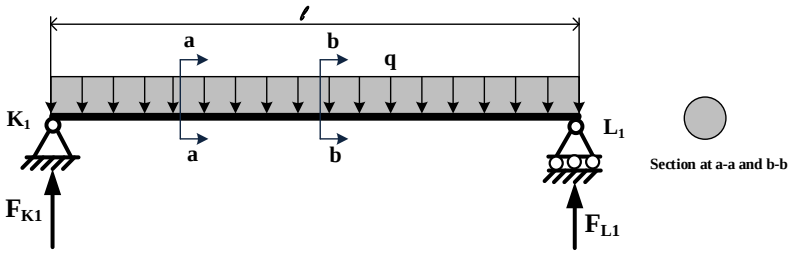

Figure 3.45. Reaction forces at supports K1 and L1.

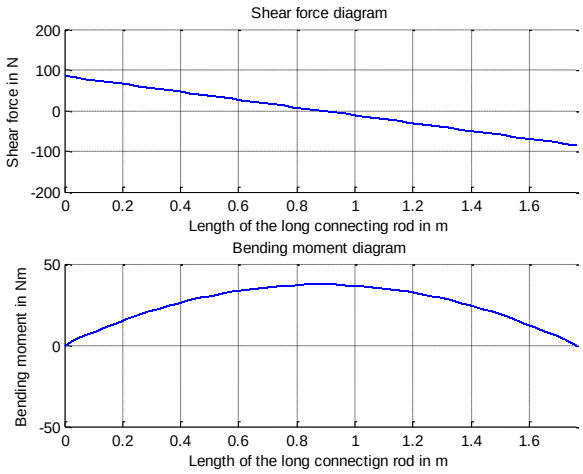

Figure 3.46. Shear force and bending moment diagrams

5. Determination of actual stress of the long connecting rod.

Actual stress of the long connecting rod can be determined by following formulas:

$$\delta = \frac{M_b^{max}}{S}; \qquad (3.16)$$

Here, M_b^{max}- maximum bending moment, Maximum value of the bending moment has been taken from the MATLAB calculation. $M_{max} = 37.25$

S – Section modulus;

Section modulus for solid circular shape - $S = \frac{\pi \cdot d^3}{32} = 0.1 \cdot d^3$;

Bending strength of the long connecting rod should be smaller than allowable bending stress as follows:

$\delta \leq [\delta]$;

Here, $[\delta]$ - Allowable stress of circular cross section,

$[\delta] = 0.60 \cdot \text{Fty} = 0.60 \cdot 310 = 186\text{MPa}$

Here, Fty - is the tensile yield strength of the medium carbon steel AISI 1045.

Equation (3.16) can be rewritten as follows:

$\frac{M_b^{max}}{0.1 \cdot d^3} \leq [\delta];$

Actual stress can be calculated as follows:

$$\delta = \frac{M_b^{max}}{0.1 \cdot d^3} = \frac{37.25Nm}{0.1 \cdot 20^3\ mm^3} = \frac{37.25Nm}{800 \cdot 10^{-9} m^3} = 46562500N/m^2 = 46.56MPa;$$

The result is acceptable when compared to the allowable stress:

$\delta < [\delta] = 46.56 < 186;$

Stress analysis of the upper shaft 2.

The proposed mechanism has two upper shafts. These shafts are not for transmission purposes, they are only used as a support for rotating members such as bearings. Two long connecting rods and two short connecting rods mount on the shaft within their end rod bearings. Two levers are raised up the upper shafts with their upper ends. The shape of the upper shaft can be considered according to the previous stress analysis, and the diameters of locations of the bearings are known (Figure 3.47). Because, the bearings of the short and long connecting rods are selected in their stress analysis.

The sketch of the upper shaft 2 is shown in Figure 3.47. It can be selected as a step shaft, because there are 6 bearings mount on the upper shaft 2. In order to find the volume, mass and weight of the upper shaft 2, each step of the shaft can be calculated separately as follows:

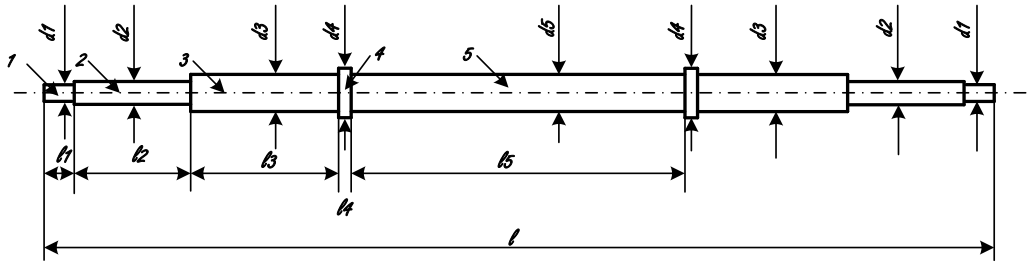

Figure 3.47. The sketch of the upper shaft 2.

Dimensions of the upper shaft 2:

$l = 1.44m; \quad l_1 = 0.03m; \quad l_2 = 0.235m; \quad l_3 = 0.2m; \quad l_4 = 0.01m; \quad l_5 = 0.49m;$

$d_1 = 0.017m;$ $d_2 = 0.02m;$ $d_3 = 0.025m;$ $d_4 = 0.03m;$ $d_5 = 0.025m;$

1. Calculation of the volume.

The volume of the upper shaft 2 can be calculated as follows standard formula for circular solid bar separately for each steps of the shaft as follows:

$V_1 = \pi \cdot r_1^2 \cdot l_1 = 3.14 \cdot 0.0085^2 \cdot 0.03 = 0.00000980m^3;$

$V_2 = \pi \cdot r_2^2 \cdot l_2 = 3.14 \cdot 0.01^2 \cdot 0.235 = 0.0000737m^3;$

$V_3 = \pi \cdot r_3^2 \cdot l_3 = 3.14 \cdot 0.0125^2 \cdot 0.2 = 0.0000981m^3;$

$V_4 = \pi \cdot r_4^2 \cdot l_4 = 3.14 \cdot 0.015^2 \cdot 0.01 = 0.00000706m^3;$

$V_5 = \pi \cdot r_5^2 \cdot l_5 = 3.14 \cdot 0.0125^2 \cdot 0.48 = 0.000235m^3;$

The total volume of the upper shaft 2:

$V_t = 2V_1 + 2V_2 + 2V_3 + 2V_4 + V_5 = 0.000423m^3;$

2. Calculation of mass of the upper shaft 2

The mass of the upper shaft 2 can be calculated as a product of volume and density of material as follows:

$m_{ush2} = V_t \cdot \rho = 0.000423m^3 \cdot \frac{7850kg}{m^3} = 3.32$ kg;

3. Calculation of weight of the upper shaft 2

The weight of the upper shaft 2 is a product of the mass and the acceleration of gravity:

$W_{ush2} = m_{ush2} \cdot g = 3.32 \cdot 9.81 = 32.62\ N;$

It is known that from the stress analysis of the longitudinal bar, the total weight of the harrow is 747.3 N. The harrow hangs on to the two ternary links and two short connecting rods. And its total weight is distributed by 4 bearings. The half of the total weight of the harrow and total weight of the short longitudinal bars, and half of the total weight of the long connecting rods act on two locations of the shaft 2 as shown in Figure 3.48, and can be written as follows:

$W_{harrow} = W_{20cb} + 2 * W_{lb} + 2 * W_{sh2};$

$F_{E_{1y}} = \frac{W_{harrow}}{4} + W_{cr3};$ $\quad F_{E_{1y}} = F_{E_{2y}};$

$F_{L_1} = \frac{W_{lcr1}}{2};$ $\quad F_{L_1} = F_{L_2};$

Total loads which are acting on the upper shaft can be calculated as follows:

$$F_{total} = F_{E_{1y}} + F_{E_{2y}} + F_{L_{1y}} + F_{L_{2y}};$$

It is considered that, a simply beam is supported at points J_1 and J_2. The vertical loads $F_{E_{1y}}$, $F_{E_{2y}}$, $F_{L_{1y}}$ and $F_{L_{2y}}$are acting on the four locations of the beam (Figure 3.48). Dimensions of the beam are:

$l_{ush1} = 0.25\ m;$ $\quad l_{ush2} = 0.2\ m;$ $\quad l_{ush3} = 0.54\ m;$ $\quad l_{ush} = 1.44\ m;$

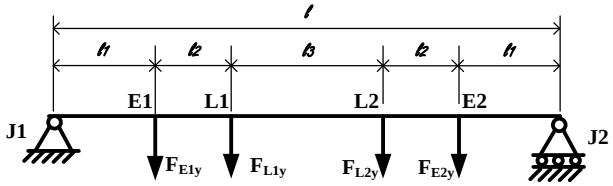

Figure 3.48. The load diagram of the upper shaft 2.

In order to find the magnitude of the uniformly distributed load, the weight of the upper shaft 2 times inertia force are divided by entire length of the upper shaft 2 as follows:

$$q_{ush2} = \frac{W_{ush2} + m_{ush2} a_{Gush2y}}{l_{ush2}}; \qquad (3.17)$$

4) Calculation of the reactions forces of the upper shaft 2.

$$F_{J1y} = F_{J2y} = \frac{F_{total} + q_{ush2}}{2};$$

5) Calculation of the shear force and the bending moment.

Shear force and bending moment can be calculated by dividing cross sections (Figure 3.53).

Free body diagram of section I:

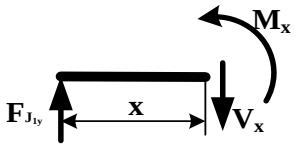

Figure 3.49. Free body diagram of the section I

Static equilibrium equations of section I:

$+\uparrow \sum Fy = 0; \qquad V_x = F_{J1y};$

$\circlearrowleft + \sum M = 0; \qquad M_x = F_{J1y} \cdot x;$

For section I following assumptions can be written: $0 \leq x \leq l_1;$

If, $x = 0; \qquad V_x = 0; \qquad M_x = 0;$

If, $x = l_{ush1}; \qquad V_x = F_{J1y}; \qquad M_x = F_{J1y} \cdot l_{ush1};$

Free body diagram of section II:

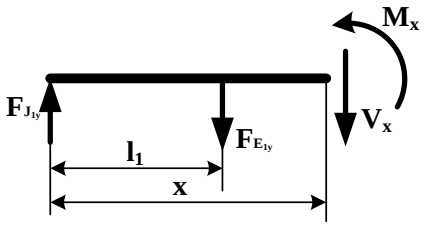

Figure 3.50. Free body diagram of section II.

Static equilibrium equations of section II:

$+\uparrow \sum Fy = 0; \qquad V_x = F_{J1y} - F_{E1y};$

$\circlearrowleft + \sum M = 0; \qquad M_x = F_{J1y} \cdot x - F_{E1y}(x - l_1);$

For section II following assumptions can be written: $l_1 \leq x \leq l_2;$

If, $x = l_{ush1} + \frac{l_{ush2}}{2}; \quad V_x = F_{J1y} - F_{E1y}; \quad M_x = F_{J1y} \cdot l_{ush1} + \frac{l_{ush2}}{2} - F_{E1y} \cdot \frac{l_{ush2}}{2};$

If, $x = l_{ush1} + l_{ush2}; \quad V_x = F_{J1y} - F_{E1y}; \quad M_x = F_{J1y} \cdot l_{ush1} + l_{ush2} - F_{E1y} \cdot (l_{ush1} + l_{ush2});$

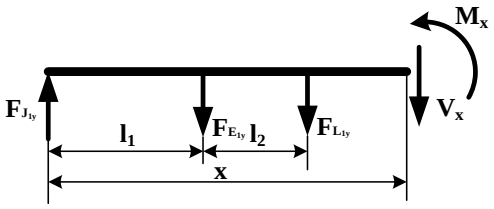

Figure 3.51. Free body diagram of section III.

Static equilibrium equations of section III:

$+\uparrow \sum Fy = 0;$ $V_x = F_{J1y} - F_{E1y} - F_{L1y};$

$\circlearrowleft + \sum M = 0;$ $M_x = F_{J1y} \cdot x - F_{E1y}(x - l_{ush1}) - F_{L1y}(x - l_{ush1} + l_{ush2});$

For section III following assumptions can be written: $l_1 + l_2 \leq x \leq l_3;$

If, $x = \frac{l_{ush}}{2};$ $V_x = F_{J1y} - F_{E1y} - F_{L1y};$

$$M_x = F_{J1y} \cdot \frac{l_{ush}}{2} - F_{E1y}\left(\frac{l_{ush}}{2} - l_{ush1}\right) - F_{L1y}\left(\frac{l_{ush}}{2} - l_{ush1} + l_{ush2}\right);$$

Shear force and bending moment diagrams are shown in Figure 3.53.

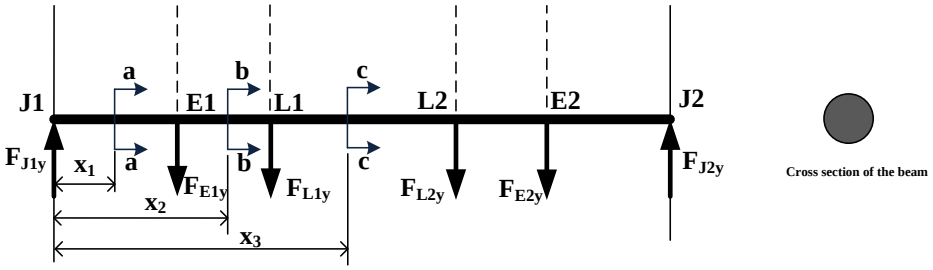

Figure 3.52. Cross sections of the beam

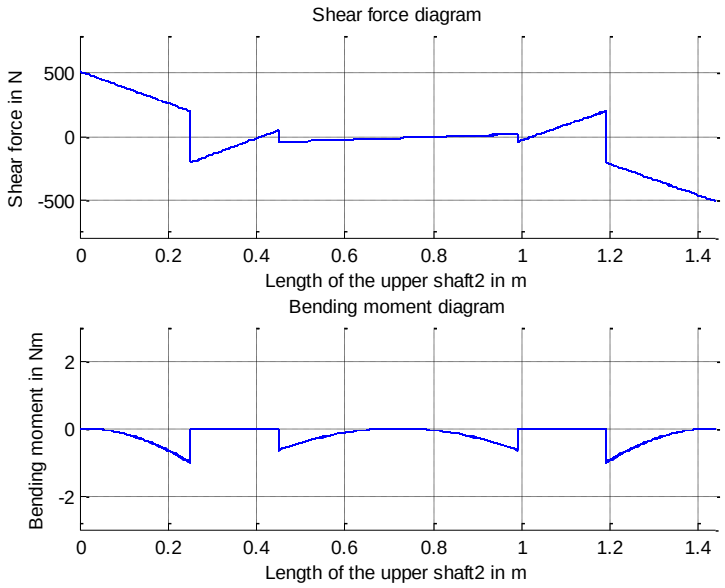

Figure 3.53. Shear force and bending moment diagrams.

6. Determination of the actual stress of the upper shaft.

The actual stress of the upper shaft 2 can be determined by following formulas:

$$\delta = \frac{M_b^{max}}{S}; \qquad (3.18)$$

Here, M_b^{max}- maximum bending moment. Maximum value of the bending moment has been taken from the MATLAB calculation. $M_{max} = 1.03$

S – Section modulus; section modulus for solid circular shape - $S = \frac{\pi \cdot d^3}{32} = 0.1 \cdot d^3$;

d - Diameter of the shaft.

Bending stress of the upper shaft 2 should be smaller than allowable bending stress as follows:

$\delta \leq [\delta]$;

$[\delta]$ - Allowable stress of circular cross section,

$[\delta] = 0.60\text{Fty} = 0.60 \cdot 310 = 186\text{MPa}$

Here, Fty - is the tensile yield strength of the medium carbon steel AISI 1045.

Equation (3.18) can be rewritten as follows:

$$\frac{M_b^{max}}{0.1 \cdot d^3} \leq [\delta];$$

Actual stress can be calculated as follows:

$$\delta = \frac{M_b^{max}}{\frac{\pi \cdot d^3}{32}} = \frac{1.03Nm}{0.1 \cdot 25^3\ mm^3} = \frac{1.03Nm}{1562.5 \cdot 10^{-9} m^3} = 659411.01N/m^2 = 0.65MPa;$$

The result is acceptable when compared to the allowable stress:

$\delta < [\delta] = 0.65 < 186;$

Stress analysis of the lever 3

There are four levers in the proposed mechanism. Levers connect to the upper shafts with their upper ends, and to the bottom shafts with their bottom ends by end rod bearings.

It is considered that, the shape of the cross section of the lever 3 is a circular form. The inner diameter of the end rod bearings should be equals to the small diameter of the upper shaft 2. The small diameter of the upper shaft 2 is known from the previous stress analysis and equals to 17 mm or 0.017 m. End rod bearing DIN ISO 12240-4 (DIN 648 E series) has been selected from the MBO catalogue [58]. The inner diameter of the selected bearing equals to 20 mm. The diameter of the threaded hole equals M16. From the center of the inner diameter of the bearing to the end equals 67 mm. The depth of the threaded hole equals to 33 mm. The difference between these lengths equals to 34 mm. The total difference of two bearings equal 68 mm. The distance between centers of the mounted bearings known from the position analysis of the proposed machine and equals to 793 mm or 0.793m. The section 3.3 gives detailed information about selected bearings.

In order to find the real length l of the lever 3 (Figure 3.54), the total differences of the bearings should be subtracted from the distance of the bearing centers as follow:

$$l = 793 - 68 = 725mm = 0.725m;$$

$$l_1 = l - 2 * l_2 = 725 - 2 * 33 = 659mm = 0.659m;$$

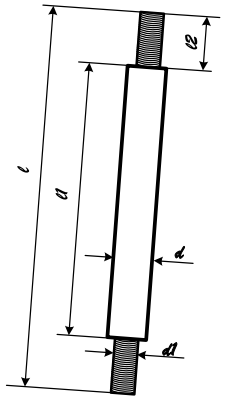

Figure 3.54. The sketch of the lever3

The selected dimensions of the lever 3:

$l = 725mm = 0.725m; \quad l_1 = 659mm = 0.659m; \quad l_2 = 33mm = 0.033m;$
$d = 20mm = 0.02m; \quad d_1 = 16mm = 0.016m;$

Volume, mass and the weight of the lever3 can be calculated as follows:

Radius of the lever: $r = \frac{d}{2} = \frac{20}{2} = 10mm = 0.01m;$

$V = \pi \cdot r^2 \cdot l = 3.14 \cdot 0.01^2 \cdot 0.725 = 0.00023m^3;$

The mass of the lever 3 can be calculated as product of volume and density of material. Carbon plane steel AISI 1045 has been selected for the lever 3. The density of the selected material equals to $7850\ \frac{kg}{m^3}$;

$m_{lever3} = V_t \cdot \rho = 0.00023m^3 \cdot \frac{7850kg}{m^3} = 1.81$ kg;

The weight of the lever 3 is a product of the mass and the gravity force:

$W_{lever3} = m_{lever3} \cdot g = 1.81 \cdot 9.81 = 17.75N;$

According to the kinetostatic analysis, the compressive forces act on the levers. The compressive forces are illustrated in Figure 3.55.

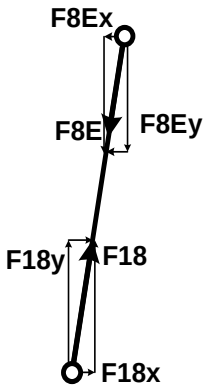

Figure 3.55. The load diagram of the lever 3.

In order to determine the maximum compressive stress of the lever 3, the reaction forces, the inertia forces and the mass moments of inertia should be taken into consideration.

Compressive stress calculates as follows:

$$\sigma_c = \frac{P}{A}; \qquad (3.19)$$

Where, σ_c – compressive stress, (N/mm^2);

P- External force (N); $P = F_{8Ex} + F_{8Ey} = F_{8E}$;

A- Cross sectional area (mm^2);

Maximum stress should be small or equals to the allowable stress as follows:

$\sigma_t = \frac{P}{A} \leq [\sigma_t]$;

$[\delta]$ - Allowable stress of circular cross section,

$[\delta] = 0.60\text{Fty} = 0.60 \cdot 310 = 186\text{MPa}$

Here, Fty - is the tensile yield strength of the medium carbon steel AISI 1045.

Actual stress of the lever 3 has been calculated by MATLAB program. The plot of the actual stress is shown in Figure 3.53. The maximum compressive stress compares with allowable stress in order to verify the diameter of the lever3.

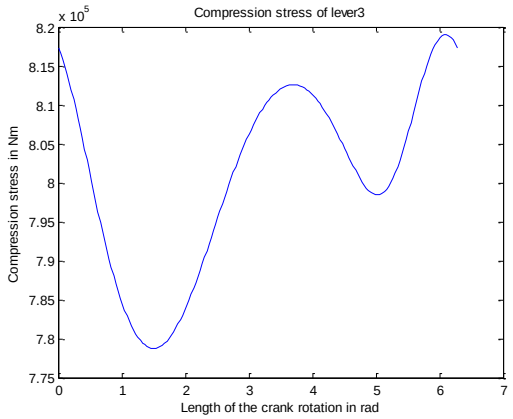

Figure 3.56. Plot of the compressive stress of the lever 3.

Maximum value of the compressive stress has been taken from the MATLAB calculation:

$\sigma_t = 818967.63 \frac{N}{m^2} = 0.819\ Mpa;$

$\sigma_t \leq [\delta] = 0.792 < 186$

The result is acceptable.

Stress analysis of the bottom shaft2

There are two bottom shafts in the proposed machine. Bottom shafts can be mounted with journal bearings on the frame of the machine. They are installed under the scouring bowl. Sketch of the bottom shaft 2 is shown in Figure 3.57.

In Figure 3.57, the section 1 represents the location of the end rod bearing. The section 2 represents the location of the pillow block journal bearing. The diameter of section 1 is known from the stress analysis of the lever 3 and equal 0.017 m. The same size with other end rod bearing has been selected, such us DIN ISO12240-4 (DIN 648 E series) from the MBO catalogue [58]. The diameter of the section 2 should be bigger than the diameter of the end rod bearing. The diameter of the journal bearing location has been selected as 0.025 m. The journal bearing SY 25 TF has been selected from the SKF catalogue [57]. The detailed information about bearings has been presented in section 3.3.

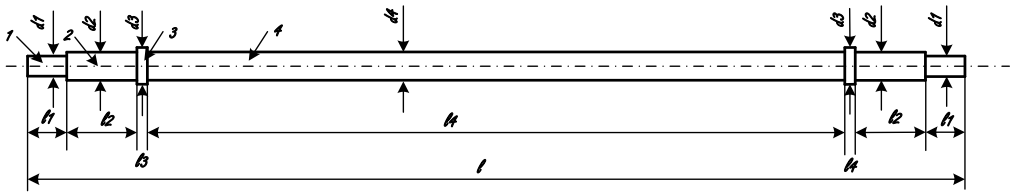

Figure 3.57. The sketch of the bottom shaft 2.

Dimensions of the bottom shaft 2:

$l = 1.44m; \quad l_1 = 0.03m; \quad l_2 = 0.09m; \quad l_3 = 0.01m; \quad l_4 = 1.18m;$
$d_1 = 0.017m; \quad d_2 = 0.025m; \quad d_3 = 0.03m; \quad d_4 = 0.025m;$

In order to find the volume, mass and weight of the bottom shaft2, each steps of the shaft can be calculated separately as follows:

1. Calculation of volume of the bottom shaft 2.

The volume of the bottom shaft 2 can be calculated as following standard formula for circular solid bar separately for each step of the shaft as follows:

$V_1 = \pi \cdot r_1^2 \cdot l_1 = 3.14 \cdot 0.0085^2 \cdot 0.03 = 0.0000068m^3;$

$V_2 = \pi \cdot r_2^2 \cdot l_2 = 3.14 \cdot 0.0125^2 \cdot 0.09 = 0.0000441m^3;$

$V_3 = \pi \cdot r_3^2 \cdot l_3 = 3.14 \cdot 0.015^2 \cdot 0.01 = 0.00000706m^3;$

$V_4 = \pi \cdot r_4^2 \cdot l_4 = 3.14 \cdot 0.0125^2 \cdot 1.18 = 0.000579m^3;$

Total volume of the bottom shaft 2:

$V_t = 2V_1 + 2V_2 + 2V_3 + V_4 = 0.000694m^3;$

2. Calculation of mass of the bottom shaft 2.

Mass of the bottom shaft 2 can be calculated as a product of volume and density of material as follows:

$m_{bsh2} = V_t \cdot \rho = 0.000694m^3 \cdot \frac{7850kg}{m^3} = 5.45$ kg;

3. Calculation of weight of the bottom shaft 2.

Weight of the bottom shaft 2 is a product of the mass and the gravity force:

$W_{bsh2} = m_{bsh2} \cdot g = 5.45 \cdot 9.81 = 53.51\ N;$

The total weight of the mechanism acts on the bottom shafts but, loads are not equal. Both bottom shafts should be analysed separately. In this section, the stress analysis can be performed for the bottom shaft2. It is known from the stress analysis of the lever3, total load and the own weight of the lever3 are equals to:

$$F_{I1y} = F_{I2y} = \frac{F_{total}}{2} + W_{lever3};$$

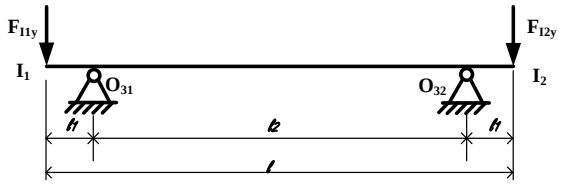

Figure 3.58. The load diagram of the bottom shaft.

It is considered that, simply beam supported at O_{31} and O_{32}. Vertical loads F_{I1y} and F_{I2y} act on the free ends of the beam as shown in Figure 3.58. The dimensions of the beam are considered as follows: $l_1 = 0.08\ m;\ \ l_2 = 1.26\ m;\ \ l = 1.44\ m;$

4. Calculation of the reaction forces.

Free body diagram of the beam is shown in Figure 3.61. The reactions F_{O31y} and F_{O32y} at supports O_{31} and O_{32} (Figure 3.61) can be calculated as follows, because the symmetry of the bottom shaft 2:

$$F_{O31y} = F_{O32y} = \frac{F_{I1y} + F_{I2y}}{2};$$

5. Calculation of the shear force and the bending moment.

The shear force and the bending moment can be calculated by dividing the cross sections as shown in Figure 3.62.

Free body diagram of section I:

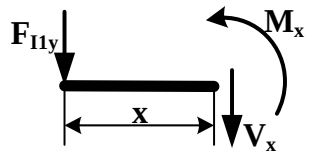

Figure 3.59. Free body diagram of section I

Static equilibrium equations of section I can be written as follows:

$+\uparrow \sum Fy = 0; \qquad V_x = -F_{I1y};$

$\circlearrowleft + \sum M = 0; \qquad M_x = -F_{I1y} \cdot x;$

For section I following assumptions can be written: $0 \leq x \leq l_1;$

If, $x = 0; \qquad V_x = -F_{I1y}; \qquad M_x = 0;$

If, $x = l_1; \qquad V_x = -F_{I1y}; \qquad M_x = -F_{I1y} \cdot l_1;$

Free body diagram of section II:

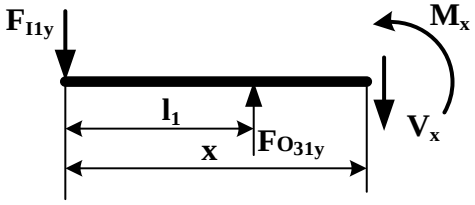

Figure 3.60. Free body diagram of section II

Static equilibrium equations of section II can be written as follows:

$+\uparrow \sum Fy = 0; \qquad V_x = \mathrm{F_{O31y}} - F_{I1y};$

$\circlearrowleft + \sum M = 0; \qquad M_x = F_{O31y}(x - l_1) - F_{I1y} \cdot x;$

For section II following assumptions can be written: $l_1 \leq x \leq l_2;$

If, $x = l_1 + \frac{l_2}{2}; \qquad V_x = \mathrm{F_{O31y}} - F_{I1y};$

$M_x = F_{O31y}\left(l_1 + \frac{l_2}{2} - l_1\right) - F_{I1y} \cdot l_1 + \frac{l_2}{2};$

If, $x = l_1 + l_2; \qquad V_x = \mathrm{F_{O31y}} - F_{I1y};$

$$M_x = F_{O31y}(l_1 + l_2 - l_1) - F_{I1y} \cdot (l_1 + l_2);$$

Shear force and bending moment diagrams are shown in Figure 3.62.

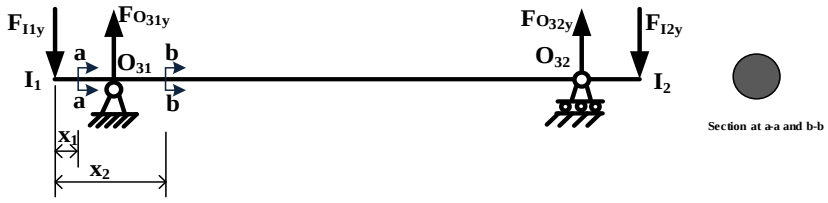

Figure 3.61. Reaction forces

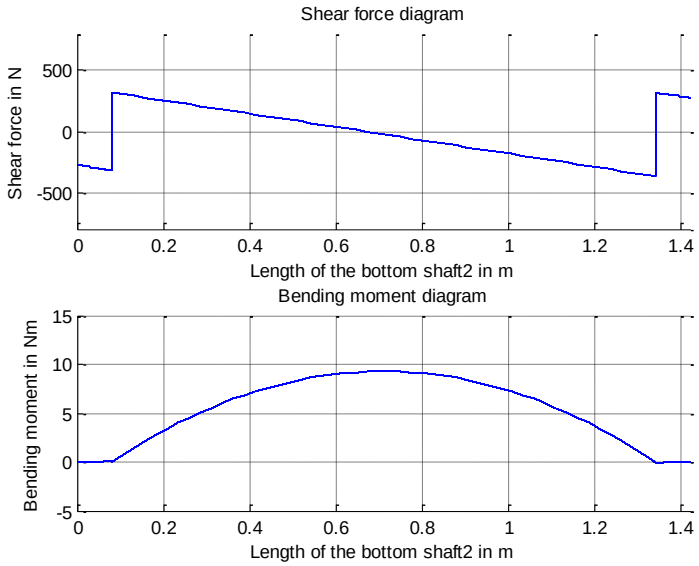

Figure 3.62. Shear force and bending moment diagrams

6. Determination of actual stress of the bottom shaft 2.

Actual stress of the bottom shaft 2can be determined by following formulas:

$$\delta = \frac{M_b^{max}}{S}; \qquad (3.20)$$

Here, M_b^{max}- maximum bending moment. Maximum value of the bending moment has been taken from the MATLAB calculation. $M_{max} = 9.28Nm$

S – Section modulus;

Section modulus for solid circular shape - $S = \frac{\pi \cdot d^3}{32} = 0.1 \cdot d^3$;

d - Diameter of the shaft.

Bending stress of the bottom shaft 1 should be small or equals than allowable bending stress as follows:

$$\delta \leq [\delta];$$

Here, $[\delta]$ - Allowable stress of circular cross section,

$[\delta] = 0.60 \cdot \text{Fty} = 0.60 \cdot 310 = 186\text{MPa}$

Here, Fy - is the tensile yield strength of the low carbon steel AISI 1045.

Equation (3.20) can be rewritten as follows:

$\frac{M_b^{max}}{0.1 \cdot d^3} \leq [\delta];$

Actual stress can be calculated as follows:

$\delta = \frac{M_b^{max}}{\frac{\pi \cdot d^3}{32}} = \frac{9.28Nm}{0.1 \cdot 20^3\, mm^3} = \frac{9.28Nm}{800 \cdot 10^{-9} m^3} = 11600000N/m^2 = 11.60MPa;$

The result is acceptable when compared to the allowable stress:

$\delta < [\delta] = 11.60 < 186;$

Stress analysis of the ternary link

One of the main working parts of the proposed mechanism is a coupler. According to the "Atlas of four bar coupler curves" [50], about 7300 coupler curves of four bar linkages have been identified. The desired motion of the harrow can be obtained by the coupler. In the proposed mechanism shape of the coupler is a ternary link as shown in Figure 3.63. The ternary link connects to the crankshaft, shaft 1, and upper shaft 1 of the mechanism with its three sides. In order to determine the stress analysis of the ternary link Finite element method can be used. In the following steps stress analysis of the ternary link can be performed:

1. Calculation of volume, mass and weight of the ternary link:

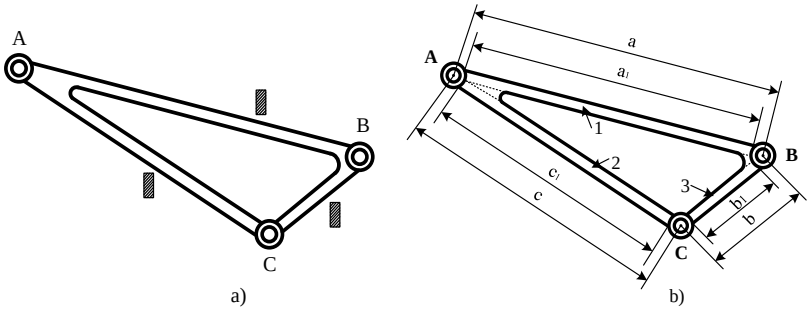

Figure 3.63. The shape of the ternary link

a) Shape of the cross sections, b) Dimensions of the ternary link

Referring to the Figure 3.63 a, it is considered that, the ternary link has two different parts, the shape of the cross sections of the three sides are rectangular solid bar, and all joints are hollow circular bar. Dimensions of the ternary link are shown in Figure 3.63 b. In order to determine the volume, the mass and the weight of the ternary link can be calculated separately as follows:

1. Calculation of volume of the joints.

The shape and the dimensions of the joint are shown in Figure 3.64. The inner diameters of the joint ***C*** is known from the stress analysis of the shaft 2. The diameter of location of the bearing has been selected 0.02 m in stress analysis of the shaft 2. From the equality of the shaft 2 and the shaft 1, the diameter of location of the shaft1 is 0.02 m as well. In order to define the inner diameter of the joints, the proper bearing should be selected. Single row cylindrical roller bearing NU 2204 EC has been selected from the SKF catalogue [57]. The outer diameter of the selected bearing equals to inner diameter of the joints of the ternary link and equals to $d = 0.047m$. Inner diameter of the joint ***A*** and joint ***B*** can be chosen the same with inner diameter of joint ***C*** until proper bearing selection. Outer diameters of the all joints are considered that $D = 0.06m$. Width of the selected bearing equals to $0.018m$. In order to mount the bearing, the depth of the joints has been selected 0.018 m. The width of the wall can be selected 0.007 m. The total width of the joint equals 0.025 m.

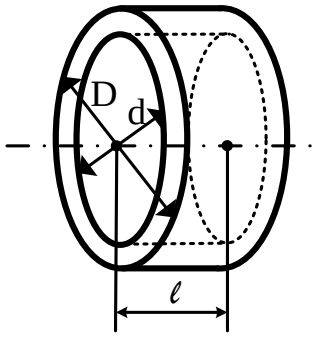

Figure 3.64. The joint of the ternary link

The volume of the hollow circular shape can be found by three steps as follows:

1. Calculation of volume of the whole joint (it is considered, the joint is fully solid): $r_1 = \frac{D}{2} = \frac{0.06}{2} = 0.03m$;

$V_1 = \pi \cdot r_1^2 \cdot l = 3.14 \cdot 0.03^2 \cdot 0.025 = 0.0000706m^3$;

2. Calculation of volume of the hole: $r_2 = \frac{d}{2} = \frac{0.02}{2} = 0.03m$;

$V_2 = \pi \cdot r_2^2 \cdot l = 3.14 \cdot 0.01^2 \cdot 0.018 = 0.00000565m^3$;

3. Calculation of total volume by subtraction of volume of the hole from volume of the whole joint:

$V_{t.c} = V_1 - V_2 = 0.0000706 - 0.00000565 = 0.0000565m^3$;

4. The volume of the solid rectangular shape.

It is assumed that, in order to determine the lengths of the sides of the ternary link, the outer diameters of the joints can be subtracted from the distance between centres of the sides. The distances of the sides (Figure 3.63.b) are known from the position analysis of the mechanism as follows:

$AB = a = 985mm = 0.985m$; $AC = c = 671mm = 0.671m$; CB= $b = 440mm = 0.44m$;

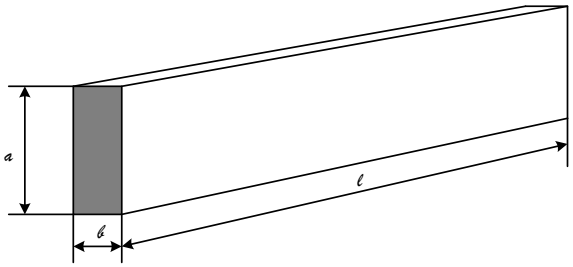

Figure 3.65. Rectangular solid bar (shape of the sides)

Referring to Figure 3.65, the width a and the height b are the same for all sides of the link, and magnitudes has been selected such as $a = 30mm = 0.03m$; $b = 15mm = 0.015m$; only the length l is different such as:

- For side 1 (Figure 3.63 b), $l_1 = a_1 = a - D = 0.985 - 0.06 = 0.925m$;
- For side 2 (Figure 3.63 b), $l_1 = b_1 = b - D = 0.671 - 0.06 = 0.611m$;

- For side 3 (Figure 3.63 b), $l_1 = c_1 = c - D = 0.44 - 0.06 = 0.38m$;

Calculation of volume of the side 1:

$V_1 = a \cdot b \cdot l_1 = 0.03 \cdot 0.015 \cdot 0.925 = 0.00042m^3$;

Calculation of volume of the side 2:

$V_2 = a \cdot b \cdot l_1 = 0.03 \cdot 0.015 \cdot 0.611 = 0.00027m^3$;

Calculation of volume of the side 3:

$V_3 = a \cdot b \cdot l_1 = 0.03 \cdot 0.015 \cdot 0.38 = 0.00017m^3$;

The total volume of the three sides:

$V_{t.s} = V_1 + V_2 + V_3 = 0.00042 + 0.00027 + 0.00017 = 0.00086m^3$;

Total volume of ternary link:

$V_{t.tl} = V_{t.c} + V_{t.s} = 0.0000565 + 0.00086 = 0.00092m^3$;

The mass of the ternary link is a product of the volume and the material density. It is considered that material of ternary link is a grey cast iron, its density equals to $\rho = 7150\frac{kg}{m^3}$. Mass of the ternary link can be found as follows:

$m_{tl} = V_{t.tl} \cdot \rho = 0.00092m^3 \cdot 7150\frac{kg}{m^3} = 6.6kg$;

Weight of the ternary link:

$W_{tl} = m_{tl} \cdot g = 6.6 \cdot 9.81 = 64.5N$;

It is known that from the stress analysis of the longitudinal bar, the total weight of the harrow is 799.66 N. The Total load distribute by four connected joints. One of the connected link is ternary link. In Figure 3.66, free body diagram of the ternary link is shown. It is considered that, total load which is acting on the ternary link equal ¼ portion of the weight of the harrow and own weight of the ternary link.

$$G = \frac{W_h}{4} + W = \frac{799.66}{4} + 64.5 = 264.4\text{N};$$

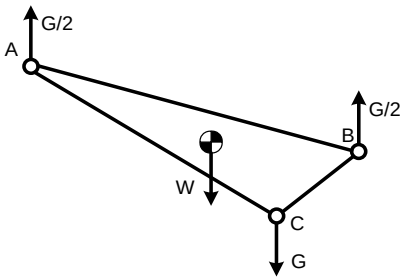

Figure 3.66. Free body diagram of the ternary link

In order to analysis of stresses of the right and left ternary links, the model has been made in SOLIDWORKS software. Two joints has been selected as a fixed, and force applied on one joint. The results of the Finite element method are shown in Figures 3.67 - 3.74.

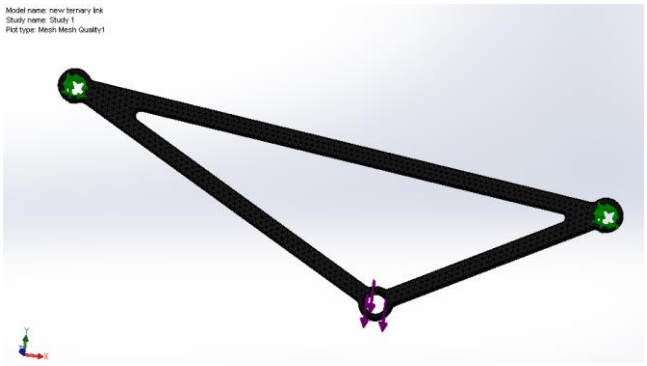

Figure 3.67. Mesh plot of the left ternary link

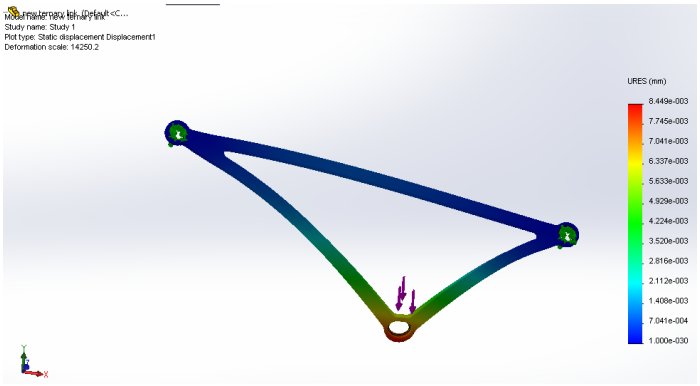

Figure 3.68. Static displacement plot of the left ternary link

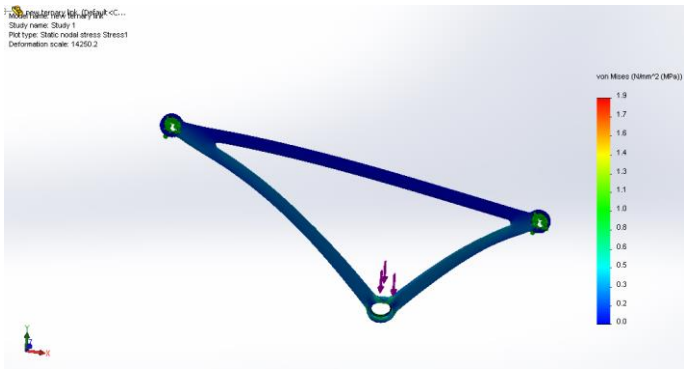

Figure 3.69. Static nodal stress plot of the left ternary link

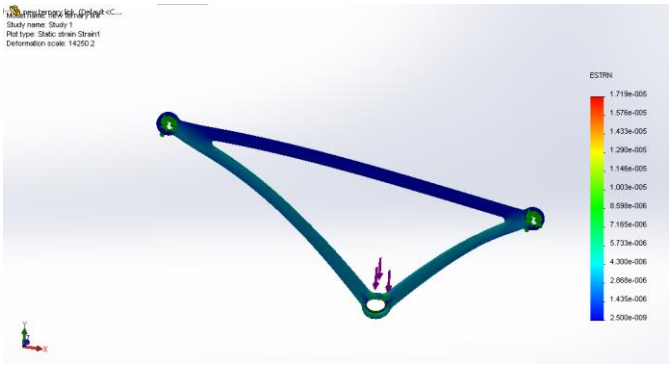

Figure 3.70. Static strain plot of the left ternary link

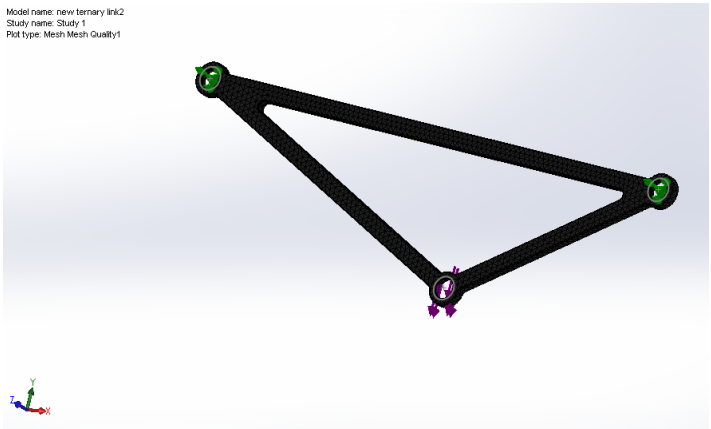

Figure 3.71. Mesh plot of the right ternary link

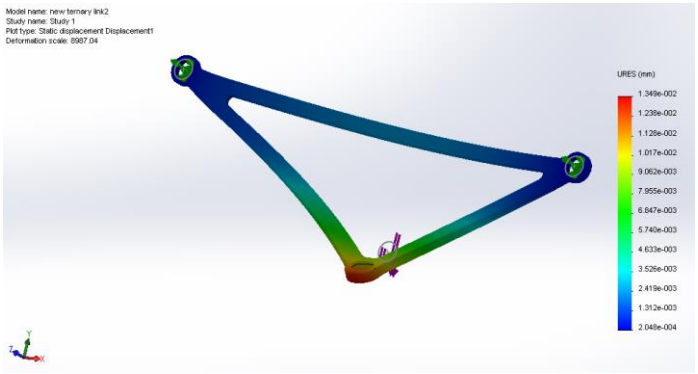

Figure 3.72. Static displacement plot of the right ternary link

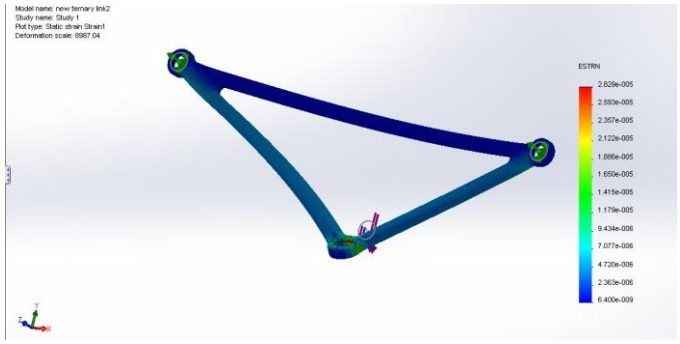

Figure 3.73. Static strain plot of the right ternary link

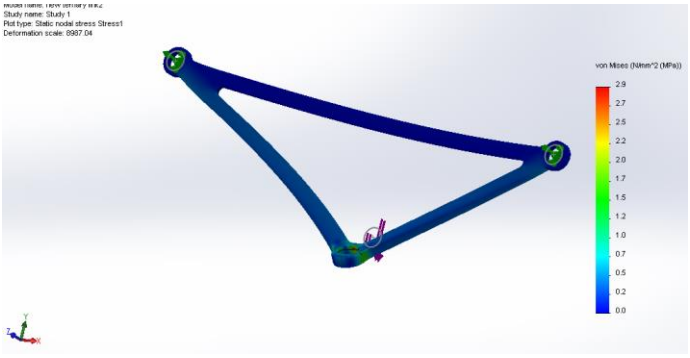

Figure 3.74. Static nodal stress plot of the right ternary link

Stress analysis of upper shaft1

In this section the upper shaft1 has been analysed in order to determine shear force and bending moment. Two long connecting rods and two ternary links are mounted on the shaft 1 with bearings.

1. Calculation of the volume, mass end weight of the upper shaft 1.
Sketch of the upper shaft 1 is shown in Figure 3.75. It is considered that the upper shaft 1 and the upper shaft 2 are the same with their all dimensions.

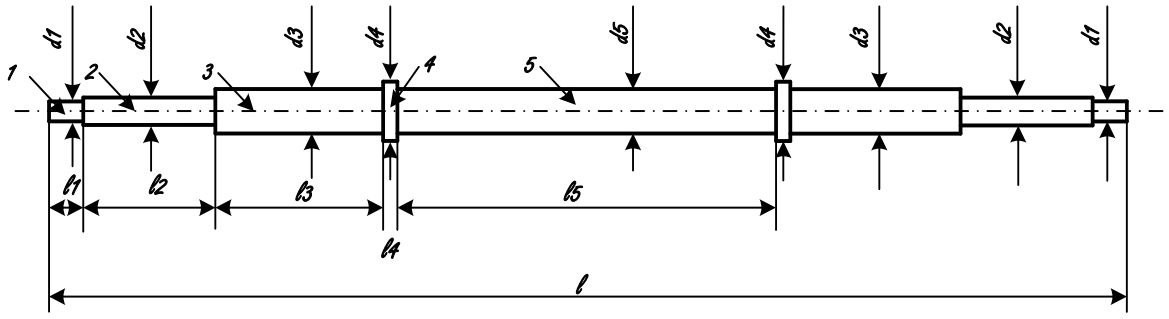

Figure 3.75. The sketch of the upper shaft 1.

In order to find the volume, mass and weight of the upper shaft1, each steps of the shaft can be calculated separately. Dimensions of the upper shaft 1 are the same with upper shaft 2 as follows:

$l = 1.44m; \quad l_1 = 0.03m; \quad l_2 = 0.235m; \; l_3 = 0.2m; \quad l_4 = 0.01m; \quad l_5 = 0.49m;$

$d_1 = 0.017m; \quad d_2 = 0.02m; \quad d_3 = 0.025m; \quad d_4 = 0.03m; \quad d_5 = 0.025m;$

The volume, mass and the weight of the upper shaft 1 are the same with mass and the weight of the upper shaft 2 as follows:

2. The total volume of the upper shaft 1 is equals to:

$V_t = 2V_1 + 2V_2 + 2V_3 + 2V_4 + V_5 = 0.000423m^3;$

3. The mass of the upper shaft1 equals to:

$m_{ush1} = V_t \cdot \rho = 0.000423m^3 \cdot \frac{7850kg}{m^3} = 3.32$ kg;

4. The weight of the shaft equals to:

$W_{ush1} = m_{ush1} \cdot g = 3.32 \cdot 9.81 = 32.62\ N;$

It is known that the total weight of the harrow equals to 747.3 N. The harrow hangs on the two ternary links and two short connecting rods. And its total weight is distributed at four locations.

The half of the total weight of the harrow, the half of the total weight of the two ternary links, and the half of the total weight of the two long connecting rods act on the four locations of the upper shaft 1 as shown in Figure 3.76, and can be written as follows:

$F_{B_{1y}} = \frac{W_{harrow}}{4} + \frac{W_{tl}}{2};$ $\quad F_{B_{1y}} = F_{B_{2y}};$

$F_{K_1} = \frac{W_{cr3}}{2};$ $\quad F_{K_1} = F_{K_2};$

Total loads which are acting on the upper shaft can be calculated as follows:

$$F_{total} = F_{B_{1y}} + F_{B_{2y}} + F_{K_{1y}} + F_{K_{2y}};$$

The upper shaft 1 hangs on the two levers which are mounted on the two sides of the scouring bowl. It is considered that, a simply beam is supported at points N_1 and N_2. The vertical loads $F_{B_{1y}}$, $F_{B_{2y}}$, $F_{K_{1y}}$ and $F_{K_{2y}}$ are act on the four locations of the beam (Figure 3.75).

Dimensions of the beam has been selected equal to the upper shaft 2 as follows:

$l_1 = 0.25\ m;$ $\quad l_2 = 0.2\ m;$ $\quad l_3 = 0.54\ m;$ $\quad l = 1.44\ m;$

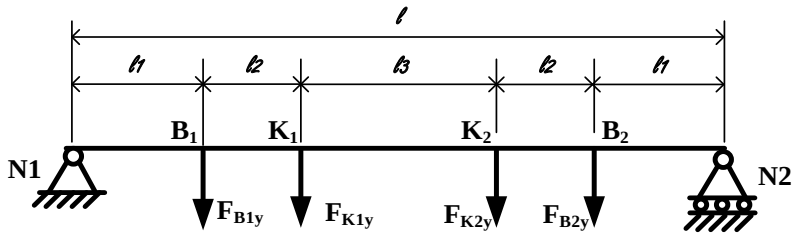

Figure 3.76. The load diagram of the upper shaft 1.

5. Calculation of reactions F_{N1y} and F_{N2y} at supports N_1 and N_2.

Referring to the free body diagram of the beam (Figure 3.77) the reaction forces can be calculated as follows:

$$F_{N1y} = F_{N2y} = \frac{F_{total}}{2};$$

6. The shear force and the bending moment of the upper shaft 1 can be calculated by dividing the cross sections as shown in Figure 3.77.

Free body diagrams and the static equilibrium equations are the same the free body diagrams and the static equilibrium equations of the upper shaft 2. Here is the only total free body diagram, shear force and bending diagrams are presented (3.77 and 3.78).

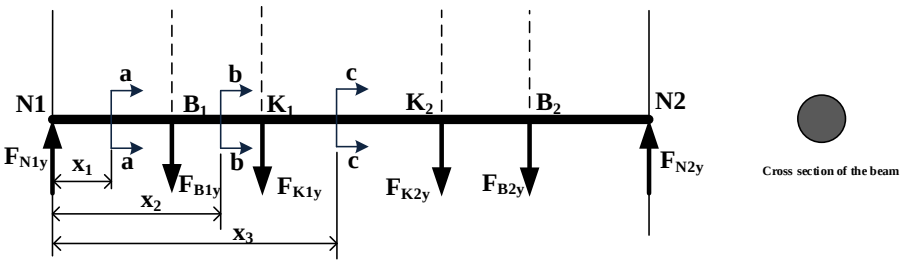

Figure 3.77. Cross sections of the beam

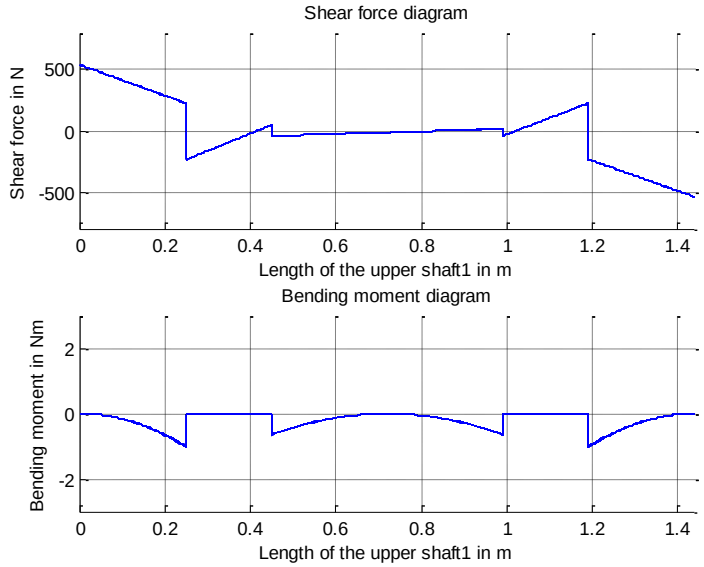

Figure 3.78. Shear force and bending moment diagrams.

7. Determination of the actual stress of the upper shaft 1.

The actual stress of the upper shaft 1 can be determined by following formulas:

$$\delta = \frac{M_b^{max}}{S}; \qquad (3.21)$$

Here, M_b^{max}- maximum bending moment. Maximum value of the bending moment has been taken from the MATLAB calculation. $M_{max} = 1.03Nm$;

S – Section modulus; section modulus for solid circular shape - $S = \frac{\pi \cdot d^3}{32} = 0.1 \cdot d^3$;

d - Diameter of the shaft.

Bending stress of the upper shaft 1 should be smaller than allowable bending stress as follows:

$\delta \leq [\delta]$;

$[\delta]$ - Allowable stress of circular cross section,

$[\delta] = 0.60\text{Fty} = 0.60 \cdot 310 = 186\text{MPa}$

Here, Fty - is the tensile yield strength of the medium carbon steel AISI 1045.

Equation (3.21) can be rewritten as follows:

$\frac{M_b^{max}}{0.1 \cdot d^3} \leq [\delta]$;

Actual stress can be calculated as follows:

$\delta = \frac{M_b^{max}}{\frac{\pi \cdot d^3}{32}} = \frac{1.03Nm}{0.1 \cdot 25^3\ mm^3} = \frac{1.03Nm}{1562.5 \cdot 10^{-9} m^3} = 659411.09/m^2 = 0.659MPa$;

The result is acceptable when compared to the allowable stress:

$\delta < [\delta] = 0.659 < 186$;

Stress analysis of the lever 1

One of the four levers of the proposed mechanism is lever1. The lever 1 connects to the upper shaft 1 and the bottom shaft 1 by end rod bearings. It is considered that the dimensions of the all levers are the same as lever 3. The sketch of the lever is shown in Figure 3.79.

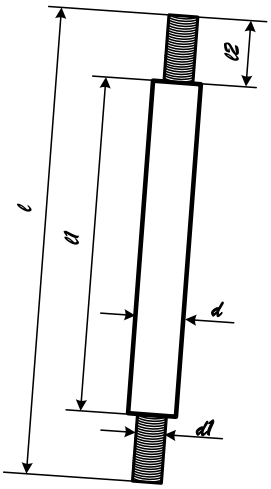

Figure 3.79. The sketch of the lever1.

The lever 1 mounts on the free end of the upper shaft 2, and the free end of the bottom shaft 2 by end rod bearings. The end rod bearing DIN ISO 12240-4 (DIN 648 E series) has been selected in stress analysis of the lever 3.

According to the kinetostatic analysis, the compressive forces act on the levers. The lever 1 illustrated in Figure 3.80.

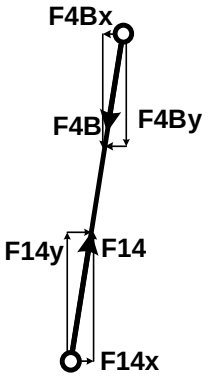

Figure 3.80. Compressive forces of the lever1.

In order to determine the maximum compressive stress of the lever 1, the reaction forces, the inertia forces and the mass moments of inertia should be taken into consideration.

Compressive stress calculates as follows:

$$\sigma_c = \frac{P}{A}; \qquad (3.22)$$

Where, σ_c – compressive stress, (N/mm^2);

P- External force (N); $P = F_{4Bx} + F_{4By} = F_{4B}$;

A- cross sectional area (mm2);

Maximum stress should be small or equals to the allowable stress as follows:

$$\sigma_t = \frac{P}{A} \leq [\sigma_t];$$

$[\delta]$ - Allowable stress of circular cross section,

$[\delta] = 0.60\text{Fty} = 0.60 \cdot 310 = 186\text{MPa}$

Here, Fty - is the tensile yield strength of the medium carbon steel AISI 1045.

Actual stress of the lever 1 has been calculated by MATLAB program. The plot of the actual stress is shown in Figure 3.81. The maximum compressive stress compares with allowable stress in order to verify the diameter of the lever1.

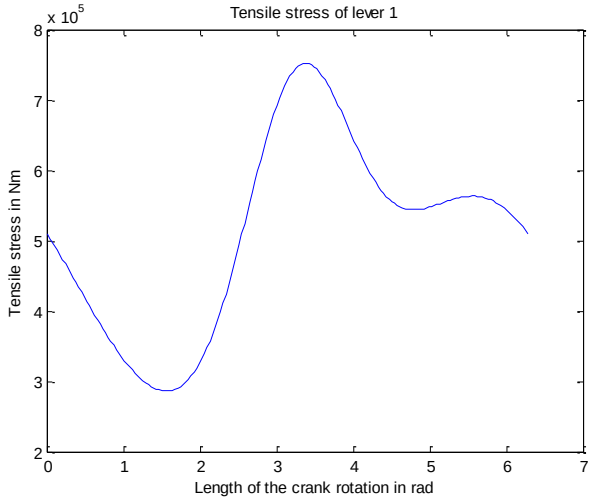

Figure 3.81. Plot of the compressive stress of the lever 1.

Maximum value of the compressive stress has been taken from the MATLAB calculation:

$\sigma_t = 752162.8 \frac{N}{m^2} = 0.752\ Mpa;$

$\sigma_t \leq [\delta] = 0.752 < 186$

The result is acceptable.

Stress analysis of the bottom shaft 1

In this section stress analysis can be performed for the bottom shaft 1. It is considered that dimensions of the both bottom shafts are the same. Sketch of the bottom shaft 1 is shown in Figure 3.82. The section 1 represents the diameter of location of the end rod bearing. The end rod bearing ISO12240-4 (DIN 648 E series) has been selected in stress analysis of the lever 3. The section 2 represents the diameter of location of the journal bearing. The journal bearing SY 25 TF has been selected in stress analysis of the bottom shaft 2.

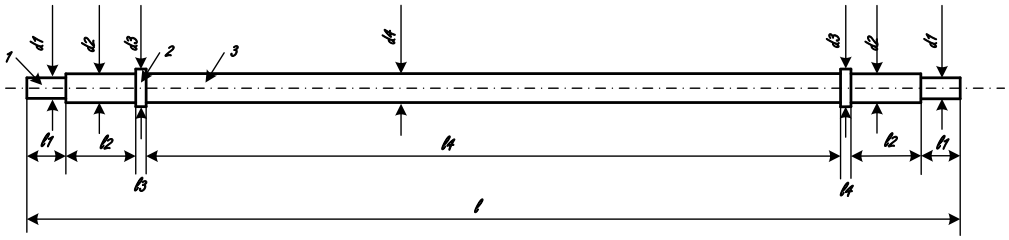

Figure 3.82. The sketch of the bottom shaft 1

Dimensions of the bottom shaft 1 are the same as bottom shaft 2 as follows:

$l = 1.44m; \quad l_1 = 0.03m; \quad l_2 = 0.09m; \quad l_3 = 0.01m; \quad l_4 = 1.18m;$
$d_1 = 0.017m; \quad d_2 = 0.025m; \quad d_3 = 0.03m; \quad d_4 = 0.025m;$

In order to find the volume, mass and weight of the bottom shaft 2, each step of the shaft can be calculated separately as follows:

2. Calculation of the volume, mass end weight of the bottom shaft.

The volume, the mass end the weight of the bottom shaft 1 are the same as bottom shaft 2 as follows:

$V_t = 2V_1 + 2V_2 + 2V_3 + V_4 = 0.000694m^3;$

$m_{bsh1} = V_t \cdot \rho = 0.000694m^3 \cdot \frac{7850kg}{m^3} = 5.45$ kg;

$W_{bsh1} = m_{bsh1} \cdot g = 5.45 \cdot 9.81 = 53.51\ N$;

It is known from the stress analysis of the lever1, sum of the total load which acts on the lever 1 and own weight of the lever1 are equal to $F_{M1y} = F_{M2y} = \frac{F_{total}}{2} + W_{lever1}$; Total load which act on the bottom shaft1: $F_{M1y} + F_{M2y}$;

It is considered that, simply beam supported at O_{21} and O_{22}. Vertical loads F_{M1y} and F_{M2y} act on the free ends of the beam as shown in Figure 3.83. Dimensions of the beam are considered as follows: $l_1 = 0.08\,m$; $l_2 = 1.26\,m$; $l = 1.44\,m$;

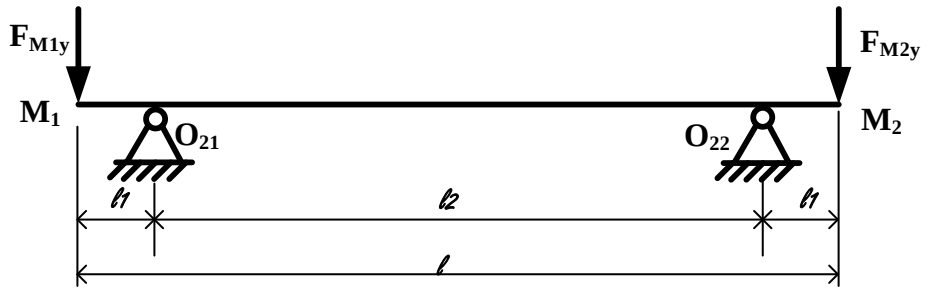

Figure 3.83. The load diagram of the bottom shaft 1

3. Calculation of the reaction forces.
Free body diagram of the beam is shown in Figure 3.84. The reactions F_{O21y} and F_{O22y} at supports O_{21} and O_{22} can be calculated as follows:

$$O_{21} = O_{22} = \frac{F_{M1y} + F_{M2y}}{2};$$

4. Calculation of the shear force and the bending moment.

Shear force and bending moment has been calculated in stress analysis of the bottom shaft 1. Shear force and bending moment has been calculated by dividing the cross sections as shown in Figure 3.85.

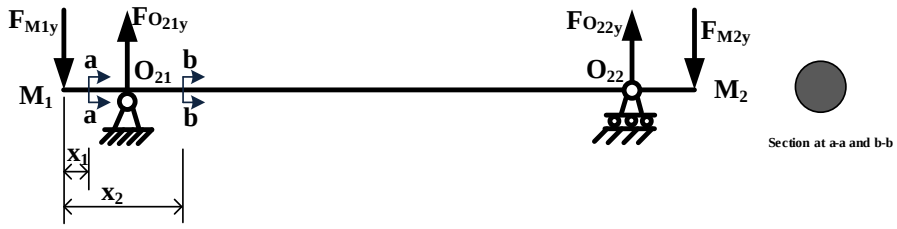

Figure 3.84. Reaction forces

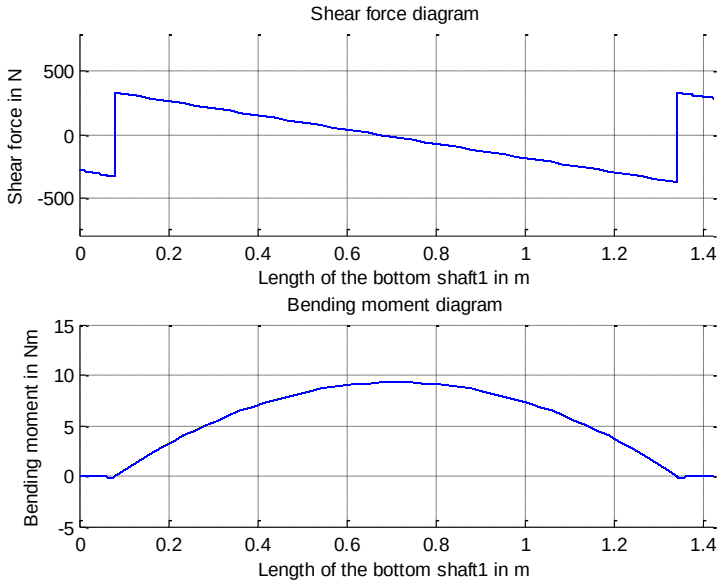

Figure 3.85. Shear force and bending moment diagram

6. Determination of actual stress of the bottom shaft 1.

Actual stress of the bottom shaft 1 can be determined by following formulas:

$$\delta = \frac{M_b^{max}}{S}; \qquad (3.23)$$

Here, M_b^{max}- maximum bending moment. Maximum value of the bending moment has been taken from the MATLAB calculation. $M_{max} = 9.28Nm$;

S – section modulus; section modulus for solid circular shape - $S = \frac{\pi \cdot d^3}{32} = 0.1 \cdot d^3$;

d - diameter of the shaft.

Bending stress of the shaft should be small or equals than allowable bending stress as follows:

$\delta \leq [\delta]$;

$[\delta]$ - Allowable stress of circular cross section,

$[\delta] = 0.60 \cdot \text{Fty} = 0.60 \cdot 310 = 186\text{MPa}$

Here, Fy - is the tensile yield strength of the low carbon steel AISI 1020.

Equation (3.23) can be rewritten as follows:

$\frac{M_b^{max}}{0.1 \cdot d^3} \leq [\delta]$;

Actual stress can be calculated as follows:

$$\delta = \frac{M_b^{max}}{\frac{\pi \cdot d^3}{32}} = \frac{9.28Nm}{0.1 \cdot 20^3\ mm^3} = \frac{9.28Nm}{800 \cdot 10^{-9} m^3} = 11600000N/m^2 = 11.60MPa;$$

The result is acceptable when compared to the allowable stress:

$\delta < [\delta] = 11.60 < 186$;

Stress analysis of the crankshaft

In this section, the crankshaft of the proposed mechanism has been analysed in order to determine torsion, shear force and bending moment. The crankshaft consists of transmission shaft, crank arms or webs and crankpin. The stress analysis of the crankshaft has been performed by finite element method using commercial software SOLIDWORKS 2012. In Figure 3.86 the sketch of the crankshaft is shown. The forces F_{A1} and F_{A2} act on the crankpin as shown in Figure 3.86. The crank arms or webs connect to the shafts and to the crankpin with bolts. As shown in Figure 3.86, the ends of the crankpin are carved in order to connect with crank arms. The crank arms are also carved at their both ends respectively. After mounting of the crankpin and crank arms, with their carved parts, they are bolted to each other in order to make a strong joint.

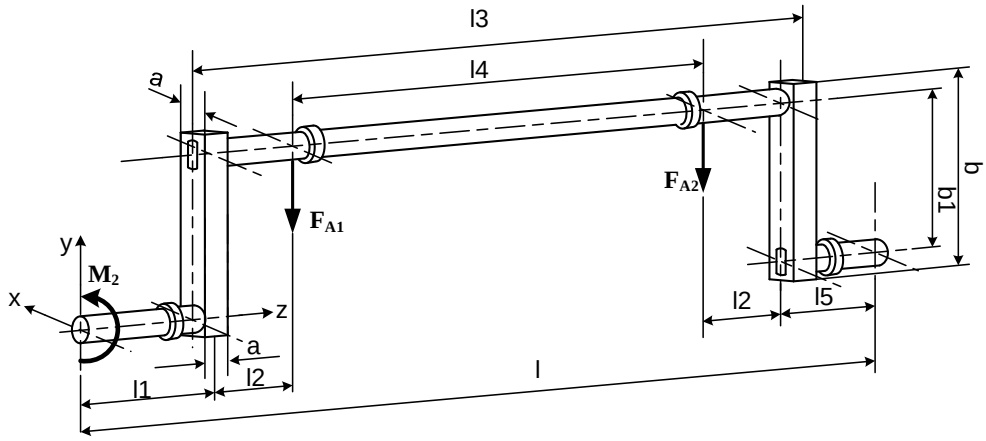

Figure 3.86. The sketch of crankshaft of the proposed machine

The load diagram of the crankshaft is shown in Figure 3.87. Torque M_2 and forces F_{A1} and F_{A2} act on the crankshaft. Forces which acting on the crank pin are known from the previous stress analysis as follows:

$$F_{A1} = F_{A2} = \frac{t.w.of\ the\ harrow}{8} + \frac{t.w.of\ the\ ter.link}{2};$$

The torque equals to acting force times length of the crank arm, and can be written as follows:

$$M_2 = (F_{A1} + F_{A2}) \times 0.25;$$

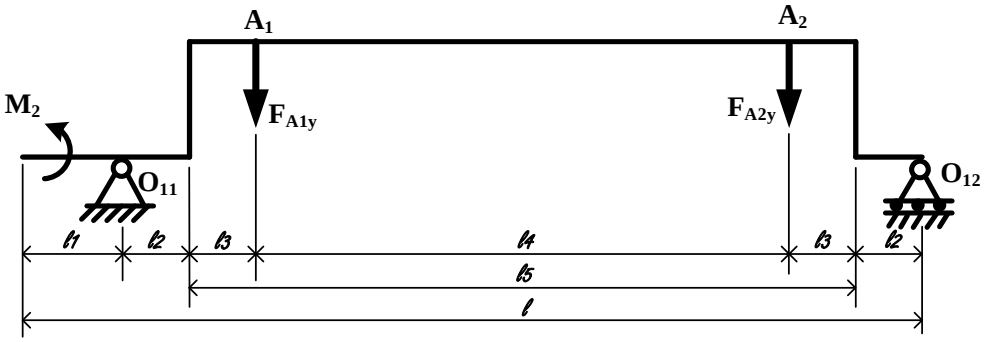

Figure 3.87. The load diagram of the crankshaft

Dimensions of the crankshaft has been selected approximately, but close to the other parts of the mechanism. In order to determine the volume, the mass and the

weight of the crankshaft, each part should be calculated separately as following sequence:

- Crankpin;
- Left transmission shaft;
- Right transmission shaft;
- Web or crank arm

1. Crankpin.

Calculation of the volume starts from the crankpin. The sketch of the crankpin is shown in Figure 3.88. Ends of the crankpin can be carved in order to mount to the crank as in shown Figure 3.

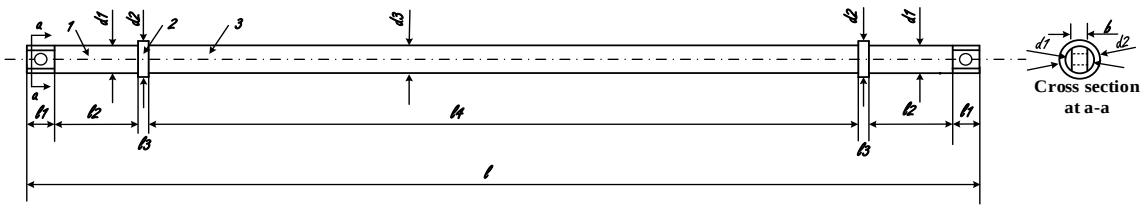

Figure 3.88. The sketch of the crankpin

The section 1 represents the diameter of location of the bearing. The single row cylindrical roller bearing NU 2204 EC has been selected in the stress analysis of the upper shaft 1 and equals to 0.020m.

The dimensions of the crankpin are:

$l = 1.11m; \quad l_1 = 0.02m;\ l_2 = 0.083m;\ \ l_3 = 0.01m; \quad l_4 = 0.884m;\ a = 0.01m;$

$d_1 = 0.02m;\ \ d_2 = 0.025m; \quad d_3 = 0.02m;$

1.1. Calculation of volume of the crankpin.

The volume of the crankpin can be calculated as following standard formula for circular solid bar separately for each steps of the crankpin:

Carved parts are neglected.

$V_1 = \pi \cdot r_1^2 \cdot (l_1 + l_2) = 3.14 \cdot 0.01^2 \cdot 0.103 = 0.0000323m^3;$

$V_2 = \pi \cdot r_2^2 \cdot l_3 = 3.14 \cdot 0.0125^2 \cdot 0.01 = 0.0000049m^3;$

$V_3 = \pi \cdot r_3^2 \cdot l_4 = 3.14 \cdot 0.01^2 \cdot 0.912 = 0.000286 m^3$;

The total volume of the crankpin is equals to:

$V_t = 2V_1 + 2V_2 + 2V_3 = 2 \cdot 0.0000323 + 2 \cdot 0.0000049 + 0.000286 = 0.00036 m^3$;

1.2. Calculation of mass of the crankpin.

The mass of the crankpin can be calculated as a product of the volume and the density of the selected material (Low carbon plain, $\rho = 7850 kg$) as follows:

$m_{pin} = V_t \cdot \rho = 0.00036 m^3 \cdot \frac{7850 kg}{m^3} = 2.82$ kg;

1.3. Calculation of weight crankpin.

The weight of the crankpin is a product of the mass and the gravity force:

$W_{pin} = m_{ush1} \cdot g = 2.82 \cdot 9.81 = 27.75\ N$;

2. Left transmission shaft

Sketch of the left transmission shaft is shown in Figure 3.89. The transmission shaft rotates by belt drive. In Figure 3.89, the section 1 represents the location of the pulley of the belt drive, the section 2 represents the location of the journal bearing, and one end of the shaft is carved and opened the hole for mounting with the crank web.

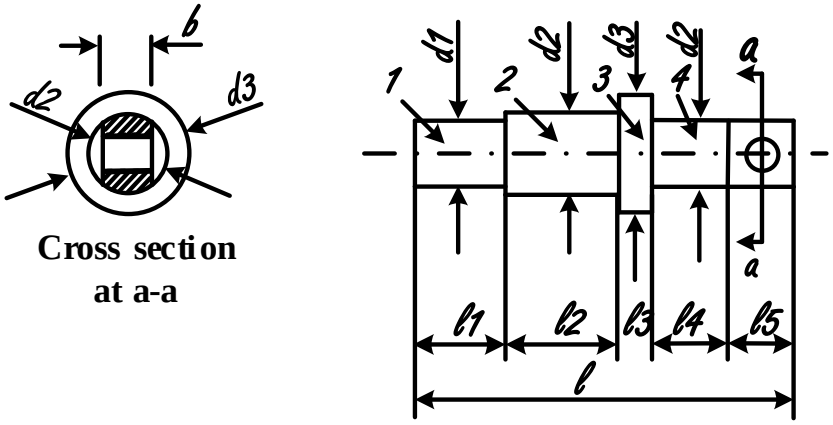

Figure 3.89. The sketch of the left transmission shaft

The dimensions of the crankpin are:

$l = 0.145m;\quad l_1 = 0.04m;\ l_2 = 0.05m;\ l_3 = 0.01m;\quad l_4 = 0.025m;\ l_5 = 0.02m;$

$d_1 = 0.02m;\ d_2 = 0.025m;\quad d_3 = 0.03m;$

2.1. Calculation of the volume of the left transmission shaft.

The volume of the left transmission shaft can be calculated as following standard formula for circular solid bar separately for each steps of the shaft (carved parts are neglected):

$V_1 = \pi \cdot r_1^2 \cdot l_1 = 3.14 \cdot 0.01^2 \cdot 0.04 = 0.0000125m^3;$

$V_2 = \pi \cdot r_2^2 \cdot (l_1 + l_4 + l_5) = 3.14 \cdot 0.0125^2 \cdot 0.085 = 0.000042m^3;$

$V_3 = \pi \cdot r_3^2 \cdot l_3 = 3.14 \cdot 0.015^2 \cdot 0.01 = 0.00000706m^3;$

The total volume of the left transmission shaft is equals to:

$V_t = V_1 + V_2 + V_3 = 0.0000125 + 0.000042 + 0.00000706 = 0.000061m^3;$

2.2. Calculation of the mass of the left transmission shaft.

The mass of the of the left transmission shaft can be calculated as a product of the volume and the density of the selected material (Low carbon plain AISI 1045, $\rho = 7850kg$) as follows:

$m_{l.sh} = V_t \cdot \rho = 0.000061m^3 \cdot \frac{7850kg}{m^3} = 0.47$ kg;

2.3. Calculation of the weight of the left transmission shaft.

The weight of the left transmission shaft is a product of the mass and the gravity force:

$W_{l.sh} = m_{ush1} \cdot g = 0.47 \cdot 9.81 = 4.61\ N;$

3. Right transmission shaft

The sketch of the right transmission shaft is shown in Figure 3.90. The location of the journal bearing is numbered 3, and one end of the shaft is carved and opened hole in order to mount to the crank web.

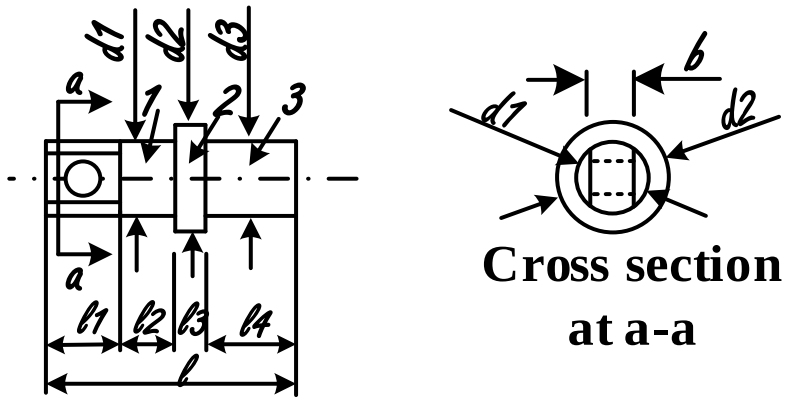

Figure 3.90. The sketch of the right transmission shaft

The dimensions of the right transmission shaft are:

$l = 0.095m;\quad l_1 = 0.02m;\ l_2 = 0.025m;\ \ l_3 = 0.01m;\quad l_4 = 0.04m;$

$d_1 = 0.02m;\ \ d_2 = 0.03m;\quad d_3 = 0.025m;$

3.1. Volume of the right transmission shaft.

The volume of the right transmission shaft can be calculated as following standard formula for circular solid bar separately for each steps of the shaft:

Carved parts are neglected.

$V_1 = \pi \cdot r_1^2 \cdot (l_1 + l_2) = 3.14 \cdot 0.01^2 \cdot 0.045 = 0.000014m^3;$

$V_2 = \pi \cdot r_2^2 \cdot l_3 = 3.14 \cdot 0.015^2 \cdot 0.01 = 0.0000071m^3;$

$V_3 = \pi \cdot r_3^2 \cdot l_4 = 3.14 \cdot 0.0125^2 \cdot 0.04 = 0.000019m^3;$

The total volume of the right transmission shaft is equals to:

$V_t = V_1 + V_2 + V_3 = 0.000014 + 0.0000071 + 0.000019 = 0.00004m^3;$

3.2. The mass of the right transmission shaft.

The mass of the of the right transmission shaft can be calculated as a product of the volume and the density of the selected material (Low carbon plain, $\rho = 7850kg;$) as follows:

$m_{r.sh} = V_t \cdot \rho = 0.00004m^3 \cdot \frac{7850kg}{m^3} = 0.31$ kg;

3.3. The weight of the right transmission shaft.

The weight of the right transmission shaft is a product of the mass and the gravity force:

$W_{r.sh} = m_{ush1} \cdot g = 0.31 \cdot 9.81 = 3.1\ N;$

4. Crank arms or crank webs.

The sketch of the crank arm is shown in Figure 3.91. Near the two ends of the crank arms are carved and opened holes for bolts in order to connect to the shafts and crankpin. The shape of the crank arm is considered as a rectangular prism. Dimensions of the crank arm are as follows:
$l = 0.28m;$ $l_1 = 0.25m;$ $l_2 = 0.02m;$ $l_3 = 0.015m;$ $b = 0.02m;$ $b_1 = 0.01m;$ r = $0.01m;$
Two sides of the crankpin are equal to 0.02m;

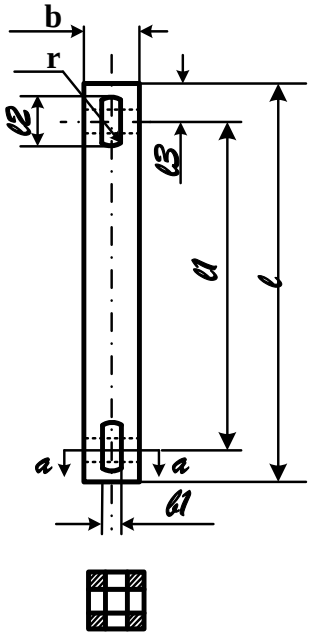

Cross section at a-a

Figure 3.91. The sketch of the crank arm

4.1. Volume of the crank arm.

The volume of the crank arm can be calculated by standard formulas for the rectangular prism as follows (holes and carved parts are neglected):

$$V = b^2 \cdot l = 0.02^2 \cdot 0.28 = 0.000112 m^3;$$

4.2. The mass of the crank arm.

The mass of the crank arm can be calculated as a product of the volume and the density of the selected material (Low carbon plain, AISI 1045, $\rho = \frac{7850kg}{m^3}$;) as follows:

$$m_{c.sh} = V_t \cdot \rho = 0.000112 m^3 \cdot \frac{7850kg}{m^3} = 0.88 \text{ kg};$$

4.3. The weight of the crank arm.

The weight of the crank arm is a product of the mass and the gravity force:

$$W_{l.sh} = m_{ush1} \cdot g = 0.88 \cdot 9.81 = 8.62\ N;$$

5. Total mass and total weight of the crankshaft**.**

$$m_{t.c} = m_{pin} + m_{l.sh} + m_{r.sh} + m_{c.sh} = 2.82 + 0.47 + 0.31 + 0.88 = 4.48 kg;$$

$$W_{t.c} = m_{t.c} \cdot g = 4.48 \cdot 9.81 = 43.94 N;$$

6. Modelling of the crankshaft by computer program.

In order to perform the stress analysis of the crankshaft, the model of the crankshaft has been made in commercial software SOLIDWORKS. Each part of the crankshaft has been modelled separately and assembled (Figures 3.87-3.91). The results of the Finite element method are shown Figures 3.92-3.96.

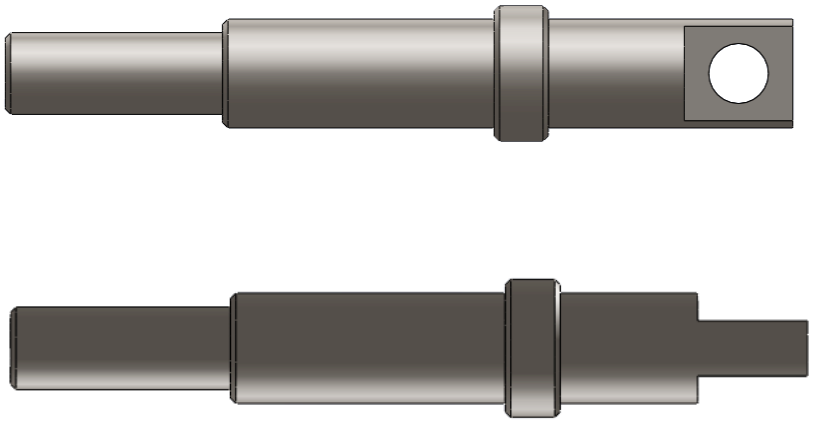

Figure 3.92. 3D model of the left transmission shaft

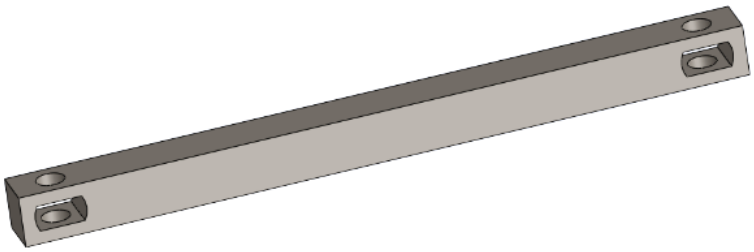

Figure 3.93. 3D model of the crank arm or crank web

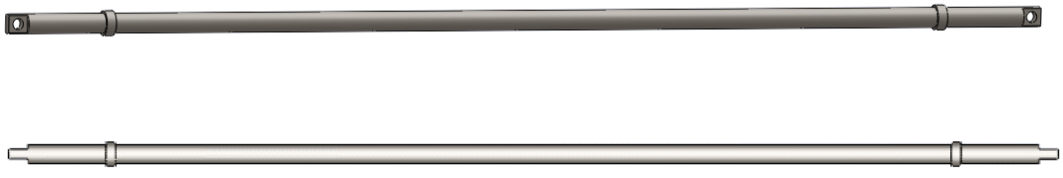

Figure 3.94. 3D model of the crankpin

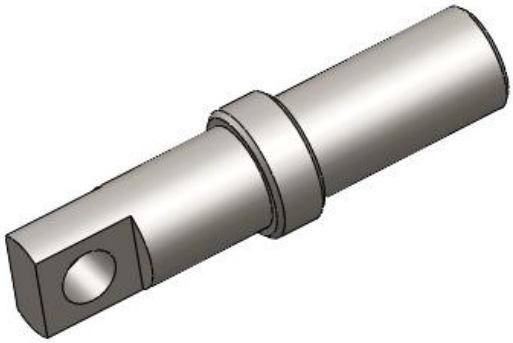

Figure 3.95. 3D model of the right transmission shaft

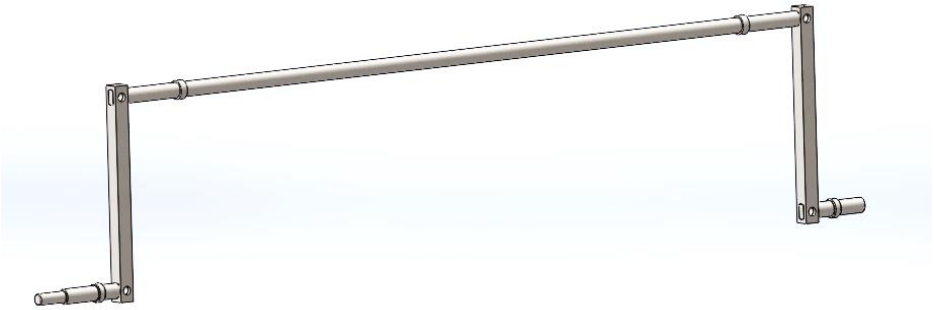

Figure 3.96. Assembled model of crankshaft

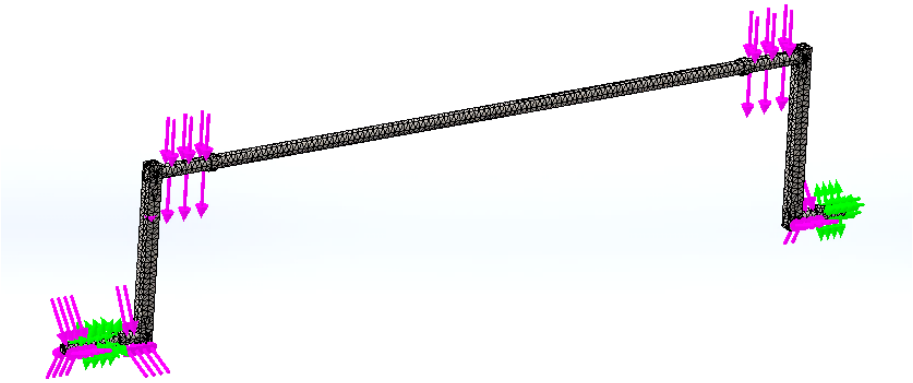

Figure 3.97. Mesh plot of the crankshaft

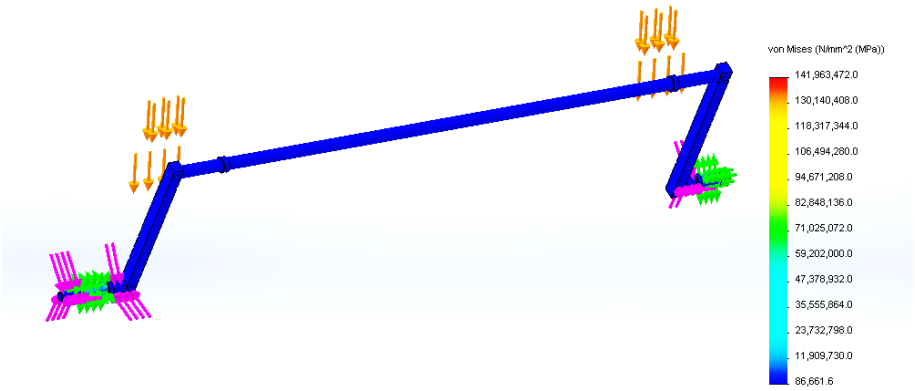

Figure 3.98. Stress analysis of the crankshaft

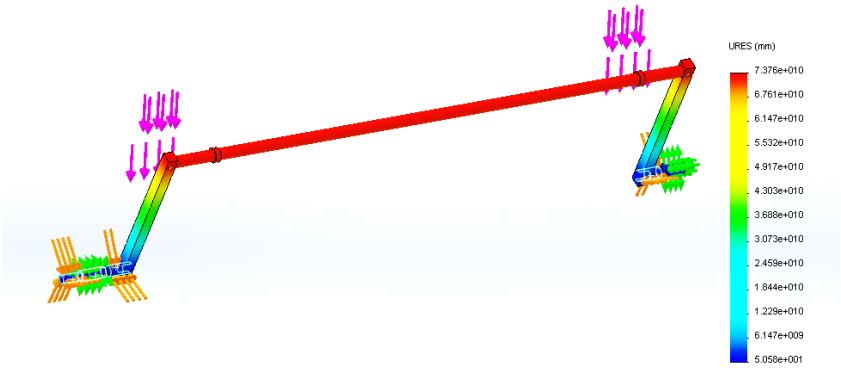

Figure 3.99. Static displacement plot of the crankshaft

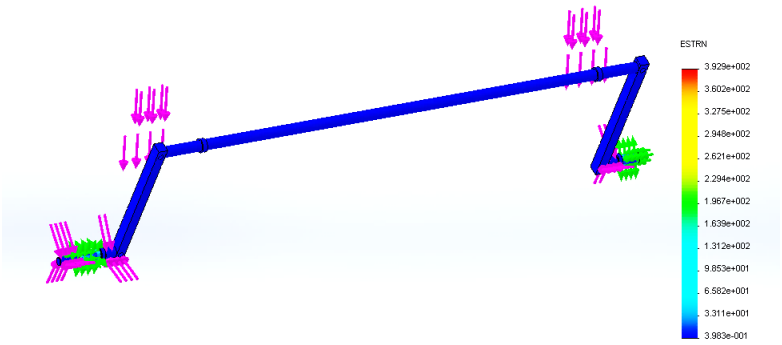

Figure 3.100. Static strain plot of the crankshaft.

Figure 3.101. Factor of safety.

3.2. Material selection for the new mechanism

Proper materials has been selected during stress analyses of links. Selected materials are tabulated in Table 3.4.

3.3. Bearing selection for the crank and pivots

During stress analyses of links of the proposed mechanism the proper bearings have been selected. Mechanical properties of the selected materials are presented in Tables 3.5-3.7. In order to select proper bearings, actual loads and to suit the nature of the machine, precision, rigidity have been taken into consideration.

3.4. Motor, reducer and belt drive selection

Selection of most appropriate motor and gearbox starts checking the required specifications such as positioning accuracy, holding of position, speed range, operating voltage and other environmental resistances.
The velocity of the driving link is known from the kinematic analysis, and it is equal 1.5 rad/s or 14.32 rpm. From the kinetostatic analysis the required torque has been found and equals to 311 Nm. The required power of the machine can be found as follow:

$$P = \frac{M(Nm)\cdot n(rpm)}{9550} = \frac{311\cdot 14.32}{9550} = 0.47kW; \qquad (3.24)$$

The motor and gearbox can be installed bottom of the proposed machine, under the crank location. Because, the bowl has been designed as a conical form, from up to down its size shrinks. There is enough space for installation the required motor and gearbox. From the Standard Line, S.T.M. Teams catalogues [61] type of the motor and gearbox assemble has been selected. There are two options in the catalogue. One of them is only for gearbox selection, second one is for gearbox and motor assembling. From next option, version of the gearbox and motor assembling has been selected, and then from the first option, only gearbox has been selected according to the input link torque, driving link velocity and required power. Proper gearbox has been selected from the "Standard Line", S.T.M. Teams catalogues, Table 1.6, "Gearboxes performances".

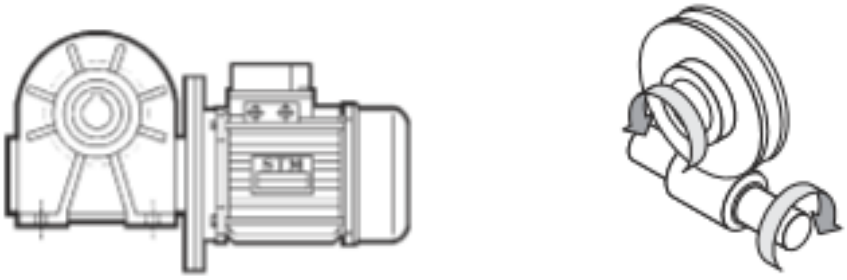

a) b)

Figure 3.102. Gearbox and motor coupling.
a - selected motor and gearbox, b-b direction of the warm rotation.

The technical data of the selected gearbox has been tabulated in Table 3.4. According to the Table 3.4, the given technical data are suitable for proposed machine. In Table 3.4 the column RMI shows the type of the suitable motor for selected gearbox. This data can be used in order to select proper motor. The proper motor M90Sa6 has been selected from the catalogue of the Carpanelli Motori elettrici brand [62]. The technical data of the selected motor are tabulated in Table 3.5.

In order to select the proper belt drive, diameters of the pulleys, and distance between gearbox and crankshaft should be known.

In table 3.4, $n2$ shows the velocity of given output shaft of the gearbox, and equals to $n2 = 18.4\,rpm$. The velocity of the driving link is known from the kinematic analysis of the proposed machine and equals to 1.5 rad/sec or 14.32 rpm. The velocity of output shaft of the gearbox is not equal to the required velocity of the mechanism. The ratio between gearbox and crankshaft velocities

can be obtained by dividing the output velocity of gearbox by required velocity of mechanism as follow:

$$Drive\ ratio = \frac{output\ shaft\ of\ the\ gearbox,rpm}{input\ shaft\ of\ the\ mechanism,rpm} = \frac{18.4rpm}{14.32rpm} = 1.28; \quad (3.25)$$

The obtained ratio can be used for proper belt drive selection. That is to say, diameter of pulley of the transmission shaft 1.28 times larger than the diameter of pulley of output shaft of the gearbox. 8PM type High torque timing keyless pulley belt drive can be selected from MISUMI bearing manufacturer catalogue [63]. The pulley selection process has been started according to the shaft diameter of the gearbox. The diameter of the gearbox shaft is known from its technical data and equals to 19 mm (Table 3.2). From the next columns diameter and number of teeth of the pulley has been selected. 86.58 mm diameter pulley has been selected, number of teeth equals 34. Ratio of the diameters equal to 1.28. In this case number of teeth for driving shaft pulley equals to 34*1.28=43.52. From the pulley selection table of the catalogue, number of teeth 44 has been selected. The diameter of the crankshaft is known from its stress analysis and equals to 20 mm. Respect to the shaft diameter and number of teeth of the pulley, from the pulleys diameter column in Table 3.6, 112.05 mm has been selected.

In order to define the distance between transmission shafts, their locations in the machine should be defined. It is considered that, the crankshaft locates upper part of the mechanism and mounts on the two columns or standards. The height of the machine frame has been selected as equals to 1000 mm. The height of the columns has been selected as equals to 188 mm according to the position analysis. The height from base to the center of the selected bearing equals 36.5 mm (Table 3.2). In order to determine the distance between the total lengths from base of the machine can be found by adding the all lengths.

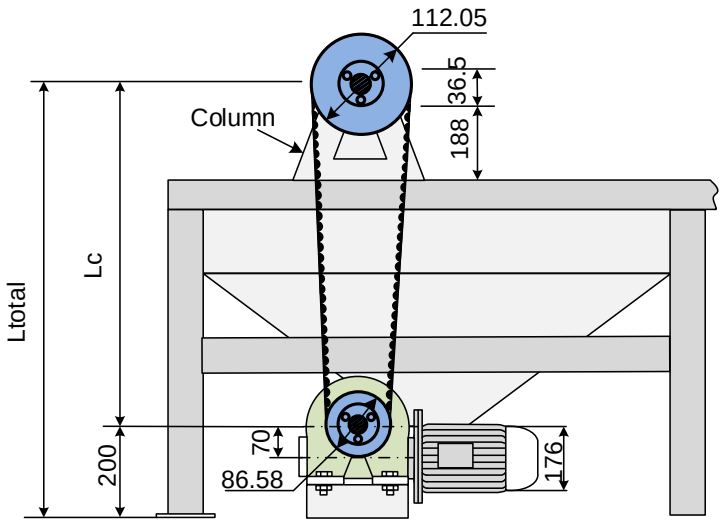

Figure 3.103. Position of the gearbox and motor in proposed machine.

$$Ltotal = 1000 + 118 + 36.5 = 1224.5mm$$
$$L_C = 1224.5 - 200 = 1024.5mm$$

It is considered that the distance from the base of the machine to the center of the gearbox equal to 200 mm (Figure 3.103). The length of the belt can be found by following equation [54]:

$$Lb = 2L_C C + 1.57(D + d) + \frac{(D-d)^2}{4C}; \qquad (3.26)$$

Here is, L = Pitch Length of Belt
C = Center Distance of pulleys
d = Pitch of small pulley diameter
D = Pitch of large pulley diameter

$$Lb = 2 \cdot 1024.5 + 1.57(112.05 + 88.56) + \frac{(112.05 + 88.56)^2}{4 \cdot 1024.5} = 2373.77;$$

2373 mm length is not available in the catalogue, nearly number can be selected for proper belt. There are two numbers are close, which are 2064mm and 2496.mm. 2496 has been selected, because it is closer than 2064 mm. In order to apply to the pulleys, frame of the machine has been increased. The technical data of the selected belt was tabulated in Table 3.7

Table 3.4. Physical and mechanical properties of selected materials [54 and 57]

N	Machine elements	Designation	Tensile strength	Yield strength	Ductility (percent elongation in 2 inches)	Density	Modulus of elasticity
			MPa	MPa	%	Kg/m^3	GPa
1	Prong	Stainless steel, S31600	552	207	70	8000	193-200
2	Crossbar	Aluminum 6061-T6	310	276	12	2635-2829	69-73
3	Longitudinal bar	Aluminum 6061-T6					
4	Shafts, which mounted on harrow	Steel 1045	565	310	16	7850	200
5	Short connecting rods	Steel 1045					
6	Upper shafts	Steel 1045					
7	Levers	Steel 1045					
8	Bottom shafts	Steel 1045					
9	Long connecting rods	Steel 1045					
10	Crankshaft	Steel 1045					
11	Ternary links	Gray cast iron	430	276		7200	103.4

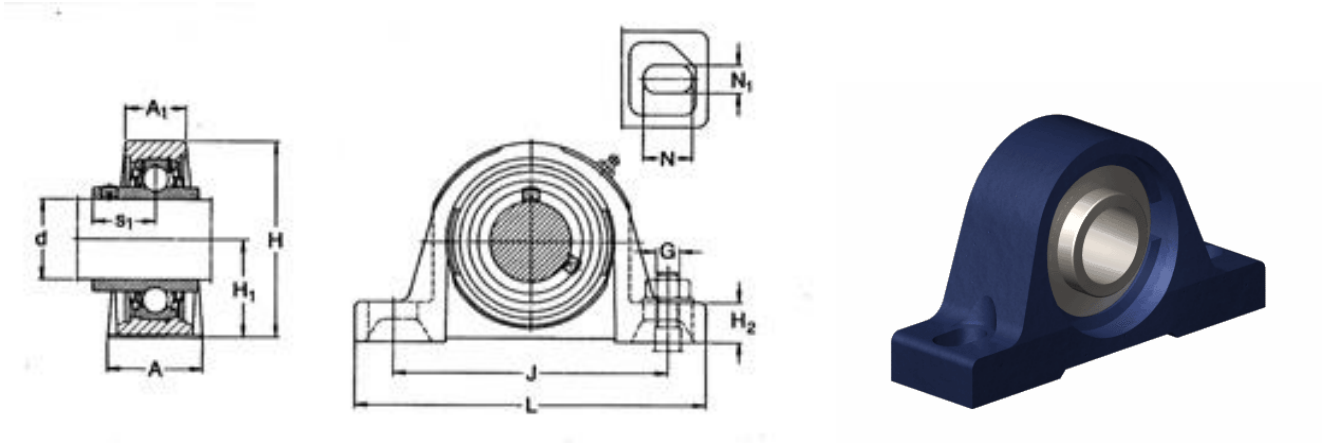

Table 3.5. Technical data of the Y-bearing plummer block units with cast housing [58].

N	Machine elements	Designation	Housing	Y-bearing	d	A	A1	H	H1	H2	J min	J max	L	N	N1	G	S1	Mass
					mm													kg
1	Shaft 1 and shaft 2	SY 25 TF	SY 505 M	YAR 205-2F	25	36	21	70	36.5	16	94	110	130	19.5	11.5	10	19.8	0.73
2	Bottom shafts																	
3	Crankshaft																	

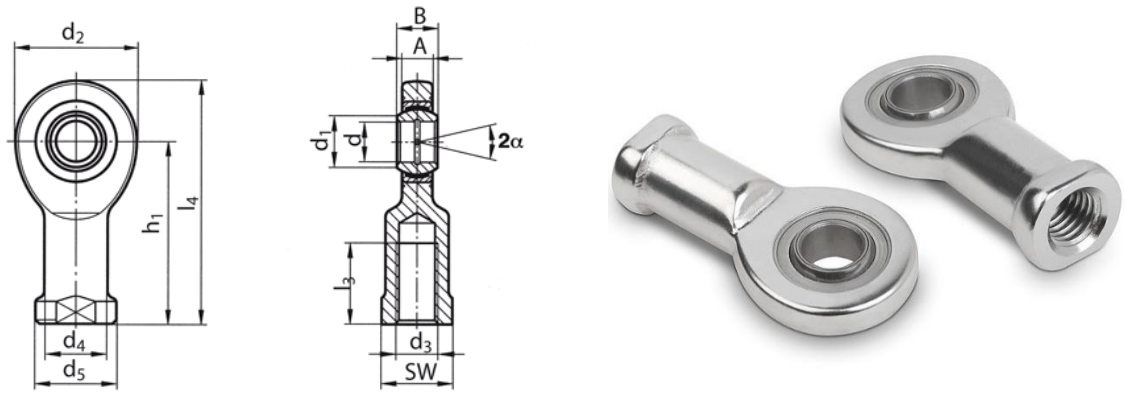

Table 3.6. Technical data of the end rod bearings [59]

N	Machine elements	Designation	Order number	d	A	B	d1	d2	Thread d3	D4	D5	H1	L3	L4	SW	Static basic loading C_0,	Angle of misalignment	Weight per piece
				mm												kN		g
1	Levers	DIN ISO 12240-4 (DIN 648) E series, with female thread	10806481 1017/013	17	11	14	20.7	46	M16	24	30	67	33	90	27	54.5	10	220
2	Short connecting rods		16806481 1020/013	20	13	16	24.2	53	M20x1.5	27.5	35	77	40	103.5	32	62.5	9	350
2	Long connecting rods		18806481 1025/013	25	17	20	29.3	64	M24x2	33.5	42	94	48	126	36	92	7	640

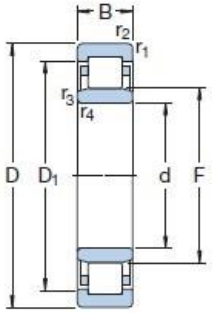

Type NU

Table 3.7. Technical data of the single row cylindrical roller bearing [60]

N	Machine elements	Designation	d	D	B	Basic load ratings		Fatigue load limit, P_u	Speed ratings		Mass
						Dynamic, C	Static, C_0		Reference speed	Limiting speed	
			Mm	Mm	Mm	kN	kN	kN	r/min	r/min	kg
1	Ternary link	NU 2204ECP	20	47	18	29.7	27.5	3.45	16000	19000	0.14

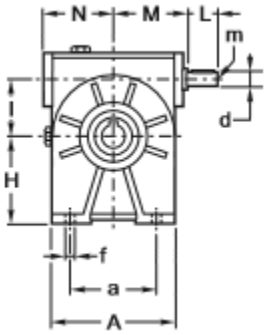

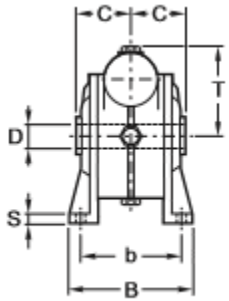

Table 3.8 Technical data of the selected gearbox [61]

Designation	**Version**	**RI gearboxes performances**					**RMI (suitable motor number)**	**Dimensions**																
RMI RI	I-28-180	Ratio	n1=900 min $^{-1}$					A	a	B	b	C	D	d	E	f	H	l	L	M	m	N	s	T
		49	n_2	T_{2M}	P kW	RD %																		
			18.4	329	1.0	62	90-80	158	120	140	116	60	28	19	87	11	115	70	40	97	M8	92	13	108

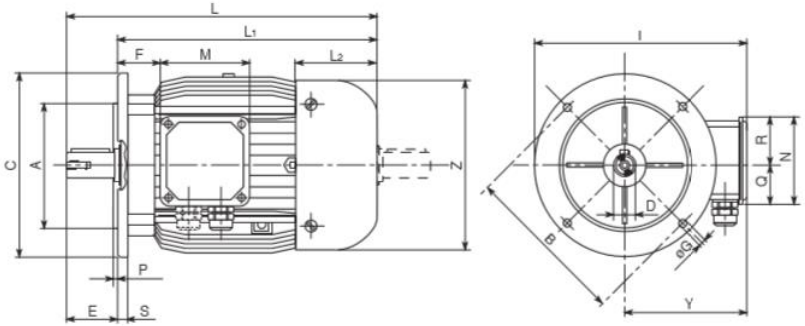

Table 3.9 Technical data of the selected asynchronous three phase motor (6 Pole, 1000 rpm-50Hz, Multi voltage winding. Volt 230/400/50 ±10% V) [62].

Type	Power	Velocity	Moment of inertia J	n	Power factor	Current, in A	Nominal torque Cn	Mass	Dimensions																			
	KW	Rpm	Kgm^2	%	cos φ	V 400	Nm	Kg	A	B	C	D	E	F	G	l	L	L1	L2	M	N	P	Q	R	S	Y	Z
M90Sa6	0.75	930	0.00249	69	0.66	2.8	7.6	11.8	130	165	200	24	50	33	12	246	325	275	85	110	110	3.5	57	57	10	146	176

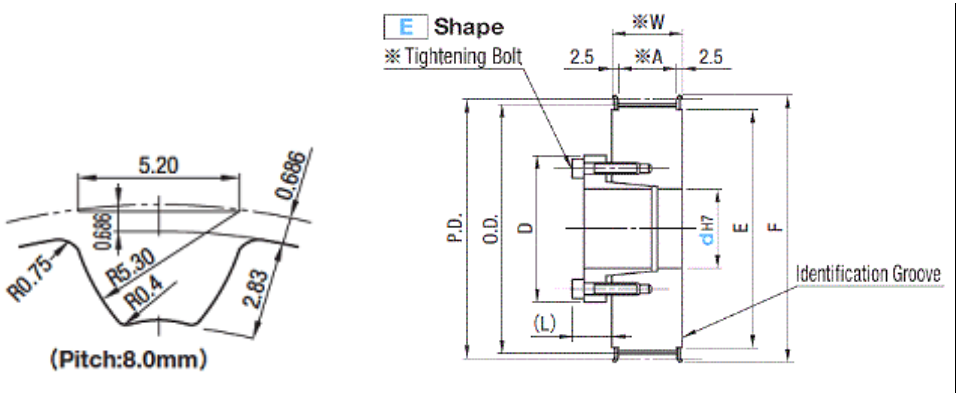

Table 3.10. Technical data of 8PM type High torque timing keyless pulley [63].

Type	Number of teeth	Pulley profile	Shaft diameter, mm	D.P.
P8M250	34	E	19 (Gearbox shaft)	86.58
	44		20 (Crankshaft)	112.05

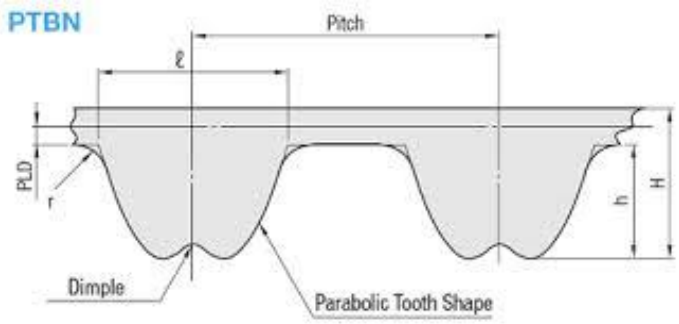

Table 3.12. Technical data of 8PM type High torque timing keyless pulley belt [63].

Type	Pitch	l	H	h	PLD	r	Mass g/m	Component code	Belt number	Number of teeth	Length of the belt, mm
P8M	8	5.20	5.5	2.90	0.686	0.8	56.0	PTBN	2496P8M	312	2496

Chapter 4
Technical drawings of the proposed mechanism.

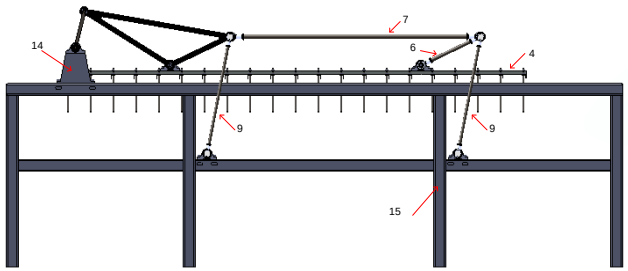

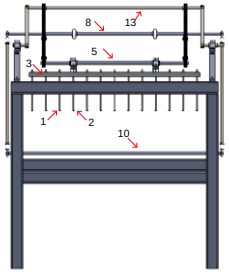

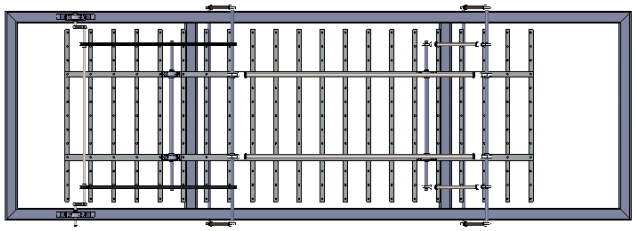

In order to manufacturing the new proposed mechanism, the all links have been drawn by Drawing tool of the commercial software SOLIDWORKS:

1. Drawing of the short prong;

2. Drawing of the short prong;

3. Drawing of the cross bar;

4. Drawing of the longitudinal bar;

5. Drawing of the shaft (which is mounted on longitudinal bar);

6. Drawing of the short connecting rod;

7. Drawing of the long connecting rod;

8. Drawing of the upper shaft;

9. Drawing of the lever;

10. Drawing of the bottom shaft;

11. Drawing of the left ternary link;

12. Drawing of the right ternary link;

13. Drawing of the crankshaft;

14. Drawing of the column (which is mounted journal bearing);

15. Drawing of frame of the proposed mechanism.

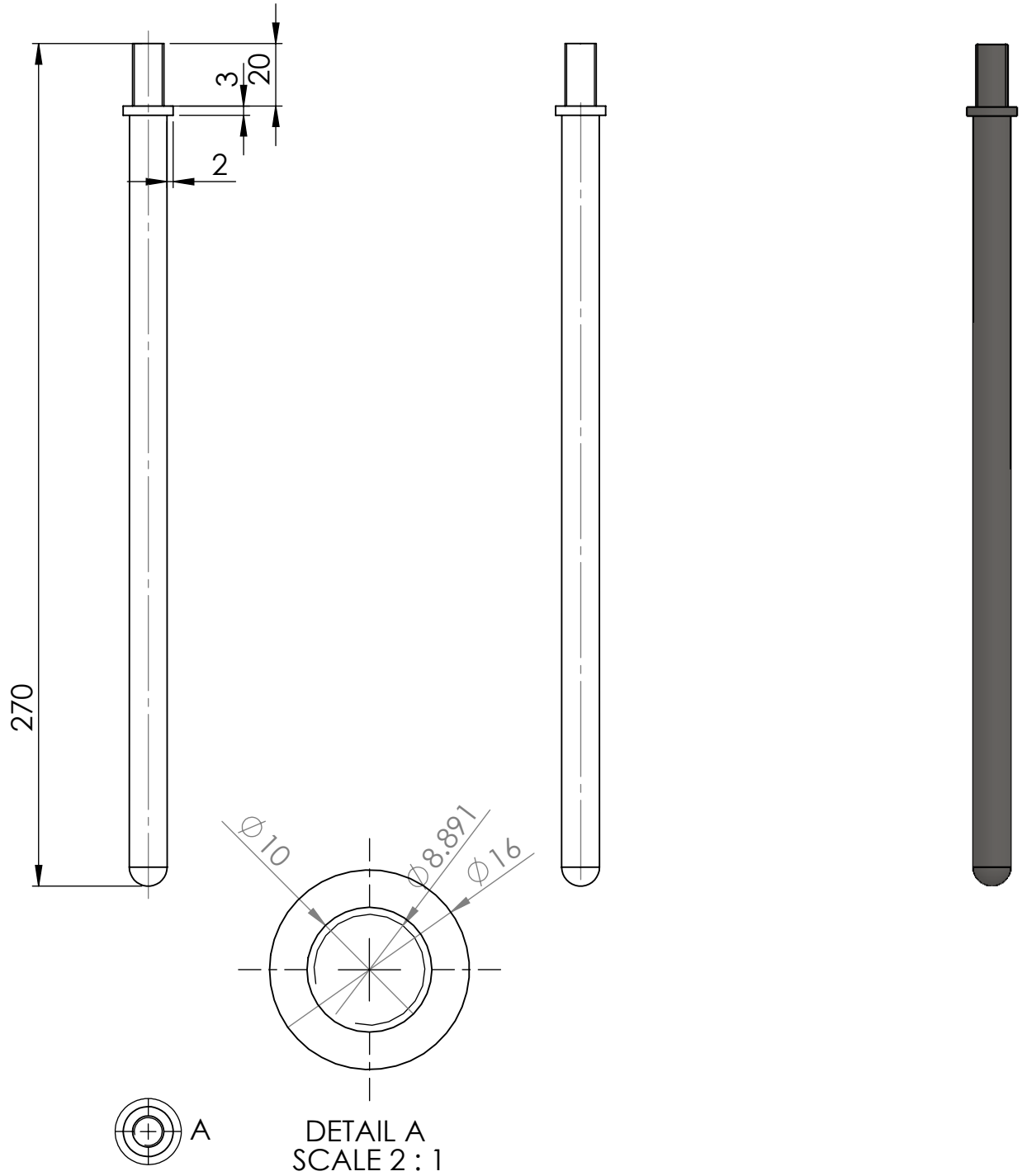

UNLESS OTHERWISE SPECIFIED: DIMENSIONS ARE IN MILLIMETERS SURFACE FINISH: TOLERANCES: LINEAR: ANGULAR:	FINISH:		DEBUR AND BREAK SHARP EDGES	DO NOT SCALE DRAWING	REVISION	
	NAME	SIGNATURE	DATE	TITLE:		
DRAWN	J.Kayumov		17.12.2014	Short prong		
CHK'D	V.P.Castelli		17.12.2014			
APPV'D	V.P.Castelli		17.12.2014			
MFG						
Q.A				MATERIAL: Stainless steel	DWG NO. 1	A4
				WEIGHT: 0.234 g	SCALE:1:2	SHEET 1 OF 1

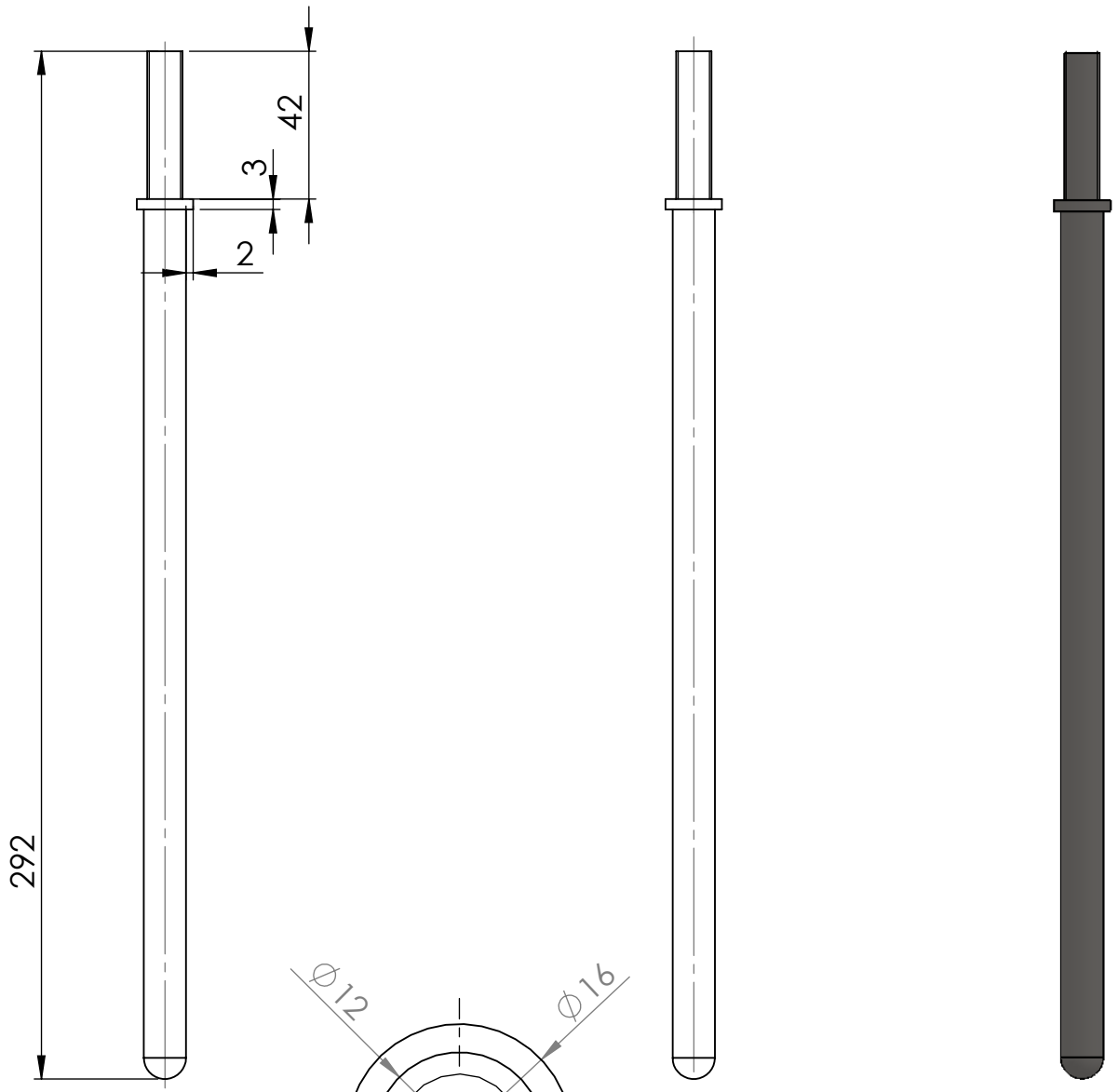

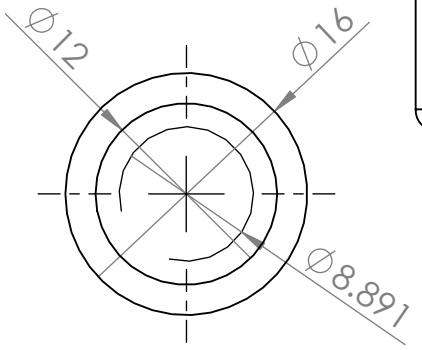

DETAIL A
SCALE 2 : 1

UNLESS OTHERWISE SPECIFIED: DIMENSIONS ARE IN MILLIMETERS SURFACE FINISH: TOLERANCES: LINEAR: ANGULAR:	FINISH:		DEBUR AND BREAK SHARP EDGES	DO NOT SCALE DRAWING	REVISION	
	NAME	SIGNATURE	DATE			
DRAWN	J.Kayumov					
CHK'D	V.P.Castelli					
APPV'D	V.P.Castelli					
MFG						
Q.A				MATERIAL: Stainless steel	DWG NO. 2	A4
				WEIGHT: 0.25 g	SCALE:1:2	SHEET 1 OF 1

TITLE:

Long prong

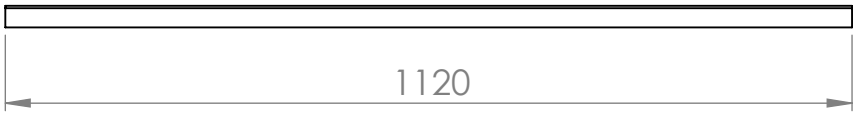

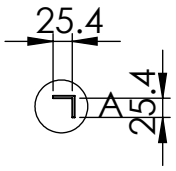

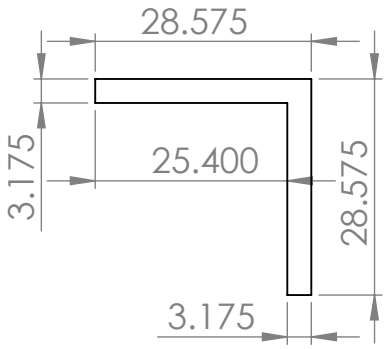

DETAIL A
SCALE 1 : 1

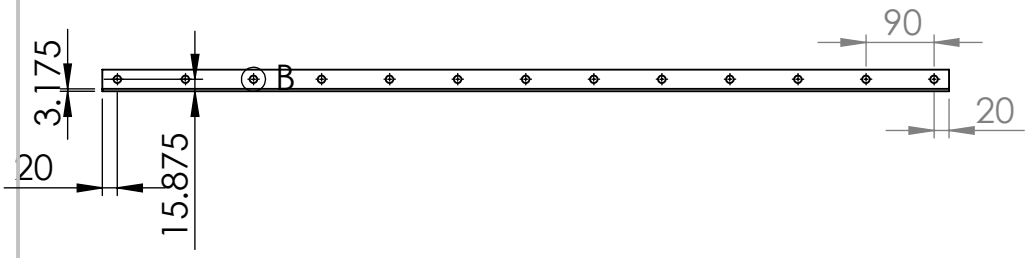

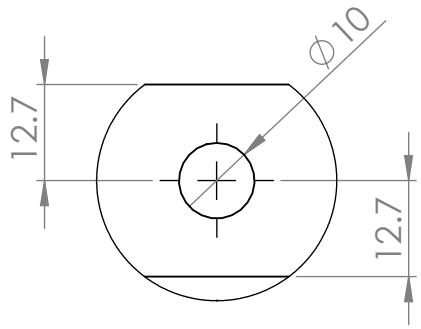

DETAIL B
SCALE 1 : 1

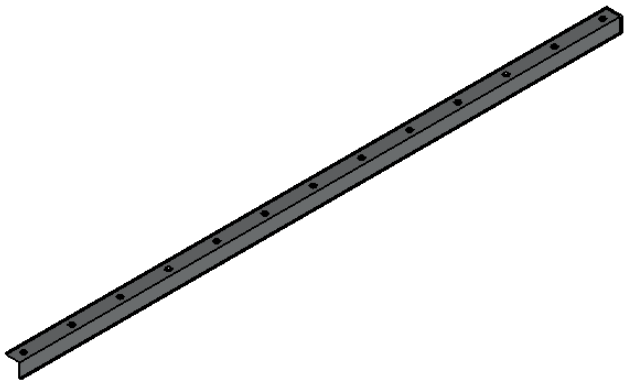

UNLESS OTHERWISE SPECIFIED: DIMENSIONS ARE IN MILLIMETERS SURFACE FINISH: TOLERANCES: LINEAR: ANGULAR:		FINISH:		DEBUR AND BREAK SHARP EDGES	DO NOT SCALE DRAWING	REVISION
	NAME	SIGNATURE	DATE		TITLE:	
DRAWN	J.Kayumov		17.12.2014		Cross bar	
CHK'D	V.P.Castelli		17.12.2014			
APPV'D	V.P.Castelli		17.12.2014			
MFG						
Q.A				MATERIAL: Aluminium 6061	DWG NO. 3	A4
				WEIGHT: 0.457 g	SCALE:1:10	SHEET 1 OF 1

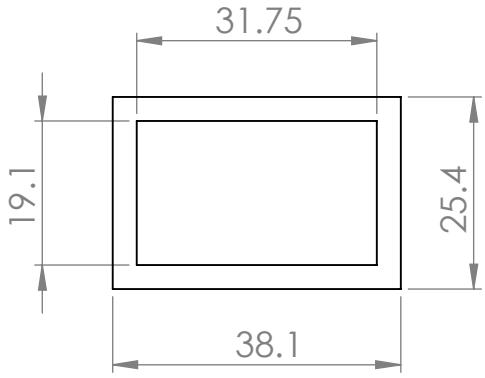

DETAIL A
SCALE 1 : 1

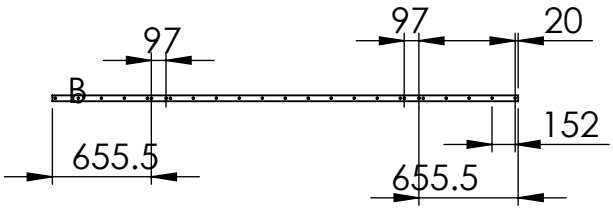

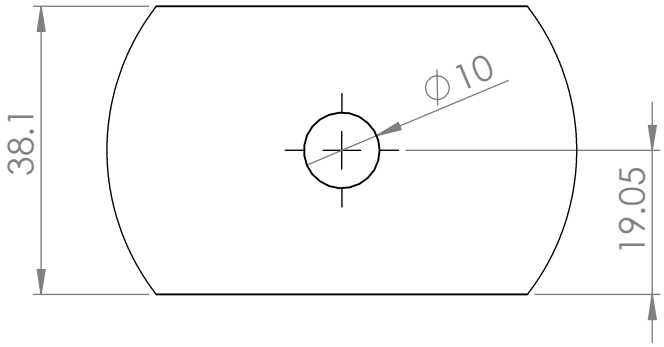

DETAIL B
SCALE 1 : 1

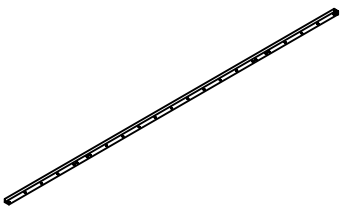

UNLESS OTHERWISE SPECIFIED: DIMENSIONS ARE IN MILLIMETERS SURFACE FINISH: TOLERANCES: LINEAR: ANGULAR:	FINISH:		DEBUR AND BREAK SHARP EDGES	DO NOT SCALE DRAWING	REVISION	
	NAME	SIGNATURE	DATE	TITLE:		
DRAWN	J.Kayumov		17.12.2014	Longitudinal bar		
CHK'D	V.P.Castelli		17.12.2014			
APPV'D	V.P.Castelli		17.12.2014			
MFG						
Q.A				MATERIAL: Aluminium 6061	DWG NO. 4	A4
				WEIGHT: 3.01 kg	SCALE:1:50	SHEET 1 OF 1

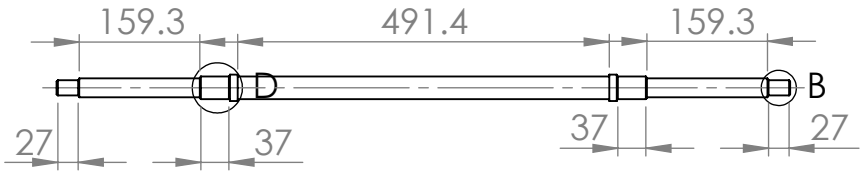

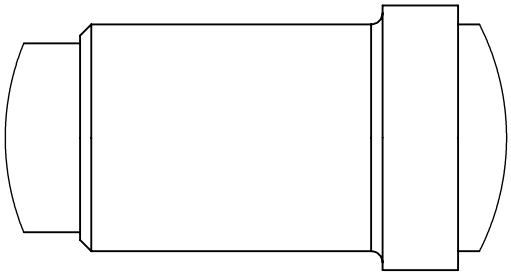

DETAIL D
SCALE 1 : 1

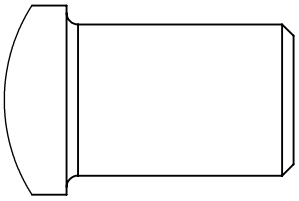

DETAIL B
SCALE 1 : 1

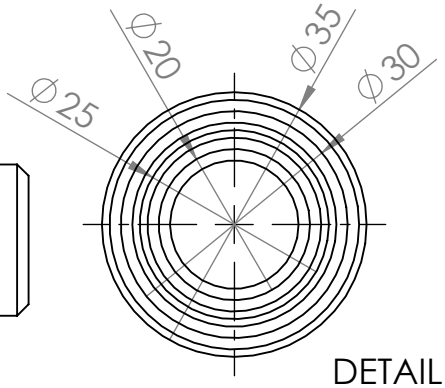

DETAIL A
SCALE 1 : 1

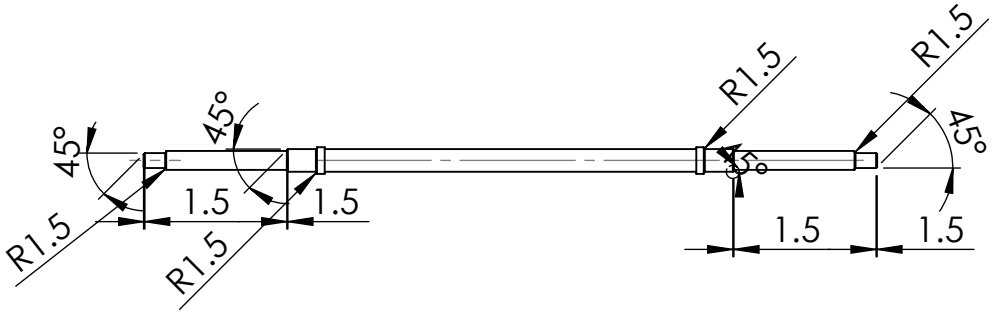

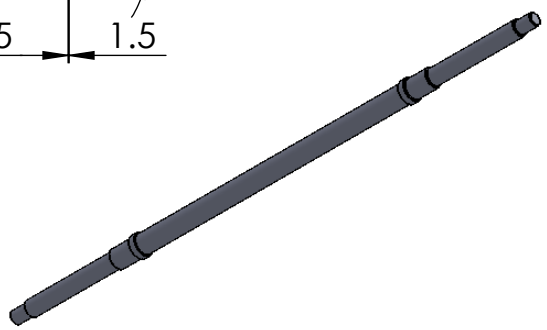

UNLESS OTHERWISE SPECIFIED: DIMENSIONS ARE IN MILLIMETERS SURFACE FINISH: TOLERANCES: LINEAR: ANGULAR:	FINISH:		DEBUR AND BREAK SHARP EDGES		DO NOT SCALE DRAWING	REVISION
	NAME	SIGNATURE	DATE		TITLE:	
DRAWN	J.Kayumov		17.12.2014		Shaft	
CHK'D	V.P.Castelli		17.12.2014			
APPV'D	V.P.Castelli		17.12.2014			
MFG						
Q.A				MATERIAL: Plain carbon steel AISI 1045	DWG NO. 5	A4
				WEIGHT: 2.67 kg	SCALE:1:10	SHEET 1 OF 1

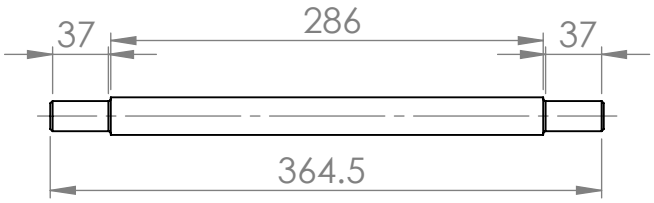

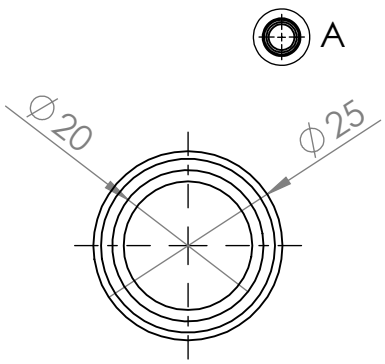

DETAIL A
SCALE 1 : 1

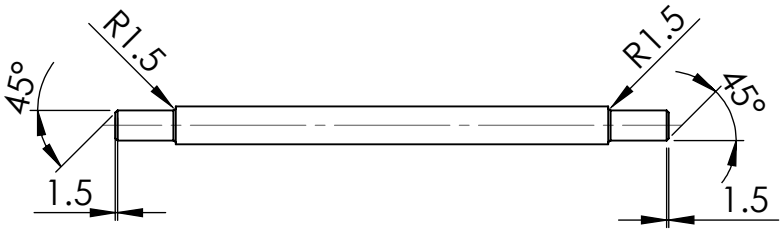

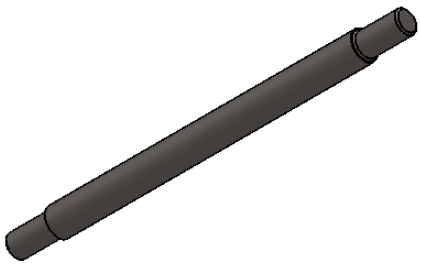

UNLESS OTHERWISE SPECIFIED: DIMENSIONS ARE IN MILLIMETERS SURFACE FINISH: TOLERANCES: LINEAR: ANGULAR:		FINISH:		DEBUR AND BREAK SHARP EDGES	DO NOT SCALE DRAWING	REVISION
	NAME	SIGNATURE	DATE		TITLE:	
DRAWN	J.Kayumov		17.12.2014		Short connecting rod	
CHK'D	V.P.Castelli		17.12.2014			
APPV'D	V.P.Castelli		17.12.2014			
MFG						
Q.A				MATERIAL: Carbon plain steel AISI 1045	DWG NO. 6	A4
				WEIGHT: 1.4 kg	SCALE:1:5	SHEET 1 OF 1

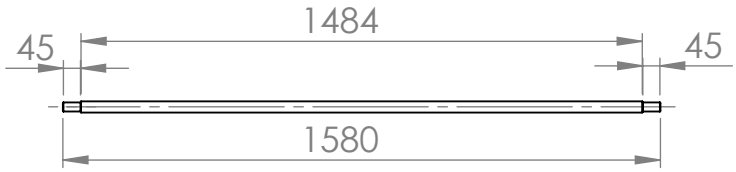

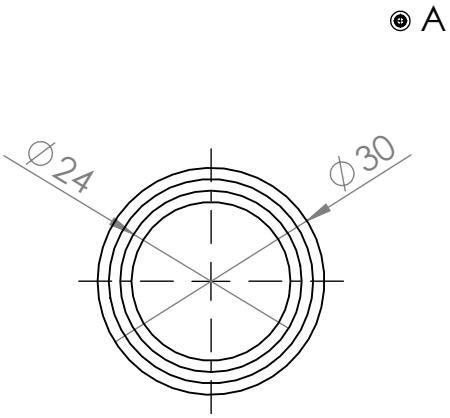

DETAIL A
SCALE 1 : 1

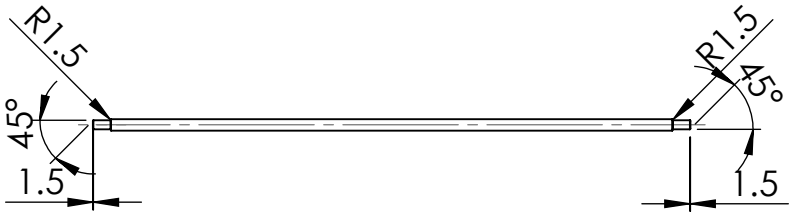

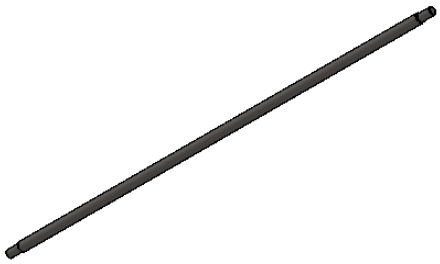

UNLESS OTHERWISE SPECIFIED: DIMENSIONS ARE IN MILLIMETERS SURFACE FINISH: TOLERANCES: LINEAR: ANGULAR:		FINISH:		DEBUR AND BREAK SHARP EDGES	DO NOT SCALE DRAWING	REVISION
	NAME	SIGNATURE	DATE		TITLE:	
DRAWN	J.Kayumov		17.12.2014		Long connecting rod	
CHK'D	V.P.Castelli		17.12.2014			
APPV'D	V.P.Castelli		17.12.2014			
MFG						
Q.A				MATERIAL: Carbon plain steel AISI 1045	DWG NO. 7	A4
				WEIGHT: 8.96 kg	SCALE:1:20	SHEET 1 OF 1

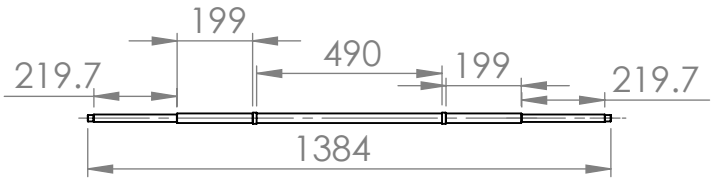

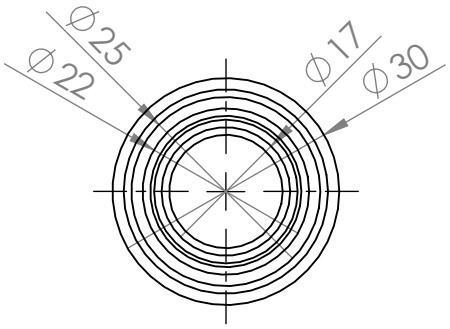

DETAIL A
SCALE 1 : 1

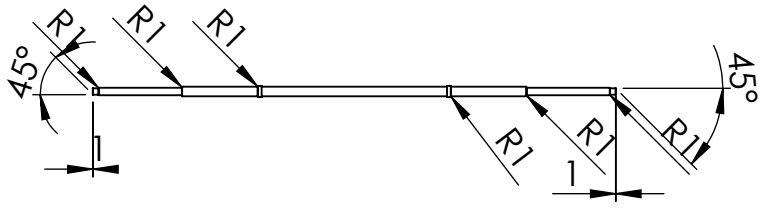

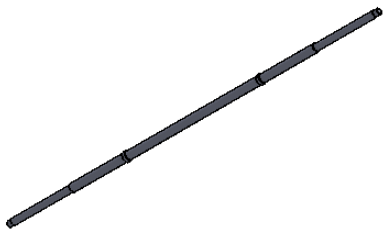

UNLESS OTHERWISE SPECIFIED: DIMENSIONS ARE IN MILLIMETERS SURFACE FINISH: TOLERANCES: LINEAR: ANGULAR:	FINISH:		DEBUR AND BREAK SHARP EDGES		DO NOT SCALE DRAWING	REVISION
	NAME	SIGNATURE	DATE		TITLE:	
DRAWN	J.Kayumov		17.12.2014		Upper shaft	
CHK'D	V.P.Castelli		17.12.2014			
APPV'D	V.P.Castelli		17.12.2014			
MFG						
Q.A				MATERIAL: Carbon plain steel AISI 1045	DWG NO. 8	A4
				WEIGHT: 3.22 kg	SCALE:1:20	SHEET 1 OF 1

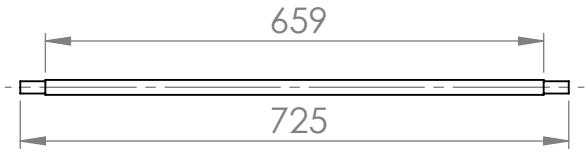

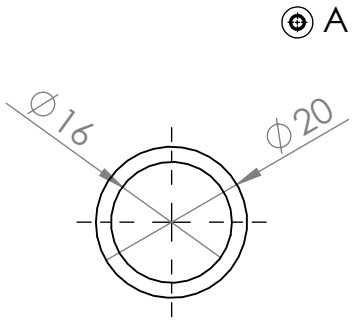

DETAIL A
SCALE 1 : 1

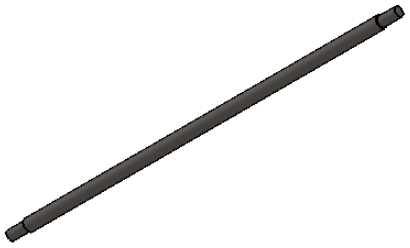

UNLESS OTHERWISE SPECIFIED: DIMENSIONS ARE IN MILLIMETERS SURFACE FINISH: TOLERANCES: LINEAR: ANGULAR:		FINISH:		DEBUR AND BREAK SHARP EDGES	DO NOT SCALE DRAWING	REVISION
	NAME	SIGNATURE	DATE		TITLE:	
DRAWN	J.Kayumov		17.12.2014		Lever	
CHK'D	V.P.Castelli		17.12.2014			
APPV'D	V.P.Castelli		17.12.2014			
MFG						
Q.A				MATERIAL: Plain carbon steel AISI 1045	DWG NO. 9	A4
				WEIGHT: 1.81 kg	SCALE:1:10	SHEET 1 OF 1

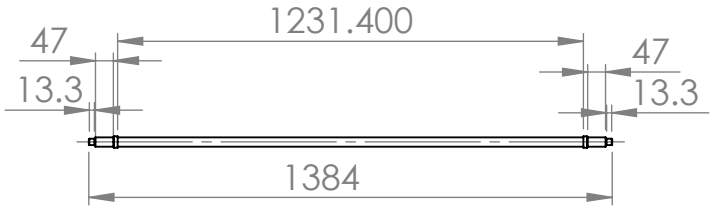

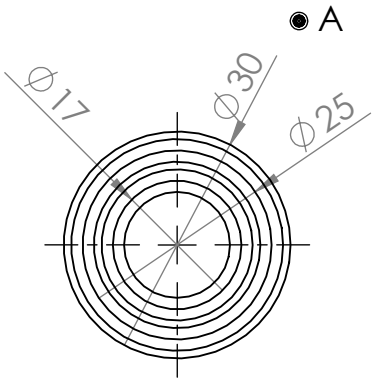

DETAIL A
SCALE 1 : 1

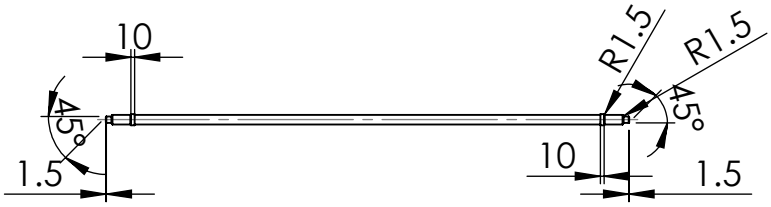

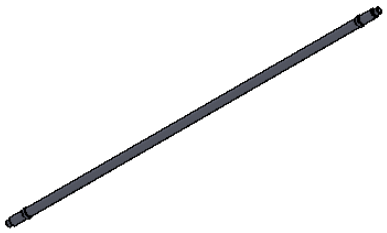

UNLESS OTHERWISE SPECIFIED: DIMENSIONS ARE IN MILLIMETERS SURFACE FINISH: TOLERANCES: LINEAR: ANGULAR:		FINISH:		DEBUR AND BREAK SHARP EDGES		
				DO NOT SCALE DRAWING		REVISION
	NAME	SIGNATURE	DATE			
DRAWN	J.Kayumov		17.12.2014			
CHK'D	V.P.Castelli		17.12.2014			
APPV'D	V.P.Castelli		17.12.2014			
MFG						
Q.A				MATERIAL: Plain carbon steel AISI 1045		
				WEIGHT: 5.45 kg		

TITLE:

Bottom shaft

DWG NO. 10	A4
SCALE:1:20	SHEET 1 OF 1

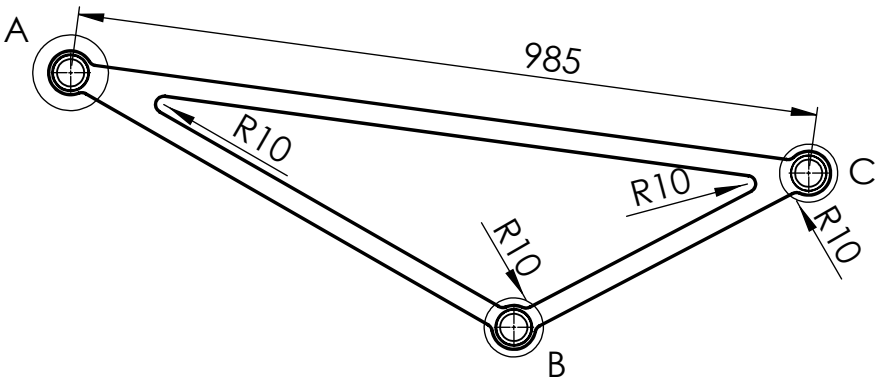

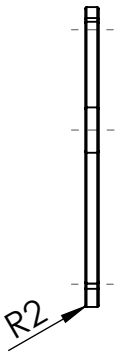

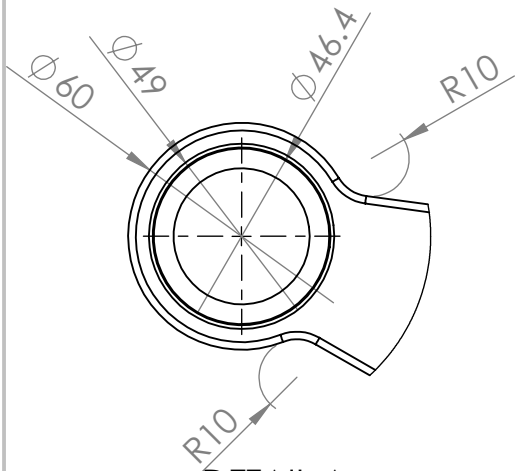

DETAIL A
SCALE 1 : 2

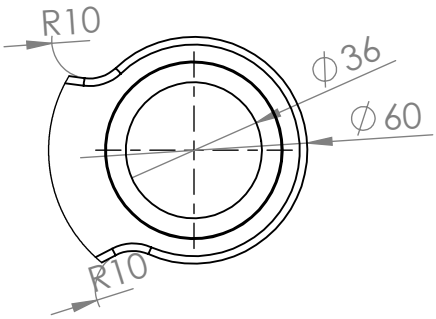

DETAIL C
SCALE 1 : 2

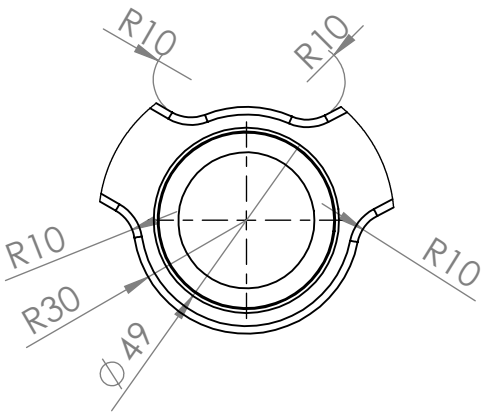

DETAIL B
SCALE 1 : 2

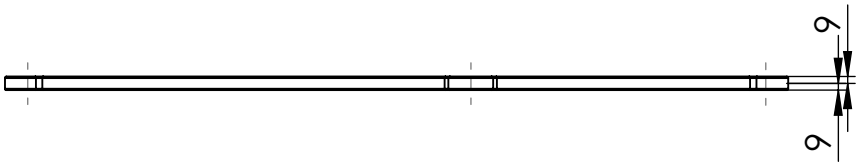

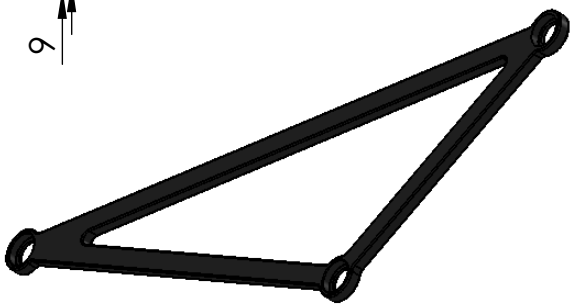

UNLESS OTHERWISE SPECIFIED: DIMENSIONS ARE IN MILLIMETERS SURFACE FINISH: TOLERANCES: LINEAR: ANGULAR:	FINISH:		DEBUR AND BREAK SHARP EDGES		DO NOT SCALE DRAWING	REVISION
	NAME	SIGNATURE	DATE		TITLE:	
DRAWN	J.Kayumov		17.12.2014		Left ternary link	
CHK'D	V.P.Castelli		17.12.2014			
APPV'D	V.P.Castelli		17.12.2014			
MFG						
Q.A				MATERIAL: Cast iron	DWG NO. 11	A4
				WEIGHT: 6.6 kg	SCALE:1:10	SHEET 1 OF 1

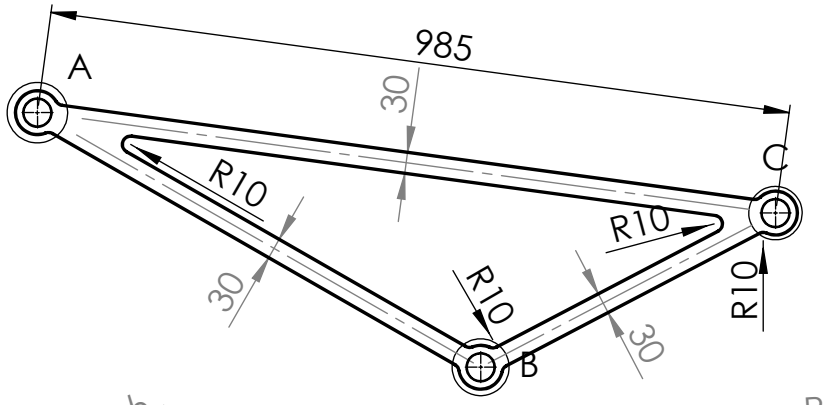

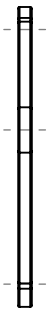

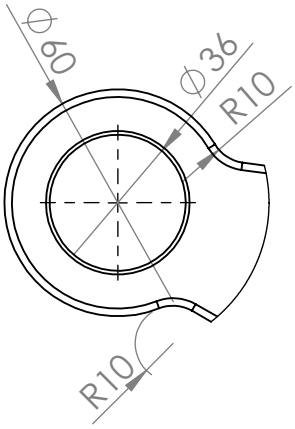

DETAIL A
SCALE 1 : 2

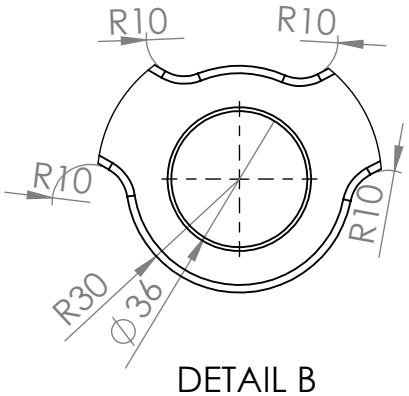

DETAIL B
SCALE 1 : 2

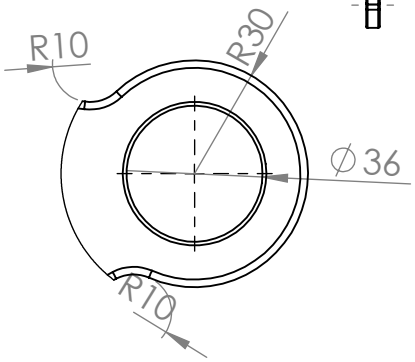

DETAIL C
SCALE 1 : 2

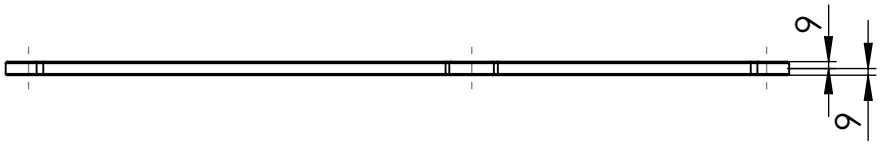

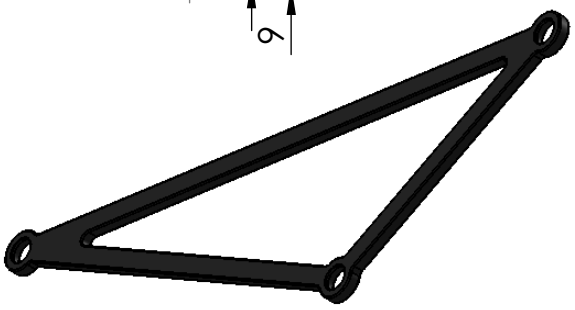

UNLESS OTHERWISE SPECIFIED: DIMENSIONS ARE IN MILLIMETERS SURFACE FINISH: TOLERANCES: LINEAR: ANGULAR:	FINISH:		DEBUR AND BREAK SHARP EDGES		DO NOT SCALE DRAWING	REVISION
	NAME	SIGNATURE	DATE		TITLE:	
DRAWN	J.Kayumov		17.12.2014		Right ternary link	
CHK'D	V.P.Castelli		17.12.2014			
APPV'D	V.P.Castelli		17.12.2014			
MFG						
Q.A				MATERIAL: Gray cast iron	DWG NO. 12	A4
				WEIGHT: 6.6 kg	SCALE:1:10	SHEET 1 OF 1

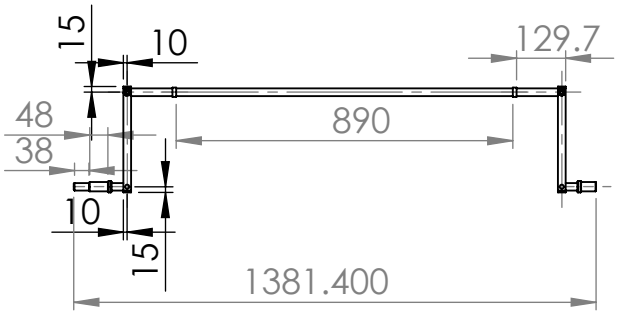

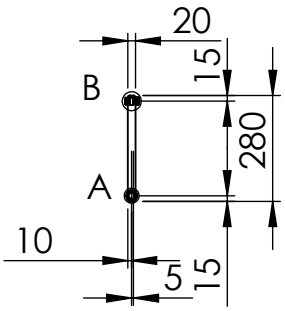

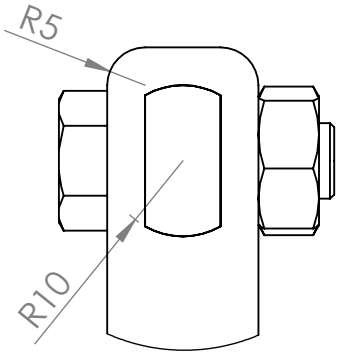

DETAIL B
SCALE 1 : 1

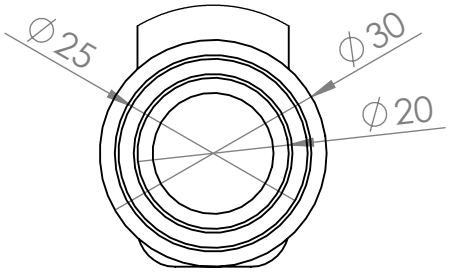

DETAIL A
SCALE 1 : 1

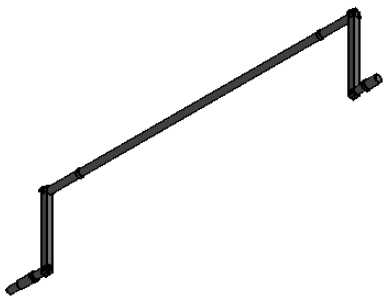

UNLESS OTHERWISE SPECIFIED: DIMENSIONS ARE IN MILLIMETERS SURFACE FINISH: TOLERANCES: LINEAR: ANGULAR:	FINISH:		DEBUR AND BREAK SHARP EDGES		DO NOT SCALE DRAWING	REVISION
	NAME	SIGNATURE	DATE		TITLE:	
DRAWN	J.Kayumov		17.12.2014		Crankshaft	
CHK'D	V.P.Castelli		17.12.2014			
APPV'D	V.P.Castelli		17.12.2014			
MFG						
Q.A				MATERIAL: Plain carbon steel AISI 1045	DWG NO. 13	A4
				WEIGHT: 4.48 kg	SCALE:1:20	SHEET 1 OF 1

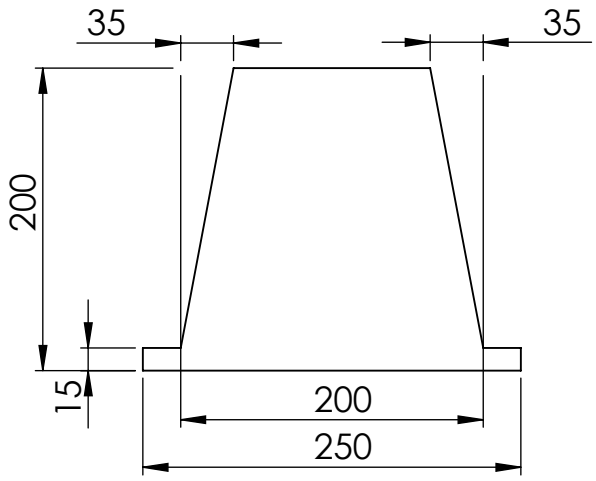

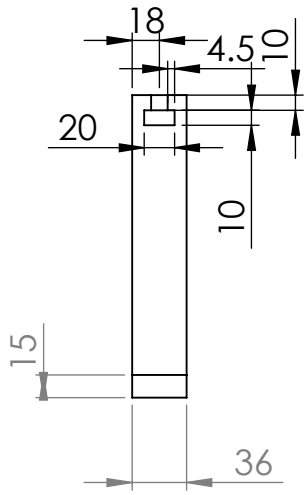

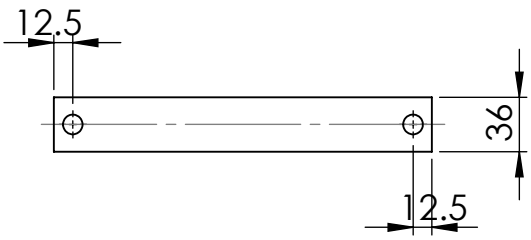

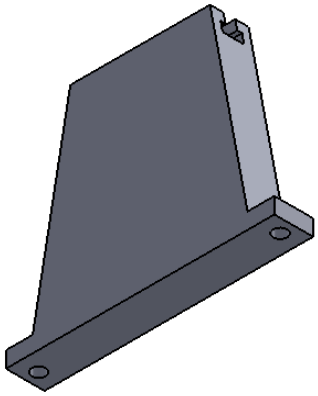

UNLESS OTHERWISE SPECIFIED: DIMENSIONS ARE IN MILLIMETERS SURFACE FINISH: TOLERANCES: LINEAR: ANGULAR:	FINISH:		DEBUR AND BREAK SHARP EDGES	DO NOT SCALE DRAWING	REVISION	
	NAME	SIGNATURE	DATE	TITLE:		
DRAWN	J.Kayumov		17.12.2014	Column		
CHK'D	V.P.Castelli		17.12.2014			
APPV'D	V.P.Castelli		17.12.2014			
MFG						
Q.A				MATERIAL: Grey cast iron	DWG NO. 14	A4
				WEIGHT: 1.1 kg	SCALE:1:5	SHEET 1 OF 1

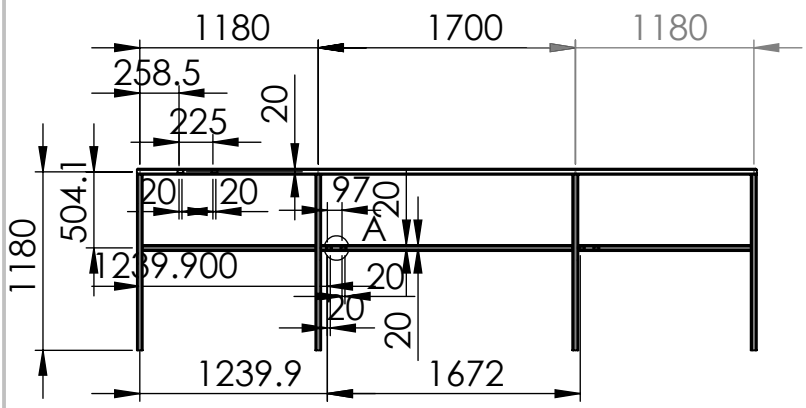

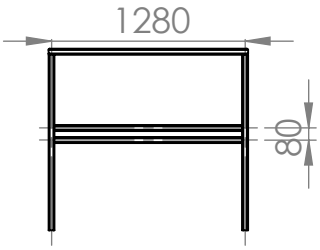

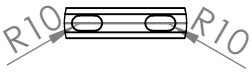

DETAIL A
SCALE 1 : 10

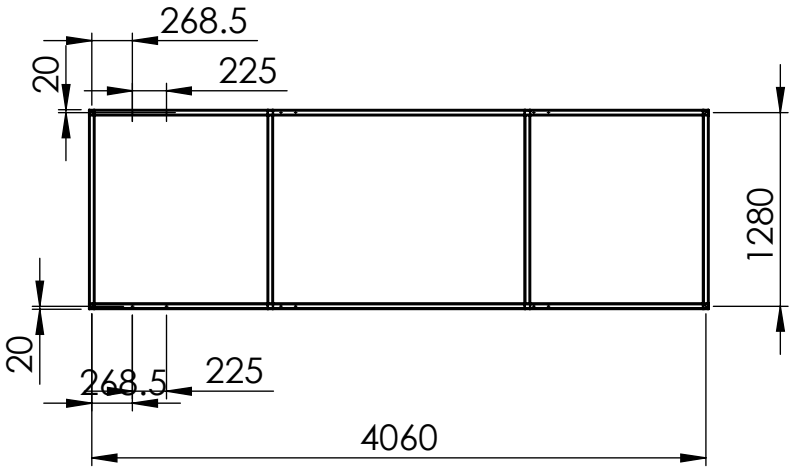

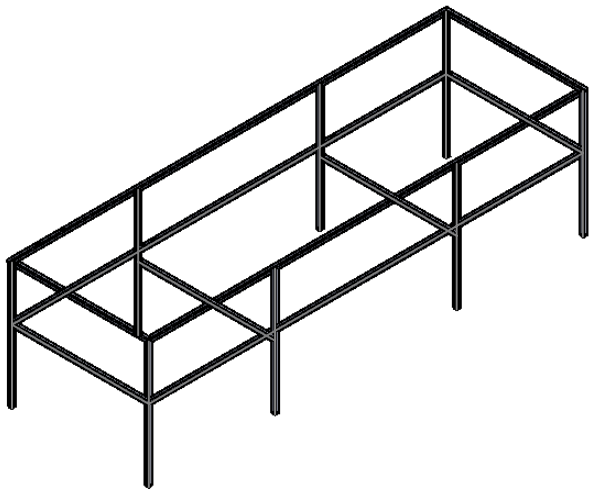

UNLESS OTHERWISE SPECIFIED: DIMENSIONS ARE IN MILLIMETERS SURFACE FINISH: TOLERANCES: LINEAR: ANGULAR:	FINISH:		DEBUR AND BREAK SHARP EDGES		DO NOT SCALE DRAWING	REVISION
	NAME	SIGNATURE	DATE		TITLE:	
DRAWN	J.Kayumov		17.12.2014		Frame	
CHK'D	V.P.Catelli		17.12.2014			
APPV'D	V.P.Catelli		17.12.2014			
MFG						
Q.A				MATERIAL: Plain carbon steel AISI 1045	DWG NO. 15	A4
				WEIGHT:	SCALE:1:50	SHEET 1 OF 1

Conclusion

The fibre entanglement is one of the main problems of the wool processing. Raw wool can be entangled during its pre-treatment. The main working points of the wool feeder, wool transport mechanisms and squeeze rollers of the conventional scouring machines provoke the fibre entanglement and the fibre damage. Several research work has been done in order to reduce the fibre entanglement. In spite of the existing technologies, the conventional scouring machines are widely used in wool processing.

In this thesis a new harrow type wool transport mechanism has been designed. The developed mechanism has been synthesized relying upon a four bar linkage. In one part of the thesis, the kinematic analysis of the mechanism has been performed. The positions of all links of the mechanism has been determined. Then, the velocity and the acceleration analyses of the mechanism have been performed. Moreover, the kinetostatic analysis of the developed mechanism has been introduced. The internal and the external forces have been calculated by the free body diagram method, by using the static and dynamic equilibrium equations.

In order to design the proposed mechanism, all links of the mechanism have been analyzed in terms of stress analysis. The proper materials, the bearings, the motor and the gearbox have been selected. The proposed mechanism has been designed such that, it can be easily installed and easily removed from the frame of the scouring machine. The proposed mechanism has been modelled by commercial software SOLIDWORKS. The last part of the thesis, the technical drawings of the proposed mechanism have been performed for manufacturing purposes. In the proposed mechanism can be installed instead of the first bowl of the scouring line. It is possible to install it also as a hybrid scouring machine, with suction drum, such as the ANDAR hopper bottom scouring machine. The new proposed mechanism can be widely used also in other industrial transportation purposes.

In the future work, the length of the straight line trajectory of the motion of the transport mechanism can be analyzed in order to increase the quality of the wool.

Bibliography

[1] Werner Von Bergen. Wool handbook. Volume two. Third enlarged edition. Part 1: Spinning, Weaving, Knitting. "Inter Science Publishers". A division of John Wiley & Sons, 1969. USA.

[2] Rogachev, N.V, Fedorov V.A. Primary treatment of wool. "Light Industry", Moscow, 1967 (in Russian).

[3] Gusev V.E. Raw materials for wool and non-woven products and primary treatment of wool, 1977 (in Russian).

[4] Simpson W.S., Crawshaw G.H. Wool: Science and technology, The Textile Institute. "Woodhead Publishing Limited", Cambridge, England, 2002. ISBN 1855735741.

[5] Cristoe J.R., Entanglement and wool scouring, Proceedings of the 2nd China Wool Textile Conference. April 15-17, 1998. Xian, China.

[6] Jamieson R.G., Wool Research Organization of New Zealand Report No. 90, 1982. (Cited in [5]).

[7] A. Samson and M. Chaikin, CIRTEL, Paris, III, 141, 1965. (Cited in [5]).

[8] Karsch F., Melliand Textilber., 49, 885, 1968. (Cited in [5]).

[9] Caunce J.F., "Mathematic modelling of wool scouring". PhD thesis, March, 2007. The University of New South Wales.

[10] Karmakar S.R., Chemical technology in the pre-treatment processes of textiles. Elsevier Science B.V. Amsterdam, The Netherlands.1999, ISBN:0-444-50060-X

[11] Choudhuri A.K., Textile preparation and dyeing. "Published by Science Publishers", Enfield, NH, USA, 2006. ISBN 1-57808-402-4

[12] "Solvent scouring of wool", Wool Sci. Rev., 1963, 23, 40-54. Cited in [5].

[13] J. Lindberg and S. Ekergen, "A new method for solvent scouring of raw wool", Prospect of International Wool Textile Conference, Melbourne, CSIRO, 1955, **E**, 342-6.

[14] Stewart R.G., Woolscouring and Allied Technology, Wool Research Organization of New Zealand, Third edition, 1988

[15] G.F.Wood, A.J.C. Pearson, J.R. Christoe, The CSIRO Low-Flow process, an in-process Effluent Treatment for Aqueous Woolscouring, CSIRO Division of Textile Industry report No G39, 1979.

[16] Vigo, Tyrone L. Textile processing and properties: Preparation, dyeing, finishing and performance. Vol. 11. Elsevier, 2013.
[17] http://www.woolmark.com/learn-about-wool/wool-scouring.
[18] Sargent, Charles G. "Improvement in machines for washing wool." U.S. Patent No. 41,324. 19 Jan. 1864.
[19] Sargent, Charles G. "Improvement in wool-washing machines." U.S. Patent No. 184,301. 14 Nov. 1876.
[20] Sargent, Frederick G. "Improvement in wool-washing machines." U.S. Patent No. 206,489. 30 Jul. 1878.
[21] Sargent, Frederick G. "Wool-washing machine." U.S. Patent No. 258,322. 23 May 1882.
[22] Sargent, Frederick G. "Wool washer." U.S. Patent No. 354,245. 14 Dec. 1886.
[23] F.P.Pendleton and J.K.Proctor, "Wool washing machine". U.S. Patent No. 180,370. July 25, 1876.
[24] F.P.Pendleton and J.K.Proctor, "Wool-scouring machine". U.S. Patent No. 206,192. July 23, 1878.
[25] J.H.Knowles, J.K.Proctor and F.P.Pendleton, "Wool-scouring machine". U.S. Patent No. 187,643. 20 Feb. 1877.
[26] Sargent, Frederick G. "Wool-washing machine". U.S. Patent No. 433,581. 5 Aug. 1890.
[27] Sargent, Frederick G. "Wool-washing machine." U.S. Patent No. 480,283. 9 Aug. 1892.
[28] McNaught J. and McNaught W. "Machinery for scouring and washing wool". U.S. Patent No. 385,761. July 10, 1888.
[29] McNaught W. "Wool washing machine". U.S. Patent No. 650,727. May 29, 1900.
[30] W. McNaught and T.W. Hawkins, "Wool washing machine". U.S. Patent No. 650,728. May 29, 1900.
[31] Sargent, Frederick G. "Wool washing machine". U.S. Patent No. 675,069. May 28, 1901.
[32] Sargent, Frederick G. "Wool washing machine". U.S. Patent No. 889,157. May 26, 1908.
[33] Frederick G. Sargent and C. Allan, "Wool washing machine". U.S. Patent No. 889,157. Apr. 20, 1909.

[34] Friedrich Bernhard, “Washing and rinsing machine for fibrous materials”. 862,233. 6 Aug, 1907.
[35] Joseph H. Tillinghast, “Wool-scouring machine”. U.S. Patent No. 821,139, May 22, 1906.
[36] Walter Oscar Milne, “Wool-scouring machine”. U.S. Patent No. 854,372. May 21, 1906.
[37] L.A. Peckham, "Wool washing machine". U.S. Patent No. 558,305, Apr. 14, 1896.
[38] W. Lund, "Wool washing machine". U.S. Patent No. 395,498. Jan 01, 1889.
[39] J. Keefe, "Wool washing machine". U.S. Patent No. 709,227. 16 Sep, 1902.
[40] C.Sargent and H.Harrison, "Wool washing machine". U.S. Patent No. 1,186,043. June 6, 1916.
[41] H.Walker, "Apparatus for scouring, dyeing or otherwise treating with liquor, wool yarn or other fibrous material". U.S. Patent No. 1,354,081 28 Sep,1920.
[42] J.F. White, "Wool washing machine". U.S. Patent No. 1,537,720. May 12, 1925.
[43] W.W. Windle, "Wool washing machine". U.S. Patent No. 2,037,841, May 12, 1936.
[44] W.W. Windle, "Wool washing machine". U.S. Patent No. 2,040,162. 21 Apr. 1936.
[45] M. Lewin, Handbook of Fiber Science and Technology Volume 2: Chemical Processing of Fibers and Fabrics--Functional Finishes. – CRC Press, 1984. – T. 2.
[46] http://www.fibre2fashion.com/industry-article/20/1958/wool-scouring1.asp.
[47] C.S.Sharma and K. Purohit, Theory of Mechanisms and machines, Prentice-Hall of India Private Limited, New Delhi, 2006.
[48] A.B.Kempe, How to draw a straight line mechanisms, “MacMillan and Co”, London, 1877.
[49] Eugene S.Ferguson, Kinematics of mechanisms from the time of Watt, “Smithsonian Institution”, Washington DC, 1962.

[50] J.A.Hrones and G.L.Nelson, Analysis of four bar linkage: Its application to the synthesys of the mechanisms, The Technology Press of the Massachusettes Institute of Technology, 1951.

[51] R.S.Hartenberg and J.Denavit, Kinematic synthesis of linkages, McGraw-Hill Book Company, Unated States of Amerika, 1964.

[52] Cengel, Yunus A., and John M. Cimbala. *Fluid mechanics*. Vol. 1. Tata McGraw-Hill Education, 2006.

[53] http://wovember.com/2012/11/14/processing-wool-by-susan-gibbs/.

[54] Mott, L. Robert, "Machine elements in mechanical design", Pearson Prentice Hall, 2004.

[55] Aluminium Design Manual-2005. The aluminium association. Specifications and guidelines for aluminium structures. 1525 Wilson Boulevard, Suite 600, Arlington, VA 22209. Page 334.

[56] The American Association of State Highway and Transportation Officials (AASHTO) Standard Specifications for Structural Supports for Highway Signs, Luminaries and Traffic Signals, fifth edition, 2009.

[57] Robert Norton Machine design: An integrated approach. Third edition, Pearson Prentice Hall, 2006.

[58] Y-bearings and Y-bearing units. SKF group 2013.

[59] DIN ISO 12240-4 (DIN 648 E series). MBO-Oswald catalogue.

[60] Cylindrical roller bearings. SKF Interactive Engineering Catalogue. May 2004.

[61] Worm Gearboxes. S.T.M. Team technical catalogue.

[62] Carpanelli motori elettrici. Technical catalogue. Bologna, Italy.

[63] MISUMI Componenti mecanici per la realizzazione di macchinari specializzati e l'automazione industriale. Volume 1/2. Edizione Italiana 2011-2012.